STATE OF OREGON
DEPARTMENT OF GEOLOGY AND MINERAL INDUSTRIES
Suite 177
800 NE Oregon St. #28
Portland, Oregon 97232

OPEN-FILE REPORT O-95-05

# EXPLANATION OF MAPPING METHODS AND USE OF THE TSUNAMI HAZARD MAP OF THE SILETZ BAY AREA, LINCOLN COUNTY, OREGON

George R. Priest, editor
Oregon Department of Geology and Mineral Industries

Funded in part by

Oregon Coastal Management Program, Oregon Department of Land Conservation and Development, from funds provided by the Oregon Legislature, US Department of Commerce National Oceanographic and Atmospheric Administration office of Coastal Resource Management under Section 306 Coastal Zone Management grants, and Section 309 Program Enhancement grants

with additional support from

State lottery, State General Fund, and donated in-kind support from the Oregon Graduate Institute of Science & Technology.

**NOTICE**

The Oregon Department of Geology and Mineral Industries is publishing this paper because the information furthers the mission of the Department. To facilitate timely distribution of information, this report has not been edited to our usual standards.

# CONTENTS

**Chapter 1**
**Simplified Explanation of the Tsunami Hazard Map of the Siletz Bay Area, Lincoln County, Oregon**



**Chapter 2**
**Siletz Bay: A Pilot Investigation of Coastal Inundation by Cascadia Subduction Zone tsunamis**

**Chapter 3**
**Evidence for Coseismic Subsidence and Tsunami Inundation During the Past 3000 Years at Siletz Bay, Oregon**



## TABLES

**Chapter 1**



**Chapter 2**



**Chapter 3**



## FIGURES

**Chapter 1**

**Chapter 2**



**Chapter 3**

## CHAPTER 1

# SIMPLIFIED EXPLANATION OF THE TSUNAMI HAZARD MAP OF THE SILETZ BAY AREA, LINCOLN COUNTY, OREGON

by

George R. Priest, Oregon Department of Geology and Mineral Industries
António M. Baptista and Ming Qi ,Oregon Graduate Institute of Science and Technology
Curt D. Peterson and Mark E. Darienzo, Portland State University

## EXECUTIVE SUMMARY

This report explains the results of a pilot tsunami hazard mapping project focused on the Siletz Bay area. Tsunami hazard maps were published by the Oregon Department of Geology and Mineral Industries (DOGAMI) at two different scales: an initial, hand-drawn compilation (Open-File Report O-95-6) at 1:4,800 (1 inch = 400 feet) and a final publication (GMS-99) at the 1:12,000 (1 inch = 1,000 feet)-scale. Small-scale illustrations of the mapped inundation are also included in this chapter as Appendix 1.2. The maps depict areas potentially vulnerable to tsunami flooding for three different scenarios:

***Scenario 1:*** Magnitude 8.8[1] subduction zone earthquake; no factor of safety applied; tsunami striking while tide is at mean sea level; 1 m (3 ft) coseismic subsidence (regional subsidence during a great earthquake); **wave height at the open coastal shoreline of approximately 6-8 m (20-25 ft)**; scenario depicts the minimum hazard from a locally generated tsunami.

***Scenario 2:*** Magnitude 8.8 subduction zone earthquake; predicted wave amplitude (one half the crest to trough distance) in 50 m (164 feet ) of water multiplied by 2 (200 percent factor of safety); tsunami striking while tide is at mean higher high water; 1 m (3 ft) coseismic subsidence; **wave height at the open coastal shoreline of approximately 9-11 m (30-35 ft)**; scenario may be viewed as the most probable case. Inundation is identical to that adopted for implementation of Senate Bill 379 (ORS 455.446 and 455.447), limiting construction of essential and special occupancy facilities in tsunami inundation zones.

***Scenario 3.*** Magnitude 8.8 subduction zone earthquake; predicted wave amplitude in 50 m (164 feet ) of water multiplied by 4 (400 percent factor of safety); tsunami striking while tide is at mean higher high water; 0 m of coseismic subsidence; **wave height at the open coastal shoreline of approximately 15-17 m (50-55 ft)**. Scenario simulates the model tsunami used for evacuation planning in northern California hazard maps and may be viewed as an extreme case.

The hazard map can be used to find following risk zones:

***Extreme Risk:*** Elevations **below** the run-up elevation of **Scenario 1**.

***High Risk:*** Elevations **between** the run-up elevation of **Scenarios 1 and 2**.

***Moderate Risk:*** Elevations **between** the run-up elevation of **Scenarios 2 and 3**.

***Low Risk:*** Elevations **between** the run-up elevation of **Scenario 3 and 30 m (100 ft)**.

***Negligible Risk:*** Elevations **above 30 m (100 ft).**

The three scenarios were developed from numerical simulations of Baptista and coworkers to estimate the tsunami flooding from a large subduction zone earthquake immediately offshore of the study area. **Scenario 2** contains a number of correction factors that reflect uncertainties in the modeling technique and tides, whereas **Scenario 1** is free of correction factors. **Scenario 3** approximates the numerical modeling methodology used by the State of California and the National Oceanographic and Atmospheric Administration for a tsunami hazard map of Humbolt Bay and Crescent City in California. While **Scenario 3** simulates flooding from a large subduction zone earthquake, it has

[1] The scenario magnitude is to some extent arbitrary, since earthquakes from M8 to M9 are possible, so the tenth decimal place listing does not imply that we know the scenario magnitude to that precision.

additional factors of safety that account for increases in wave height that may be caused by storm surges, larger uplift or subsidence of the sea floor than estimated here, and submarine landslides.

Peterson and coworkers conducted mapping and hazard analysis of prehistoric tsunami deposits to check the numerical simulations. They also estimated on the basis of buried soils that a maximum of 1 m of coastal subsidence would accompany a great earthquake. This value was used for the numerical simulations of **Scenarios 1 and 2.** The prehistoric tsunami data is most consistent with open coastal run-up on the order of 8-10 m (26-33 ft), decreasing to 3 m (10 ft) or less in areas more than 1.6 km (1 mile) inland. **The prehistoric data is therefore compatible with Scenario 2 run-up elevations at the open coast and Scenario 1 run-up predictions about 1.6 km (1 mile) or more inland.**

The numerical simulations and the evidence from prehistoric tsunami deposits clearly show that **Scenario 1 and 2** tsunamis with open-coastal run-up elevations on the order of 6-11 m (20-35 ft) are possible, and that areas near the banks of estuaries at least 4.0 km (2.5 mi.) inland (the edge of the study area) are at risk from tsunami flooding. **The Scenario 2 run-up elevation (the boundary between the moderate and high risk zones) is probably the most likely case, Scenario 1 and 3** boundaries may be viewed as the potential error about this middle case. Areas above 30 m (100 ft) elevation are above nearly any conceivable earthquake-generated tsunami.

Coastal erosion is likely to result from the sudden subsidence that accompanies great (M 8-9) earthquakes. Most beaches and foredunes on the open coast will be removed over a period of years when the area subsides the predicted 0.5-1 m (2-3 ft), since waves will reach that much higher. Loss of the buffering effect of beaches will make all open coastal shorelines in the study area subject to severe erosion by storm waves.

In the event of a large undersea earthquake in this area, there will be about 15 minutes to evacuate before the flooding from the first wave crest becomes severe; therefore ***if you feel an earthquake with 20 seconds or more of strong ground shaking, head immediately inland or to high ground. A number of waves will come in over a period of several hours, so do not go back to the shoreline until an official "all clear" is issued.*** Strong shaking is enough to make it hard to stand up during the earthquake. These guidelines will eliminate most false alarms, but, ***since tsunamis can in some cases be generated by less felt shaking, local jurisdictions may choose to use more conservative thresholds for evacuation (e.g. any felt earthquake).*** Owing to the generally low seismicity of this area, a lower threshold of shaking could be justified; this is a decision for local authorities.

Owing to unresolved problems with the numerical simulations (see Chapter 2), the flooding lines are not in general recommended for site-specific land use and engineering decisions. However, they are a useful guide to broad areas that may be at risk from tsunami flooding.

## INTRODUCTION

Scientific findings of the last several years have shown that the Oregon coast is vulnerable to shaking and tsunami flooding from great (M 8-9) undersea earthquakes that can occur on the offshore Cascadia subduction zone fault system (Figure 1.1; see Madin, 1992, and Atwater and others, 1995, for summaries). The estimated chance in the next 50 years of a great subduction zone earthquake is between 10 and 20 percent (Peterson and others, 1991; Darienzo and Peterson, 1995). To prepare the State for this threat, the Oregon Department of Geology and Mineral Industries (DOGAMI) solicited support from the Oregon Department of Land Conservation and Development (DLCD) to produce a pilot tsunami hazard map of the Siletz Bay area (Figure 1.2).

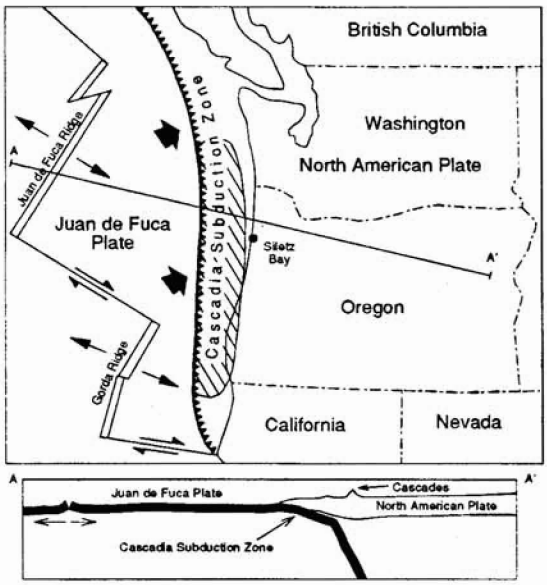


*Figure 1.1. The length of the crosshatched area is the approximate length of the postulated fault rupture for a magnitude 8.8 earthquake on the Cascadia subduction zone. During the earthquake, the shaded area will be thrust upward, creating a series of tsunami waves. Areas east of the shaded area will subside up to 1-2 m. This subsidence will persist for a number of years, causing flooding during high tides and erosion during winter storms. Neither subsidence nor uplift will occur at the eastern edge of the shaded area ("hinge zone" or "zero isobase" between subsidence and uplift).*


*Figure 1.2. Location of the study area and regional geographic place names mentioned in the text*

Undersea earthquakes of magnitude 8-9 will produce tsunamis when the sea floor and overlying ocean is deformed by faulting and submarine landslides. These waves will travel at hundreds of kilometers per hour (kph) in the deep ocean but will rapidly slow as they approach shore. As they slow, the tsunami waves increase in height from as little as a few centimeters in the deep ocean to many meters at the shoreline. When they strike shore, they will still be traveling at speeds greater than one can run and can cause severe loss of life and property.

Tsunamis from distant undersea earthquakes in Alaska and Chile can strike the Oregon coast several hours after the earthquake, giving the Alaska Tsunami Warning Center (ATWC) time to issue warnings. In the Siletz Bay area these tsunamis have statistically predicted run-up elevations (Figure 1.3) of 2.4 m (8 ft) at a recurrence of 100 years and 4.3 m (14 ft) at a recurrence of 500 years (Charland and Priest, 1995 from graphs of Houston and Garcia, 1978). The Alaskan earthquake of 1964, which approximates a 500-year event, caused tsunami waves to run up to elevations of about 4.4 m (15 ft) in this part of the coast (during a high tide), but did no reported damage to the study area (Schatz and others, 1964; Lander and others, 1993). Therefore this report focuses on the much more serious threat from locally generated Cascadia tsunamis.

In contrast to distant earthquakes, a local undersea earthquake on the Cascadia subduction zone could send tsunamis to the Siletz Bay area within minutes, leaving no time for an ATWC warning. Advance emergency evacuation planning aided by an accurate map of the hazardous areas is therefore essential to prepare for prompt response to this event.

This project responds to this need by producing a tsunami hazard map and by exploring methods for mapping this hazard in other coastal communities. Small-scale illustrations of the tsunami hazard map produced for this study are given in Appendix 1.2 (Figures 1.9, 1.10, and 1.11). Published maps were released as DOGAMI maps GMS-99

(1:12,000 scale) and Open-File Report O-95-06 (1:4,800 scale). In addition, a map (DOGAMI Open-File Report O-95-25) at the 1:24,000-scale illustrating tsunami flooding identical to that of this study's middle case, Scenario 2, was produced to implement ORS 455.446 and 455.447. These statutes limit new construction of essential and special occupancy facilities in tsunami inundation zones. A preliminary version of the same 1:24,000-scale map, (included in DOGAMI Open-File Report O-95-68) illustrates tsunami flooding equivalent to this study's lowest and middle case, Scenarios 1 and 2, respectively.

A simplified explanation of the hazard map and mapping methods is given below. An expanded explanation of the numerical simulation technique is given in Chapter 2. Detailed descriptions of the geologic evidence at Siletz Bay for earthquake-induced (coseismic) coastal subsidence and tsunami hazards are given in Chapter 3 and Appendix 1.1. The following discussion explains how tsunami run-up elevation and inundation were estimated for each of three scenario tsunamis. The three hazard scenarios were selected to illustrate the uncertainty of the tsunami flooding predictions, so informed decisions can be made by local government and the public.

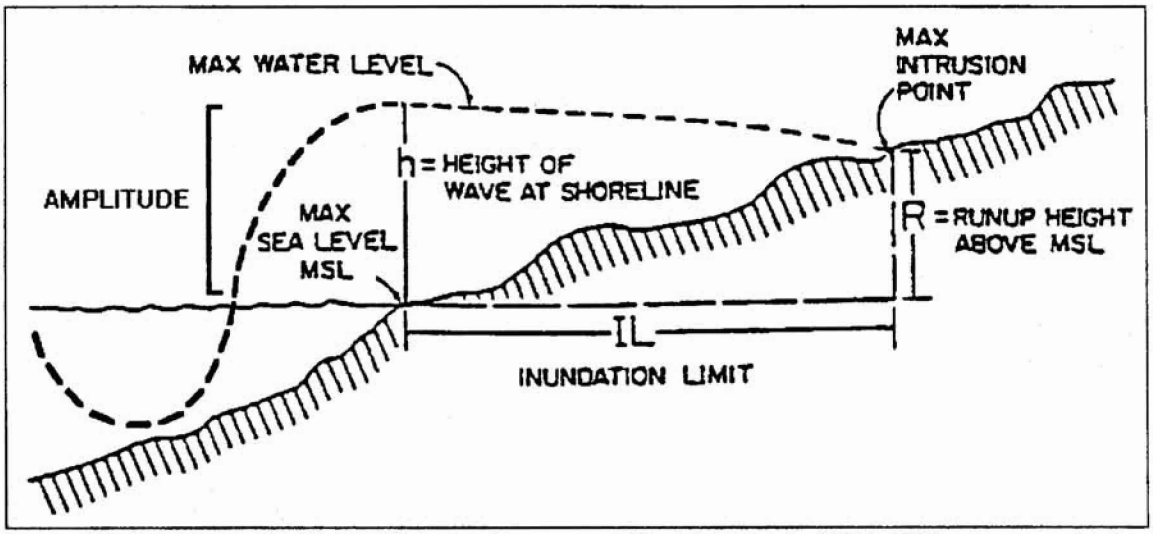


*Figure 1.3. Tsunami amplitude, inundation, and run-up (modified from Curtis, 1991). MSL = mean sea level.*

## METHODS

Tsunami run-up elevations for the three different scenarios (high, medium, and low) were estimated by numerical methods. These methods provide approximate run-up elevations and inundation distances based on an analysis of the first two hours of tsunami waves (see Chapter 2 for a technical discussion). Waves in the first 2-3 hours typically have the highest run-up elevations. See Chapter 2 for detailed explanation of the numerical simulation technique.

The first step in the procedure was to numerically simulate tsunamis generated from theoretical sea floor deformation caused by a magnitude 8.8 subduction zone earthquake. The area bowed upward by such an event is represented approximately by the cross hatched area on Figure 1.1. Landward of the cross hatched area would be a trough of subsidence similar in width to the uplifted area. A cross section across the deformed earth would therefore describe and "S" shape, which is also the initial shape of the overlying sea surface after the earthquake. This initial disturbance of the sea produces numerous waves that strike shorelines though out the Pacific. This regional simulation was used to predict the size and shape of two hours of tsunami waves arriving in the study area at offshore points in 50 m (164 ft) water depth. At that point another computer program did a detailed calculation of the tsunami flooding (inundation) that could be expected from these waves. This inundation program calculated maximum water elevations (run-up) on a rectilinear grid at a spacing of 40 m (131 ft), so actual flooding boundaries had to be extrapolated to the much more detailed topographic data.

Extrapolation of the numerical data was achieved by drawing the inundation boundaries on a 1:4800-scale orthophoto topographic map with 1.5 m (5 ft) elevation contours, inferring the boundary position using professional judgment (see Priest and others, 1994, for a technical discussion of the base map). In each case about 1.2 m (4 ft) was added to the numerically predicted run-up elevation to eliminate underestimation of the flooding hazard caused by uncertainties in the elevation contours. The contours have a vertical precision of ± 0.8 m (2.5 ft). Inspection of the orthophoto maps, which were produced from photos taken at low tide, reveals that the zero elevation isoline (geodetic mean sea level) plots in the wave swash zone at the open coast and near the low water line within the bay. This suggests that local mean sea level may be 0.3-0.4 m (1.0-1.5 ft) higher than geodetic mean sea level; hence, the correction factor.

The three flooding scenarios (Table 1.1) start with the listed wave amplitudes (Figure 1.3) in 50 m (164 ft) of water, running up to the listed elevations when they reach the open coast. A qualitative estimate of the risk zones bounded by each flooding line is listed to simplify interpretation by the public.[2]

*Table 1.1. Summary of tsunami scenarios mapped for this investigation.*

| | Risk Zone Boundary | Tsunami Amplitude3 m (ft) | Open Coastal Run-up Elevation m (ft) | Tidal Level m (ft) Above Mean Sea Level | Coseismic Subsidence m (ft) |
|---|---|---|---|---|---|
| **Scenario 1** | Extreme-High | 2.5 (8) | 6-8 (20-25) | 0 | 1 (3.3) |
| **Scenario 2** | High-Moderate | 5 (16) | 9-11 (30-35) | 1.3 (4) | 1 (3.3) |
| **Scenario 3** | Moderate-Low | 10 (33) | 15-17 (50-55) | 1.3 (4) | 0 |

**Scenario 1** is the numerical simulation without any factors of safety. **Scenario 2** adds the effect of a high tide (about 1.3 m or 4 ft) and a 200 percent factor of safety to the Scenario 1 wave amplitude. The latter factor of safety is justified by (1) uncertainties in the sea floor deformation that causes the tsunami, and (2) the common observation in modern tsunamis that actual wave heights are generally too low by varying amounts relative to the numerically predicted heights (see Chapter 2). Scenario 2 run-up is essentially the same as that used to implement Senate Bill 379 (ORS 455.446 and 455.447), even though the run-up was derived somewhat differently (see Model 2 of Priest, 1995 ). Senate Bill 379 limits construction of essential and special occupancy structures in tsunami inundation zones. **Scenario 3** adds a 400 percent factor of safety to the Scenario 1 wave and assumes high tide, but does not incorporate coseismic subsidence thought to be as much as 1 m (3 ft) from study of prehistoric buried soils in the area (see Chapter 3 for details). The 1 m of coseismic subsidence was eliminated from Scenario 3 so that it could, as closely as possible, match a scenario tsunami used by the State of California for the Humbolt Bay-Crescent City area (Toppozada and others, 1995). This was done to allow our scenarios to be more easily compared with the standard used in California for evacuation planning purposes. The additional factors of safety in Scenario 3 may be justified by the observation that tsunamis can be amplified beyond the model prediction by storm surges, submarine landslides, unusually high tides, or some combination of these factors.

For the purposes of this hazard map, the presence of prehistoric tsunami deposits (Chapter 3) is considered an indication of minimum tsunami inundation. The following observations demonstrate that this assumption is highly conservative of life and property. Alterations in the shape of the bay and spit could have allowed prehistoric tsunamis somewhat better access than at present. For example, the Highway 101 embankment, agricultural dikes, fill, shoreline

---

[2]Additional scenario tsunamis and earthquake sources were extensively investigated by Priest (1995) after the Siletz Bay study was completed. Two of these scenarios, his Model 2 and Model 3, were utilized by Priest (1995) for regional mapping of tsunami inundation on the Oregon coast. The maximum open coastal run-up for Model 3 essentially equals that of Scenario 1 in this study; likewise, Model 2 is similar to Scenario 2. An additional preliminary scenario was investigated by Priest (1995) in order to reconcile differences in Models 2 and 3. This scenario, though somewhat crude, probably represents the best time history of wave arrivals and was used in construction of the time history figure, Figure 1.5, below.

[3]Amplitude is at an offshore point at 50 m (164 ft) water depth.

protection structures, and accelerated growth and stabilization of dunes by the introduction of European beach grass, no doubt offer less access for tsunami flooding than in prehistoric times. Therefore future tsunamis will likely not reach as far inland as the prehistoric ones.

Flooding from all scenario tsunamis covered all known tsunami sand deposits, but in some cases the lowest simulated run-up, Scenario 1, did not wet flooding paths to these deposits predicted from analysis of the mineralogy of the tsunami sands (see Chapter 3). In each case a judgment was made which was as conservative of life and property as possible without seriously compromising the integrity of the numerical simulation. In general, if the elevation at the flooding path predicted from prehistoric tsunami sands was less than 1 m above the model run-up elevation, then the path was assumed to be flooded. Predicted flooding paths blocked by barriers 1 m or more higher than the model run-up were assumed not to be flooded. In all cases where the flooding paths were blocked by barriers higher than 1 m, it was obvious that the barriers had been modified from their prehistoric condition by such factors as artificial fill, rip rap, and the dune growth caused by European beach grass.

Lack of tsunami sand deposits was not considered evidence that no tsunami flooding occurred. The most easily recognized tsunami sands are those that lie atop buried marsh soils, but the prehistoric record from buried soils is fragmentary. Erosion by laterally migrating tidal and river channels can remove buried soils and tsunami sands. Buried marsh soils may not exist at all, if a marsh was not growing prior to coseismic subsidence. If coseismic subsidence is not large enough to put the soil down to intertidal or tidal levels where deposition of muds can occur, it may not be buried; then surface erosion by rain and wind can remove the tsunami sand. Even if the buried soil is well preserved, lack of a capping tsunami sand may indicate only that a sand source was not available, or that the tsunami lost sand as it slowed down and crossed vegetated areas. Multiple tsunami surges can also erode away previous deposits.

No area below 3 m (10 ft) elevation was considered safe, if it was adjacent to zones of predicted tsunami flooding. All areas below this elevation are generally in or very close to a wetland condition and will be even more likely to be flooded after coseismic subsidence.

## HOW REASONABLE ARE THE ESTIMATED RUN-UP ELEVATIONS?

## EVIDENCE FROM PREHISTORIC TSUNAMIS

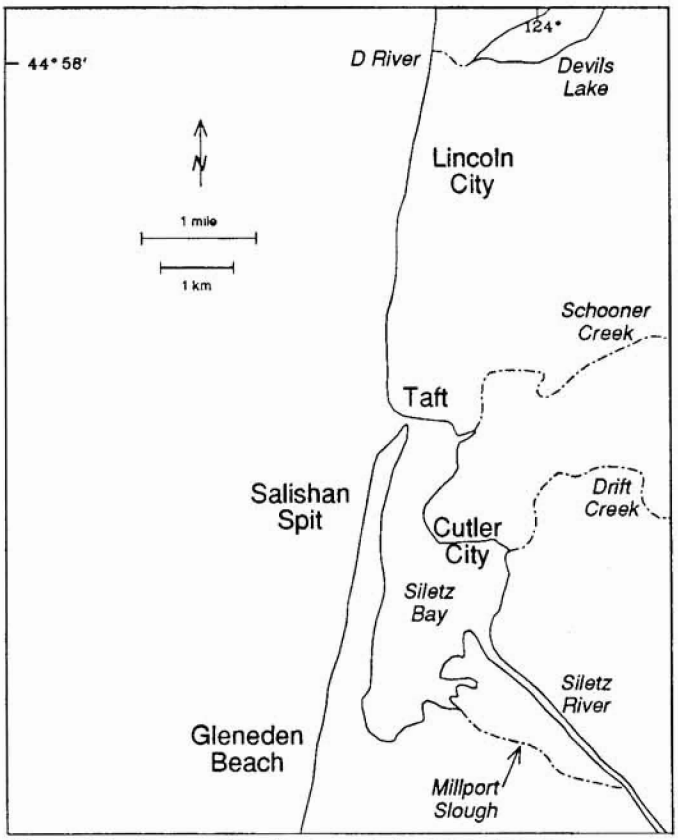


*Figure 1.4. Geographic place names in the study area..*

Salishan Spit (Figure 1.4) was a barrier to prehistoric tsunamis, offering an opportunity to estimate open coastal run-up height from the distribution of prehistoric tsunami sands immediately behind the spit. Sands deposited by tsunamis striking about 300 and 800 years ago were not deposited behind parts of the spit presently about 10-12 m (33-39 ft) above mean sea level. The actual heights of these same high spots 300-800 years ago could have been as low as 5-7 m (16-21 ft) within the uncertainties of the data (See Chapter 3 and Appendix 1.1 for detailed discussions). Assuming that the current topography of Salishan Spit is representative of times past, it is apparent that low spots on the order of 6-8 m (20-26 ft) were conduits for prehistoric tsunamis, and barriers over about 10-12 m (33-39 ft) stopped prehistoric tsunamis. Hence, the most likely open coastal run-up is on the order of 7-9 m (23-30 ft), although the uncertainties in the data cannot rule out prehistoric tsunamis as low as 5 m (16 ft) or as high as 12 m (39 ft)-(see Chapter 3 and Appendix 1.1).

Even higher tsunamis probably struck the coast in prehistoric times. The tsunami that flooded the Oregon coast about 1400 years ago may well have been higher than either the 300 or 800 yr. events (see arguments in Chapter 3). Many of these great prehistoric earthquakes have triggered submarine landslides (Adams, 1990), and landslides have been mapped on the continental slope, particularly in southern Oregon and northern California (Chris Goldfinger, 1995, personal communication). For example, a 12 km-wide landslide mass was mapped at the toe of the continental slope west of Florence (Goldfinger and others, 1992). Such landslides could have increased wave heights significantly. Unusually severe storms can force tidal levels to 1-2 m higher than normal. Any of these factors, singly or in combination, could increase tsunami run-up height beyond predictions from modeling or the prehistoric record. How much higher could the tsunamis be? The answer awaits further numerical simulation of the effect of these factors, particularly submarine landslides, but maximum run-up on the order of 16 m (50 feet),[4] the approximate value for Scenario 3, may be possible.

## EVIDENCE FROM HISTORICAL TSUNAMIS

In the Pacific Basin magnitude 8-9 earthquakes are capable of producing tsunamis with maximum run-up heights on the order of 2-30 m (6-100 ft), averaging about 9 ± 7 m (28 ± 22 ft)[5] near the epicenters (calculations on data of

---

[4]This value is derived from the average Pacific Basin run-up of 9 m plus the estimated error (one standard deviation about the mean) of 7 m (see the section on historical tsunamis).

[5]This mean was calculated from the maximum run-up elevations listed in the table of Lockridge and Smith (1984) for each of the thrust-type magnitude 8-9 earthquakes that occurred on subduction zone fault systems of the Pacific Basin. This is the faulting thought to occur on the Cascadia subduction zone. Since the type of fault mechanism was

Lockridge and Smith, 1984). Two recent earthquakes demonstrate that even those smaller than magnitude 8 can generate significant tsunamis. The magnitude 7.8 Hokkaido Nansei-Oki earthquake of 1993 produced run-up heights on the order of 6-30 m (15 to 100 ft) in areas 48-80 km (30-50 mi.) from the epicenter (Bernard and Gonzalez, 1993; run-up surveys of the Hokkaido event by G. R. Priest, A. M. Baptista, and Y. Tanioka, 1993). The 1992 magnitude 7.6 earthquake in Nicaragua produced run-up as high as 9 m (30 ft) on nearby shorelines (Baptista and others, 1993). Because of unusual characteristics of the faulting that caused this earthquake, it had very little felt shaking at the coast, so the residents had little warning.

Satake and others (1996) concluded that the 2-3 m (7-10 ft) tsunami that caused extensive damage to the Japanese Islands the morning of January 27, 1700 was possibly caused by a magnitude 9 undersea earthquake on the Cascadia subduction zone. If the conclusions of this paper are correct, then this was none other than the 300 yr. event recorded in the marshes of Siletz Bay. Although this was prehistoric to Oregon, it was very much historic to the Japanese. If the maximum run-up was 3 m (10 ft) after the tsunami traveled to Japan across thousands of kilometers of the Pacific, one can speculate that the AD 1700 waves must have reached considerably higher elevations on the Oregon coast.

## CONCLUSION

The scenario tsunamis chosen here accord well with Pacific Basin records of open coastal tsunami run-up. Scenario 2, which matches the upper limit of the prehistoric evidence for a maximum wave, is very close to the average maximum tsunami run-up elevation for the Pacific Basin. Likewise, Scenarios 1 and 3 have open coastal run-up elevations within one standard deviation above and below the mean of the Pacific Basin data. All three scenarios produce run-ups in excess of 3 m (10 ft), the maximum run-up in the Japanese islands from the AD 1700 event. While extreme in terms of the prehistoric record, a Scenario 3 tsunami with run-up elevations on the order of 16 m (50 feet) may be possible within the uncertainties caused by tides, storm surges, and submarine landslides.

## HOW REASONABLE ARE THE ESTIMATES OF INUNDATION?

Based on the distribution of tsunami sands, mainly from the last two prehistoric tsunamis, it is apparent that these two events flooded areas immediately adjacent to tidal channels and estuaries but lacked the energy (or the sand sources) to carry sands more than a few hundred meters away from the channels in the eastern part of the study area (Figure 1.7 of Appendix 1.1; Chapter 3). A soil buried as a result of coseismic subsidence during the last event lies beneath the marsh immediately east of Cutler City but lacks a tsunami sand cap or even organic debris typically washed in by tsunami waves(see core site 32 on Figure 1.7 of Appendix 1.1 and Figure 1.10 of Appendix 1.2; see also Chapter 3). Hence, it is possible that much of the area now occupied by Cutler City was not overtopped by the last prehistoric tsunami, effectively shielding this core site from flooding (see Chapter 3 for detailed discussion). These observations suggest that the prehistoric tsunamis quickly lost their strength as they traveled inland, failing to reach elevations over about 3 m (10 ft) 1.6 km (1 mile) inland. However, as discussed above, non-deposition of tsunami sand does not prove that an area was not flooded, and some tsunamis older than the last two may have been larger. In any case, this pattern of rapidly decreasing flooding potential inland is best reproduced by the numerical simulation of Scenario 1, although even that simulation puts core site 32 and some parts of Cutler City under water (Figure 1.10 of Appendix 1.2).

Relative to the run-up implied by the prehistoric record and by the experience of many who study tsunamis, Scenario 2 and 3 simulations appear to predict run-up that is somewhat high in areas 1.6 km (1 mile) or more inland. For example, Paul Whitmore of the Alaska Tsunami Warning Center wrote the following in a 1995 review comment for this paper:

---

listed in Lockridge and Smith (1984), a judgement was made regarding a thrust-type subduction zone source based on the regional geology of the area and the tsunami height If a negligible near-field tsunami was generated from a magnitude 8-9 event, it is unlikely to be a thrust mechanism. Where a range was listed, the highest value was used. The ±7 m (±22 ft) error is the one sigma error (68 percent confidence), assuming a normal Guassian probability distribution.

> "Here at the Tsunami Warning Center we have a rule-of-thumb that areas a mile or more from the open water have low tsunami danger. Historically, areas this far away from open water have only experienced small bores traveling up river, which only affect those on the river or its banks."

These observations are in accord with the inundation predicted by Scenario 1 and implied by the prehistoric tsunami sand data. This conclusion does not, however, prove that the open coastal run-up elevations for Scenarios 2 and 3 are unrealistic, only that the numerically predicted run-up elevations in the most inland (eastern) parts of the study area are somewhat high. This may be caused by assuming bottom friction that is too low, not assuming a bore-type tsunami, or using a wave with a period that is too long. Whatever the cause, use of the inundation lines for Scenarios 2 and 3 for evacuation planning in the eastern part of the study area adds an additional factor of safety.

## WHAT WILL THE SCENARIO TSUNAMIS DO TO THE SILETZ BAY AREA?

### GENERAL OBSERVATIONS

All of the scenario tsunamis will produce a number of waves, the first striking the coast within minutes of the earthquake (Figure 1.5), therefore, ***if you feel an earthquake with 20 seconds or more of strong ground shaking, head immediately inland or to high ground***. Strong shaking means that it is generally hard to stand up during the earthquake. The 20 seconds or more of shaking is typical of great undersea earthquakes that can generate big tsunamis. To get a feel for this, try shaking a chair with a family member in it for 20 seconds. Using both criteria should eliminate most false alarms. As demonstrated by the 1992 Nicaraguan earthquake, ***big tsunamis can be produced from lesser amounts of shaking, so local jurisdictions may choose to evacuate for any felt earthquake***. Check with your city or county emergency managers for local guidelines. Since the Siletz Bay area has had very little historical earthquake activity, it is unlikely that evacuating for lesser amounts of shaking would generate an undue number of "false alarms."

All of the scenario tsunamis will flood some populated areas with currents strong enough to do damage and cause loss of life. It is beyond the scope of this report to predict tsunami damage, but it is likely that single story wood frame structures, mobile homes, and light weight steel frame buildings are highly susceptible (Toppozada and others, 1995). Just about any building can be damaged by logs or cars swept against it.

The combination of shaking and tsunami flooding will do substantial damage to utilities, water front facilities, and transportation routes. Expect disruptions for several days or weeks. The following description of the aftermath of the magnitude 9.2 Alaskan earthquake that struck Seward, Alaska, in 1964 was used by Toppozada and others (1995) to give some sense of the disruption to electric power service:

> "Some storage tanks at the Standard Oil tank farm broke open during the earthquake and oil ignited. The nearby building, housing the standby generators, burned, and all the equipment was destroyed. The 69-kV transmission line across the freshwater lagoon was demolished. Power poles and spans of conductors were destroyed in the old town site by slides, destruction of the dock, movement or destruction of buildings, and by waves. The only electric service available after the earthquake was from an emergency generator that provided a limited amount of power at the hospital" (National Academy of Science, 1973).

Figure 1.5 illustrates the possible patterns of surge and withdrawal of water for the first 8 hours. Note that the waves arriving 2-2.5 hours after the earthquake may be nearly as high as the first. Similar but smaller changes of water level will continue for 8-10 hours after the earthquake, so ***do not return to low lying areas after the first tsunami wave. Wait until an official "all clear" is issued***.

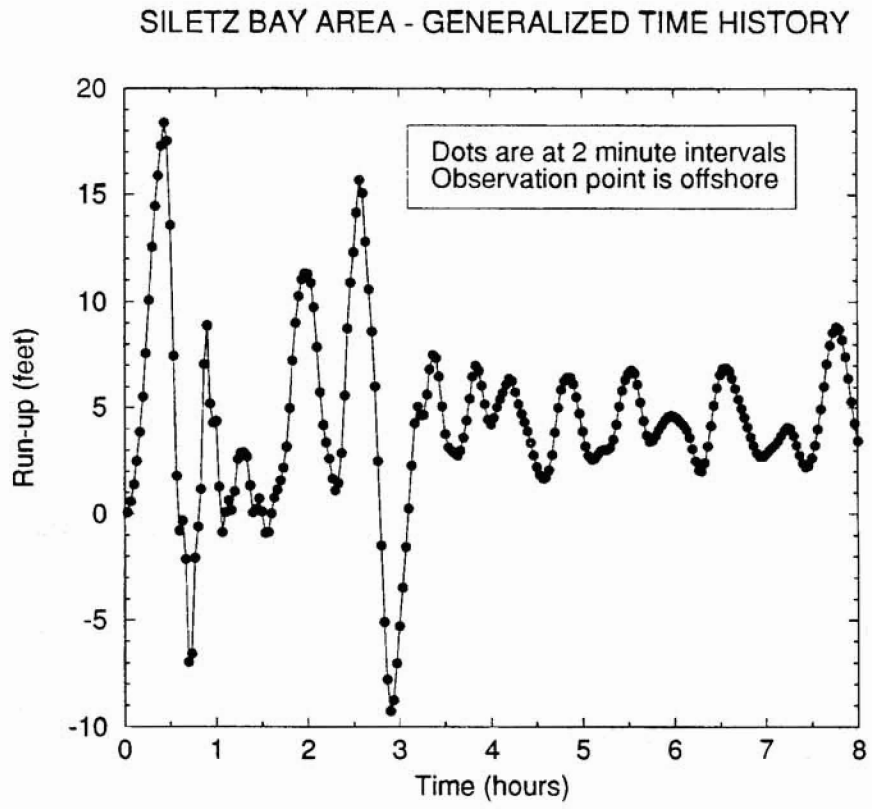


*Figure 1.5. Time history for tsunami run-up at a point immediately offshore of the Taft area. Because the point is offshore, the vertical axis does not directly predict run-up elevation at the shoreline. The figure is given to show the general pattern of wave activity, not absolute run-up elevation. Taken from a preliminary simulation by Priest (1995) using earthquake-induced bottom deformation inferred from data of Hyndman and Wang (1993).*

To visualize the meaning of Figure 1.5, imagine standing at the open shore after the earthquake and seeing the water immediately start to rise. Sea level would continue to rise at an accelerating rate, finally reaching the maximum run-up after 24 minutes. The tsunami could come in as a surge like a rapidly rising tide or as a breaking wave, depending on local conditions. Normal wind waves will produce a complex, "choppy" surface on the tsunamis, so evacuation should be well above the estimated run-up line, if possible. Tsunami waves nearly as high as the first one will continue to strike in the following 2 hours. Smaller oscillations of sea level will continue for at least the following 6-8 hours, making it risky to be near the water's edge. Hence the entire tsunami event will last for at least 8-10 hours, not counting any tsunamis caused by aftershocks.

## SCENARIO 1

A Scenario 1 tsunami will run up to elevations of 6-8 m (20-25 ft) at the open coast, decreasing to 3.7-4.6 m (12-15 ft) in Taft and 3 m (10 ft) or less south of Taft. This will flood the low lying areas of Taft, parts of Cutler City, and the D

River but will not overtop most of Salishan Spit. However, the lowest beach front homes on the spit could be damaged. The Taft area immediately adjacent to the mouth of the bay and along Schooner Creek will be heavily damaged. The tsunami will likely do little damage to the southern end of Siletz Bay, Devils Lake, or the eastern edge of the study area, except immediately adjacent to tidal channels and marshes. Bluffed areas like Gleneden Beach and Lincoln City will escape nearly unscathed. Severe currents in and around the main tidal channels will cause damage to docks and boats. People remaining at low elevations, especially on the beaches, could be swept out to sea.

## SCENARIO 2

A Scenario 2 tsunami will run up to elevations of 9-11 m (30-35 ft) at the open coast, 6-8 m (20-25 ft) in Taft and Cutler City, and generally about 3.7-4.6 m (12-15 ft) throughout most of the eastern part of the study area. This will flood low lying areas of Taft, all of Cutler City, and will overtop much of Salishan Spit, washing houses and sand into Siletz Bay. The D River area will be severely impacted. Devils Lake developments along the shoreline could get significant flooding. Most bluffed areas of Lincoln City and Gleneden Beach will escape damage, except in a few drainages that cut into the bluffs. The highest parts of Salishan Spit will be reasonably safe, especially those areas that are high and back from the open shore. Interdune lagoons will offer important protection to these back dune areas by storing and funneling water to either side. Currents much more severe than those of Scenario 1 will do damage in low lying areas throughout the study area, washing away or severely damaging all but the sturdiest structures in the flooding zone. Substantial erosion of Salishan Spit will occur, damaging roads and shoreline protection structures. Siletz Bay, roads, and local beaches will be cluttered with debris from the extensive destruction.

## SCENARIO 3

A Scenario 3 tsunami will run up to elevations of 15-17 m (50-55 ft) at the open coast, 12-14 m (40-45 ft) in Taft and Cutler City, and about 9 m (30 ft) in the eastern part of the study area. This will flood low lying areas of Taft, all of Cutler City, and will overtop nearly all of Salishan Spit. Only a few small knolls in the central spit will remain above the waves. Structures on the spit could be almost totally destroyed, and severe erosion of the spit will occur from the intense currents, damaging shoreline protection structures and roads. Extremely heavy damage can be expected at the D River and significant flooding will occur throughout Devils Lake. Even the lower parts of the bluffed areas in Lincoln City and Gleneden Beach will be inundated and heavily damaged in this scenario. Debris piled up on roads will likely make many impassable.

# WHAT DOES COSEISMIC SUBSIDENCE DO TO THE AREA?

Regional coseismic subsidence of the coastline will persist for many years and will cause high tides to be 0.5-1 m (2-3 ft) higher, flooding areas that are currently beyond the reach of these tides. Hence many shoreline developments around Siletz Bay will find themselves flooded, especially during unusually high spring tides and storm surges. Ecosystems that currently thrive on high marshes could be destroyed by intertidal environments and associated animals and vegetation. Areas presently at intertidal levels will be below most tides.

Floods from the Siletz River and adjoining drainage systems will be capable of reaching elevations as much as 1 m higher in the estuary. Of most concern will be unusually high (100-year or 500-year) floods which could be 1 m higher in the estuary than would be predicted from current flood hazard maps produced by the Federal Emergency Management Agency (FEMA). FEMA flood insurance maps will have to be revised.

As explained in Chapter 3, a rise in sea level caused by subsidence could remove the sand from all of the bluffed open-coastal beaches, allowing storm waves free access to the soft sediments which form the sea cliffs. This situation will probably persist for a number of years or even decades, greatly accelerating erosion of the entire shoreline. Indeed, the developed bluffs face far more threat from erosion than from tsunami flooding. The rate of post-earthquake bluff erosion is not known, but it will greatly exceed the current rates, which vary between 9 cm/yr. (0.3 ft/yr.) at Lincoln City to 18 cm/yr. (0.6 ft/yr.) at Gleneden Beach (Priest and others, 1994). Winter storms during a single year have caused up to 9 m (30 ft) of local sea cliffs at Gleneden Beach to fall into the sea when the buffering beach sand was removed (Priest and others, 1993). Episodes of this kind will become much more common after coseismic subsidence.

The dune-backed beaches like Salishan Spit will be particularly vulnerable to this invigorated wave erosion, especially where not cored by the previously mentioned older soil and underlying semi-consolidated sediments. It might well be

worth mapping this older resistant core to better evaluate where erosion will be slowed. Areas that probably lack the resistant deposits are the Salishan golf course at its lowest elevations and the western margin and north end of Salishan Spit, where dunes are generally lower than 8-9 m (20-25 ft).

Shoreline protection structures will offer a measure of short term protection for both bluff- and dune-backed shorelines, but the relentless attack of the sea may cause these structures to fail unless continually repaired. This is a particular concern for the Salishan development at Salishan Spit. Whereas the developed spit is largely armored with rip rap, if this were to fail, a seaway could open up in the vicinity of the golf course, cutting off road access to the spit.

## HOW SHOULD THE HAZARD MAP BE USED?

The hazard map is intended primarily for tsunami evacuation planning. In reality there is a continuum of hazard from lower elevations close to the open shore to higher elevations inland, so going inland and uphill is always the best strategy. Users should view the scenario run-up elevations as boundaries between the following risk zones:

***Extreme Risk***: Elevations below the run-up elevation of Scenario 1.

***High Risk***: Elevations between the run-up elevations of Scenarios 1 and 2.

***Moderate Risk***: Elevations between the run-up elevations of Scenarios 2 and 3.

***Low Risk***: Elevations between the run-up elevations of Scenario 3 and 30 m (100 ft).

***Negligible Risk***: Elevations above 30 m (100 ft).

Tsunami warning signs (Figure 1.6) should be posted at strategic points in the highest risk zones to warn and educate visitors and residents about the hazard. Evacuation routes should be clearly marked with signs (Figure 1.6). Contact the Oregon Department of Transportation to obtain these official state signs.


*Figure 1.6. Official tsunami evacuation and warning signs for the State of Oregon.*

The tsunami hazard map should be used in conjunction with companion maps of Wang and Priest (1995) depicting earthquake hazards from liquefaction (formation of quick sand during shaking), amplification of shaking, and slope instability (landslides and slumps). Hence, an evacuation planner should make sure that planned escape routes are not compromised by one of these other hazards. For example, bridges on liquefiable soil and roads next to unstable slopes may not be appropriate for safe evacuation.

The map should not be used to set insurance rates or for site-specific land use planning. It may, however, serve as a general guideline for regional planning. For example, when looking for general areas appropriate for schools, hospitals, and emergency response facilities, it would be wise to avoid the highest risk zones, if at all possible. The inundation boundary for Scenario 2 is the same inundation boundary utilized to implement ORS 455.446 and 455.447, limiting construction of these and other essential and special occupancy facilities in tsunami inundation zones.

## ACKNOWLEDGMENTS

Support for the project was provided in part from the Oregon Coastal Management Program, Oregon Department of Land Conservation and Development, from funds provided by the Oregon Legislature, U.S. Department of Commerce National Oceanographic and Atmospheric Administration office of Coastal Resource Management under Section 306 Coastal Zone Management grants, and Section 309 Program Enhancement grants. The project was also funded from State lottery, State General Fund, donated in-kind support from the Oregon Graduate Institute of Science & Technology, and the Sea Grant College program under grant number NA36RG0451.R/CP-78. Reviews were provided by Dennis Olmstead, John D. Beaulieu, and Donald A. Hull of DOGAMI, James N. Hawley of Lincoln County Emergency Management, John J. Marra of Shoreland Solutions, Paul M. Whitmore of the Alaska Tsunami Warning Center, Charles L. Mader of the Mader Consulting Company, and Brian F. Atwater of the U.S. Geological Survey. All of their suggestions are greatly appreciated.

## REFERENCES

Adams, J., 1990, Paleoseismicity of the Cascadia subduction zone: evidence from turbidites off the Oregon-Washington margin: Tectonics, v. 9, p.569-583

Atwater, B.F., Nelson, A.R., Clague, J.J., Carver, G.A., Yamaguchi, D.K., Bobrowsky, P.T., Bourgeois, J., Darienzo, M.E., Grant, W.C., Hemphill-Haley, E., Kelsey, H.M., Jacoby, G.C., Nishenko, S.P., Palmer, S.P., Peterson, C.D., and Reinhart, M.A., 1995, Summary of coastal geologic evidence for past great earthquakes at the Cascadia subduction zone: Earthquake Spectra, v. 11, no. 1, p. 1-18.

Baptista, A.M., Priest G.R., and Murty T.S., 1993, Field Survey of the 1992 Nicaragua tsunami: Marine Geodesy, v. 16, no. 2, p.169-203.

Bernard, E.N., and Gonzalez, F.I., 1993, Tsunami run-up distribution generated by the July 12, 1993, Hokkaido Nansei-Oki earthquake: Tsunami Newsletter, December issue, p. 3-8.

Charland, J.W., and Priest, G.R., 1995, Inventory of critical and essential facilities vulnerable to earthquake or tsunami hazards on the Oregon coast: Oregon Department of Geology and Mineral Industries, Open-File Report O-95-2, 52 p.

Curtis, G.D., 1991, Final report: Hawaii tsunami inundation/evacuation map project: Joint Institute for Marine and Atmospheric Research, Contribution No. 91-237, 29 p.

Darienzo, M.E., 1991, Late Holocene paleoseismicity along the northern Oregon coast: unpublished Ph.D. Thesis, Portland State University, 168 p.

Darienzo, M.E., and Peterson, C.D., 1995, Magnitude and frequency of subduction-zone earthquakes along the northern Oregon coast in the past 3,000 years: Oregon Geology, v. 57, no. 1, p. 3-12.

Houston, J.R., and Garcia, A.W., 1978, Type 16 flood insurance study: tsunami predictions for the West Coast of the continental United States: P.O. Box 631, Vicksburg, Miss., U.S. Army Engineer Waterways Experiment Station, Hydraulics Laboratory, Technical Report H-78-26, 38 p.

Hyndman, R.D., and Wang, K., 1993, Thermal constraints on the zone of a major thrust earthquake failure: the Cascadia subduction zone: Journal of Geophysical research, v. 98, no. b2, p. 2039-2060.

Lander, J.F., Lockridge, P.A., and Kozuch, M.J., 1993, Tsunamis affecting the west coast of the United States: Department of Commerce, National Oceanic and Atmospheric Administration (NOAA), Documentation No. 29, 242 p.

Lockridge, P.A., and Smith, R.H., 1984, Tsunamis in the Pacific Basin, 1900-1983: Boulder, Colorado, National Oceanographic and Atmospheric Administration, National Geophysical Data Center and World Data Center A for Solid Earth Geophysics, 1:7,720,000 scale map.

Madin, I., 1992, Seismic hazards on the Oregon coast, *in* Good, J.W. and Ridlington, S.S., eds., Coastal natural hazards science, engineering, and public policy: Oregon Sea Grant, No. ORESU-B-92-001, p. 3-27.

National Academy of Science, 1973, The Great Alaska Earthquake of 1964: National Academy of Science, Engineering Volume, Washington, D.C.

Peterson, C.D., Darienzo, M.E., and Clough, C., 1991, Recurrence intervals of coseismic subsidence events in northern Oregon bays of the Cascadian margin: Final technical progress report to Oregon Department of Geology and Mineral Industries, 14 p.

Priest, G.R., 1995, Explanation of mapping methods and use of the tsunami hazard maps of the Oregon coast: Oregon Department of Geology and Mineral Industries, Open-File Report O-95-67.

Priest, G.R., Saul, I., and Diebenow, J., 1993, Pilot erosion rate data study of the central Oregon coast, Lincoln County: Oregon Department of Geology and Mineral Industries, Open-File Report 0-93-10, 228 p.

Priest, G.R., Saul, I., and Diebenow, J., 1994, Explanation of chronic geologic hazard maps and erosion rate database, coastal Lincoln County, Oregon: Salmon River to Seal Rocks: Oregon Department of Geology and Mineral Industries, Open-File Report O-94-11, 45 p.

Satake, K., Shimazaki, K., Tsuji, Y., and Ueda, K., 1996, Time and size of a giant earthquake in Cascadia inferred from Japanese tsunami records of January 1700: Nature v. 379, p. 246-249.

Schatz, C.E., Curl, H.C., Jr., and Burt, W.V., 1964, Tsunamis on the Oregon coast: Oregon Department of Geology and Mineral Industries, Ore Bin, v. 26, no. 12, p. 231-232.

Toppozada, T., Borchardt, G., Haydon, W., Petersen, M., Olson, R., Lagorio, H., and Anvik, T., 1995, Planning scenario in Humbolt and Del Norte Counties, California, for a great earthquake on the Cascadia subduction zone: California Division of Mines and Geology, Special Publication 115, 157 p.

Wang, Y., and Priest, G.R., 1995, Relative earthquake hazard maps of the Siletz Bay area, coastal Lincoln County, Oregon: Oregon Department of Geology and Mineral Industries GMS-93, 3 1:12,000 scale maps and text.

## APPENDIX 1.1 - PREHISTORIC TSUNAMI RUN-UP: EVIDENCE FROM SALISHAN SPIT


## SUMMARY

Sands from the last two prehistoric tsunamis are well developed landward of low passes in Salishan Spit with present elevations between 6 and 8 m (20-27 ft) (see discussion in Chapter 2). Prehistoric tsunami sands deposited about 300 and about 800 years before present (B.P.) are absent on buried soils in marshes behind dunes 9-23 m (30-74 ft) high (Figure 1.7, core sites 14, 15 and 16; see Appendix 1.2 for more detailed locations). The real question is how high were these dune barriers 300 and 800 years ago. The following discussion shows that run-up from these two tsunamis may have been between 5 and 12 m (16-39 ft) within the uncertainties of the data. If the present is the key to past, and one assumes that the 6-8 m passes were overtopped by at least 1 m, then the most credible open coastal tsunami run-up is about 7-9 m (23-30 ft).


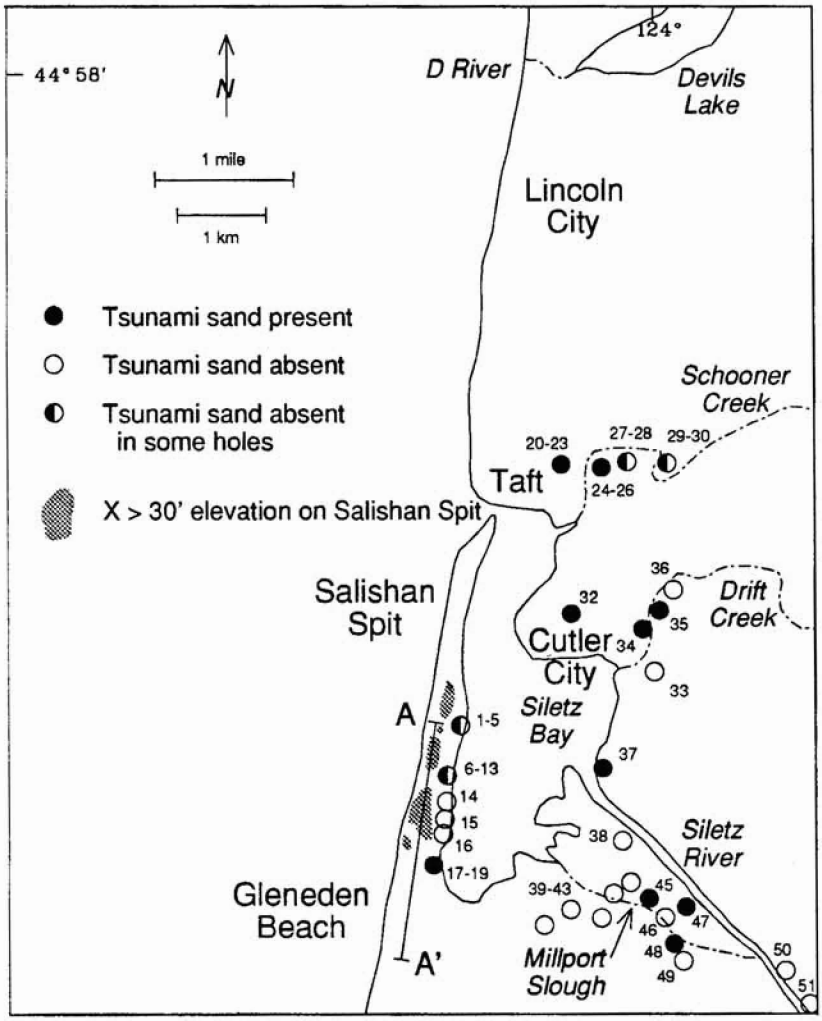


*Figure 1.7. Map of the study area showing the location of coring sites where marsh soils buried after coseismic subsidence were found. These coseismic subsidence events occurred during one or more of 7 earthquakes that struck during the last 2,800 years (see Chapter 3). As indicated, some core sites have prehistoric tsunami sands on one or more of the buried soils (see Appendix 1.2 and Chapter 3 for additional detail). A-A' is the location of the cross section of Figure 1.8. As explained in Figure 1.8 and in the text, a barrier west of sites 14, 15, and 16 (stippled area) prevented deposition of tsunami sand at those sites when earthquakes struck about 300 and 800 years ago (older records were destroyed by erosion). Sites 17, 18, and 19 have well developed tsunami sands derived from dunes and beach sand to the west, so dunes west of these sites were overtopped by tsunamis 300 and 800 years ago.*

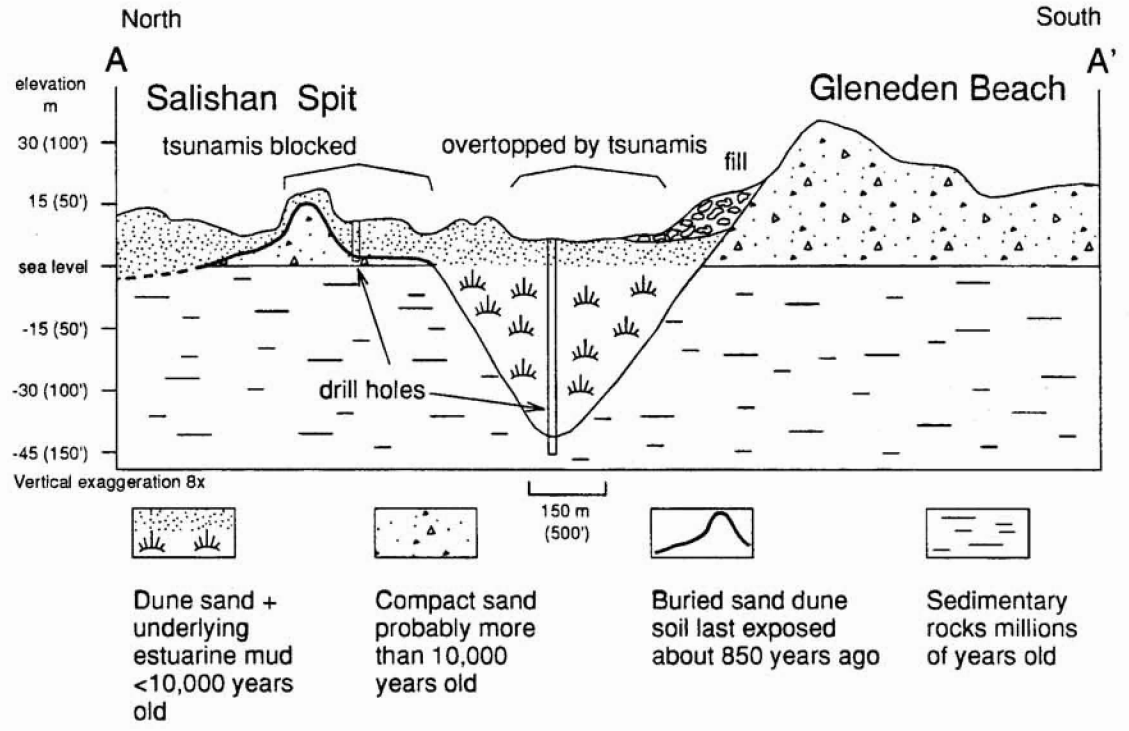


*Figure 1.8. Vertical cross section along line A-A' of Figure 1.7. Topography is the maximum elevation of the spit and bluff projected into the cross section. The soil carbon 14 dated at 850 years is located within a dune barrier that stopped prehistoric tsunamis. The area lacking the soil and the underlying semi-consolidated marine terrace sands was overtopped by prehistoric tsunamis. See the text and Figure 1.7 for further explanation.*

## EVIDENCE

The high dunes on Salishan Spit that apparently blocked prehistoric tsunamis (see distribution of tsunami sands in Figure 1.7; Peterson and others, Chapter 2) have at their core a black, organic-rich A-horizon soil carbon-14 dated at about 850 ± 60 radiocarbon years B.P. (Figure 1.8). This soil is developed on a brick red B horizon soil strongly cemented with iron oxide down to 1 m (3 ft) depth. The depth of weathering in this B-horizon soil indicates that it is likely tens of thousands of years old (Frank Reckendorf, personal communication, 1994,), so the carbon 14 age of the A horizon reflects the last time that the soil was exposed to the air, not the maximum age of the underlying sands. This soil lies at elevations as low as 4-5 m (13-15 ft) in the lowest of these high dunes, so this height plus 1-2 m (3-6 ft) to account for global sea level rise and uncertainty in tides is the minimum ancient barrier that stopped prehistoric tsunamis. Hence, the last two prehistoric tsunamis could have been lower than about 5 m (16 ft).

A prehistoric Cascadia tsunami run-up lower than 5 m is unlikely, because this height is similar to the run-up elevation inferred for distant tsunamis. A local Cascadia event should produce much higher waves than a distant earthquake; given experience world wide and the modeling results of Baptista and others (Chapter 2).[6] For example, assuming a most probable tide, the run-up from distant tsunamis at the open coast would be 2-4 m (7-13 ft) for a 100-500 year recurrence, respectively, according to Houston and Garcia (1978). If tsunamis arrived at mean higher high water, run-up would be on the order of 3-5 m. The Houston and Garcia (1978) estimate is verified by the 1964 Alaskan tsunami, which, had it arrived at a mean tide, would have had a run-up of about 3 m (10 ft) at the open coast; the actual run-up was at high tide, so it was about 4 m (Schatz and others, 1964; Lander and others, 1993), and, unlike the Cascadia events, it left no sedimentary record in Siletz Bay marshes (Curt D. Peterson, 1995, personal communication; Darienzo, 1991).

[6]This has been verified by more recent modeling of earthquake sources and derivative tsunamis by Priest (1995).

Regarding the maximum barrier height that blocked prehistoric tsunamis, any dune sand mantling the A-horizon marker soil would raise the estimated height of the barrier that stopped ancient tsunamis. Mantling sand was probably present, at least at the time of the 300 yr. B.P. tsunami, since the radiocarbon "clock" was started by burial approximately 800-900 years ago. European beach grass now present on the dunes is more efficient at stabilizing and growing dunes than the native beach grass that was available 300 years ago, so the maximum ancient barrier height in the lowest of the dune barriers is likely the present height of 9-10 m (30-33 ft) plus the 1-2 m (3-6 ft) of uncertainty for sea level. Therefore the last prehistoric tsunami could have been as high as about 12 m (39 ft) and still have been blocked at the places predicted by tsunami sediment distribution, assuming it came in on a low tide and that global sea level was about 0.5 m (1.8 ft) lower 300 years ago.

## APPENDIX 1.2 -SMALL-SCALE TSUNAMI INUNDATION MAPS SHOWING CORE SAMPLE SITES

Figures 1.9 , 1.10, and 1.11 are, respectively, small-scale illustrations of the north, central, and southern parts of the tsunami hazard map of GMS-99. These maps also show the location of the core samples taken to study prehistoric tsunami deposits and prehistoric soils buried as a result of coseismic subsidence (see Appendix 1.1 and Chapter 3 for discussions of the core data).

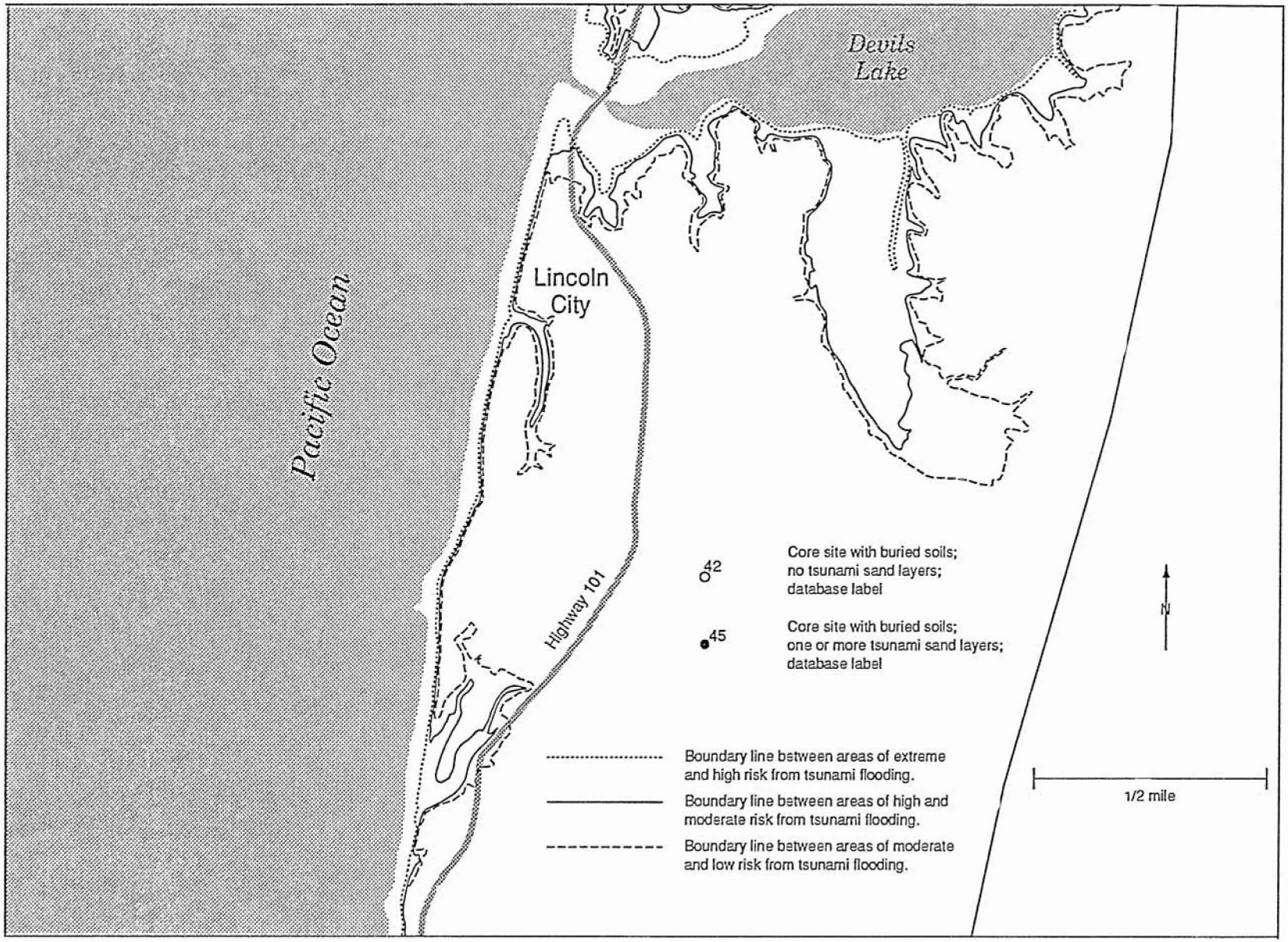


*Figure 1.9. Tsunami hazard map of the Devils Lake-Lincoln City area.*

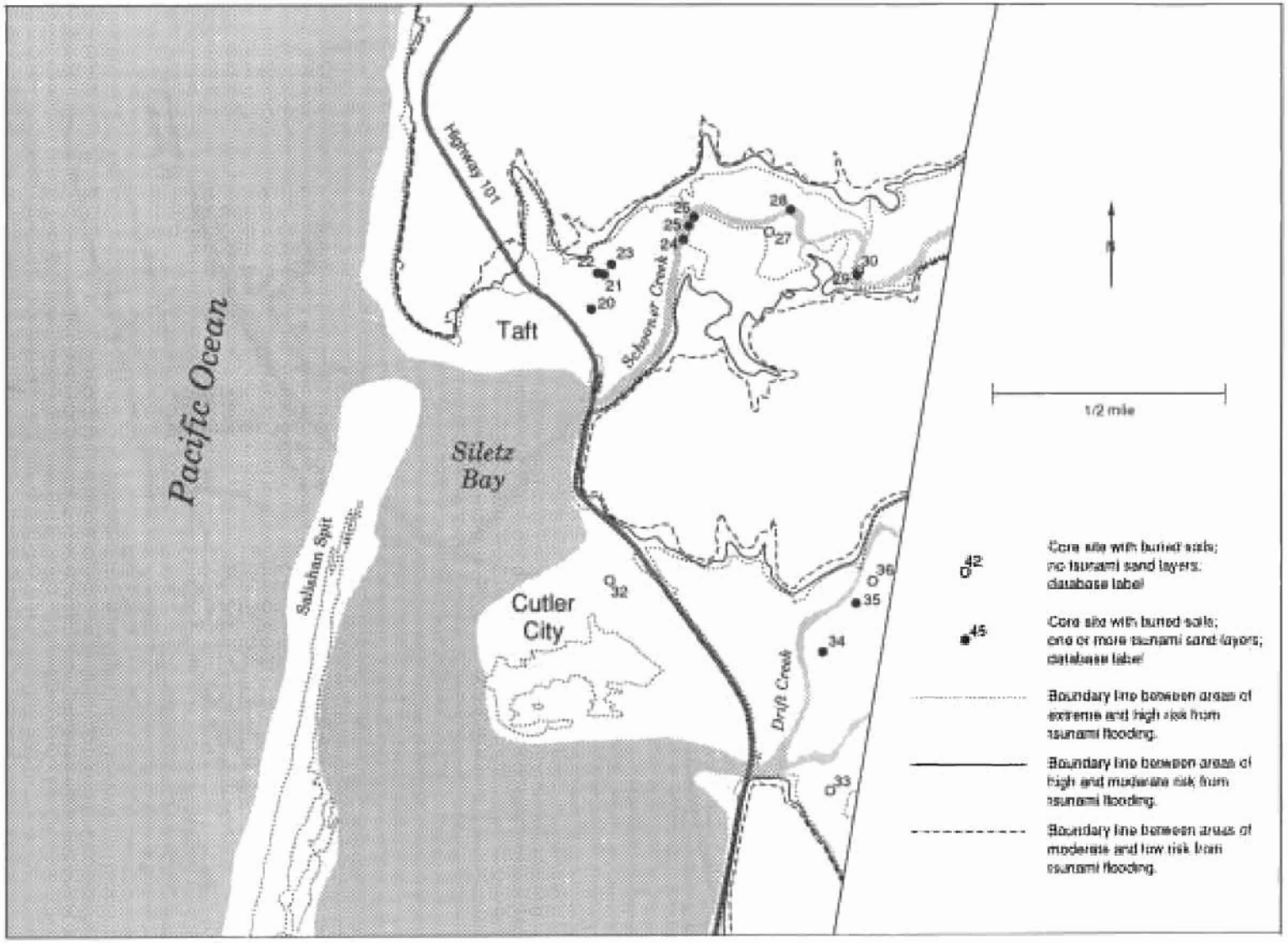


*Figure 1.10. Tsunami hazard map of the Taft-Siletz Bay area*

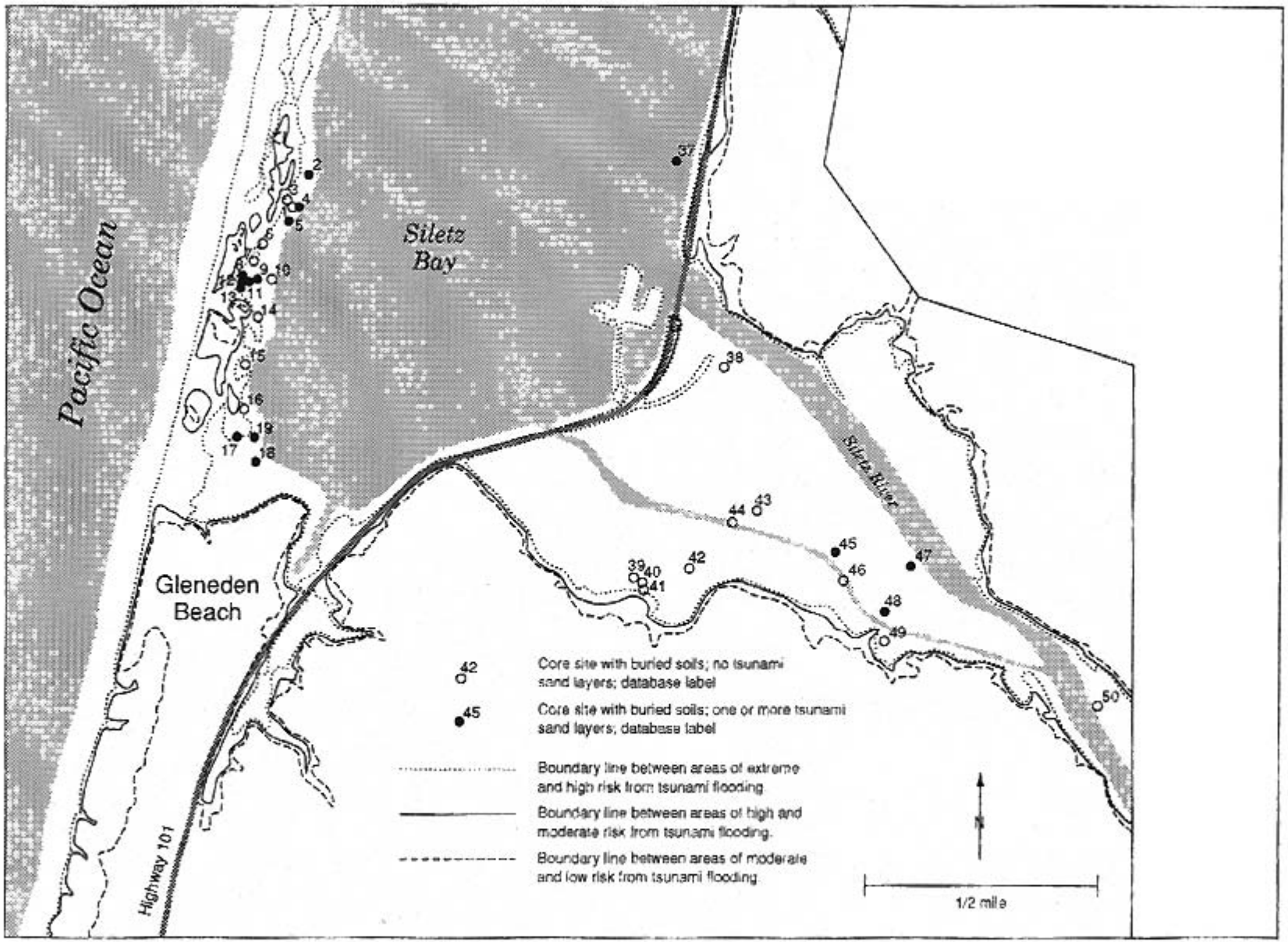


*Figure 1.11. Tsunami hazard map of the Gleneden Beach-Siletz Bay area.*

# CHAPTER 2

# SILETZ BAY: A PILOT INVESTIGATION OF COASTAL INUNDATION BY CASCADIA SUBDUCTION ZONE TSUNAMIS

By

**António M. Baptista, Ming Qi, and Edward P. Myers III**
**Center for Coastal and Land-Margin Research**
**Oregon Graduate Institute of Science & Technology**

## INTRODUCTION

The possibly devastating consequences of a tsunami generated in the Cascadia Subduction Zone (CSZ), immediately off the Pacific Northwest coast, is a cause of concern for communities in Oregon, Washington, southern British Columbia, and northern California. While scientific evidence of past large earthquakes and associated tsunamis has been the subject of controversy, the debate now centers on characteristics and impact rather than on whether those events occurred. For a summary paper of current understanding of past events, see Atwater and others, 1995.

While the need for them is incontrovertible, efforts to develop mitigation, preparedness, and emergency response strategies in the event of a future CSZ earthquake have been hampered by a lack of scientific understanding. In particular, there is no current agreement on source mechanisms, and, to a lesser but significant extent, there are questions on whether existing methodologies properly simulate regional propagation and coastal inundation of tsunamis. The problem is compounded by the fact that no CSZ tsunamis have occurred in historical times, harshly limiting the ability of researchers to validate their hypotheses and models.

From a practical perspective, scientific uncertainties regarding tsunami generation, propagation, and inundation come down to a single question: what limits of inundation should be considered?

In the present pilot study, we attempt to conciliate scientific uncertainty with practical needs of Oregon communities, by (a) developing a methodology for generation of tsunami inundation maps for Siletz Bay, and (b) critically analyzing the associated shortcomings.

The methodology adopted in this study involves a regional analysis (performed under separate funding[1]) and a local analysis (which constitutes the core of this project). The regional analysis was used to develop waveforms at about 50 m of water depth, off the Siletz coast, which were then used to investigate local inundation. Both the regional and the local analyses rely primarily on numerical modeling, but different models are used in each case.

## REGIONAL ANALYSIS

This section is based on research conducted under separate OSG funding[1], emphasizing the regional propagation of CSZ tsunamis. Detailed reports of this research are in preparation. Here, we provide only a brief summary of methods and results that will be used to define the local tsunami forcing scenarios.

## REGIONAL PROPAGATION OF CSZ TSUNAMIS

### Generation Mechanism

Strong controversy exists on the characteristics of the potential source of CSZ tsunamis. There is general agreement

1. A. Baptista (PI), "Tsunami Propagation and Run-up in the Oregon Coast", sponsored by Oregon Sea Grant.

that the primary source is seismic in nature, but there is disagreement on the magnitudes involved. In particular, does the entire fault rupture simultaneously (in a single large [e.g., Mw~8.8] event), or rather in a series of smaller [e.g., Mw~8] events separated by months to years?

Also, there are indications (Adams, 1990) that submarine landslides may have been triggered by past earthquakes, potentially furthering the tsunami energy and impact. However, the characteristics of these landslides are mostly unknown.

We have considered several different scenarios, all based on seismic sources only (i.e., no associated landslide). Three are referred here. The reference scenario was extracted from Whitmore (1993), and consists of a magnitude 8.8 earthquake extending over much of the CSZ, with associated bottom excitation generated through the deformation model of Okada (1985; Table 2.1). The first alternative scenario was that adopted by DOGAMI for Quakex 94 (a state-wide preparedness exercise, that took place in 1994), and corresponds to a smaller magnitude (Mw=8.5) earthquake (Table 2.1). The second alternative scenario represents an artificial extreme, with the same general shape as the sea floor deformation of Hyndman and Wang (1993) but with a lateral position shifted west.

**Table 2.1: Parameters used to generate bottom deformations for the reference and first alternative source scenarios**

| $M_w$ | Length (km) | Width (km) | Strike | Dip | Rake | Depth (km) | Slip (m) |
|---|---|---|---|---|---|---|---|
| 8.8 | 650.0 | 80.0 | 358.0 | 13.0 | 90.0 | 20.0 | 9.61 |
| 8.5 | 375.0 | 70.0 | 360.5 | 13.0 | 90.0 | 15.75 | 6.74 |

**Numerical Model for Regional Tsunami Propagation**

The numerical model for regional tsunami propagation is that described by Myers and Baptista (1995), and briefly reviewed in Appendix 2.1. The model is based on the finite element solution of the shallow water equations, written in continuity-wave equation form to minimize numerical oscillations. No wetting and drying is allowed, land boundaries being treated as vertical walls.

**Validation**

We strongly believe in the notion of validating numerical models against field data. Unfortunately, hydrodynamic field data for CSZ tsunamis is not available. As an attempt to partially circumvent the problem, "validation" of the regional PNW tsunami model was designed to include three phases (Baptista and others, 1995):

- Application of the model to the simulation of regional tides. This phase was considered critical, even if tides are periodic (rather than free) waves, and have typically longer periods and smaller amplitudes than tsunamis. Indeed, if accurate tidal modeling does not fully validate associated tsunami modeling, incorrect tidal modeling would strongly indicate a fundamental inability to properly simulate tsunamis. Results generally compare very favorably with tidal data from non-shore stations (Figure 2.1), outside specific regions where bathymetric information available to us is poor.

- Comparison of our tsunami simulations with independent simulations by Whitmore (1993). Results from both models are similar within a few tens of percent, in most regions along the coast. While the generally good agreement between the two models is reassuring, this again provides only limited validation (neither model is compared against actual field data).

- Application of the model to the simulation of the 1964 Alaska tsunami. This phase is in progress, and will constitute the best opportunity to compare model results with actual hydrodynamic tsunami data for the Oregon coast.

In addition, Myers and Baptista (1995) discuss limitations of the application of the same numerical model to the 1993

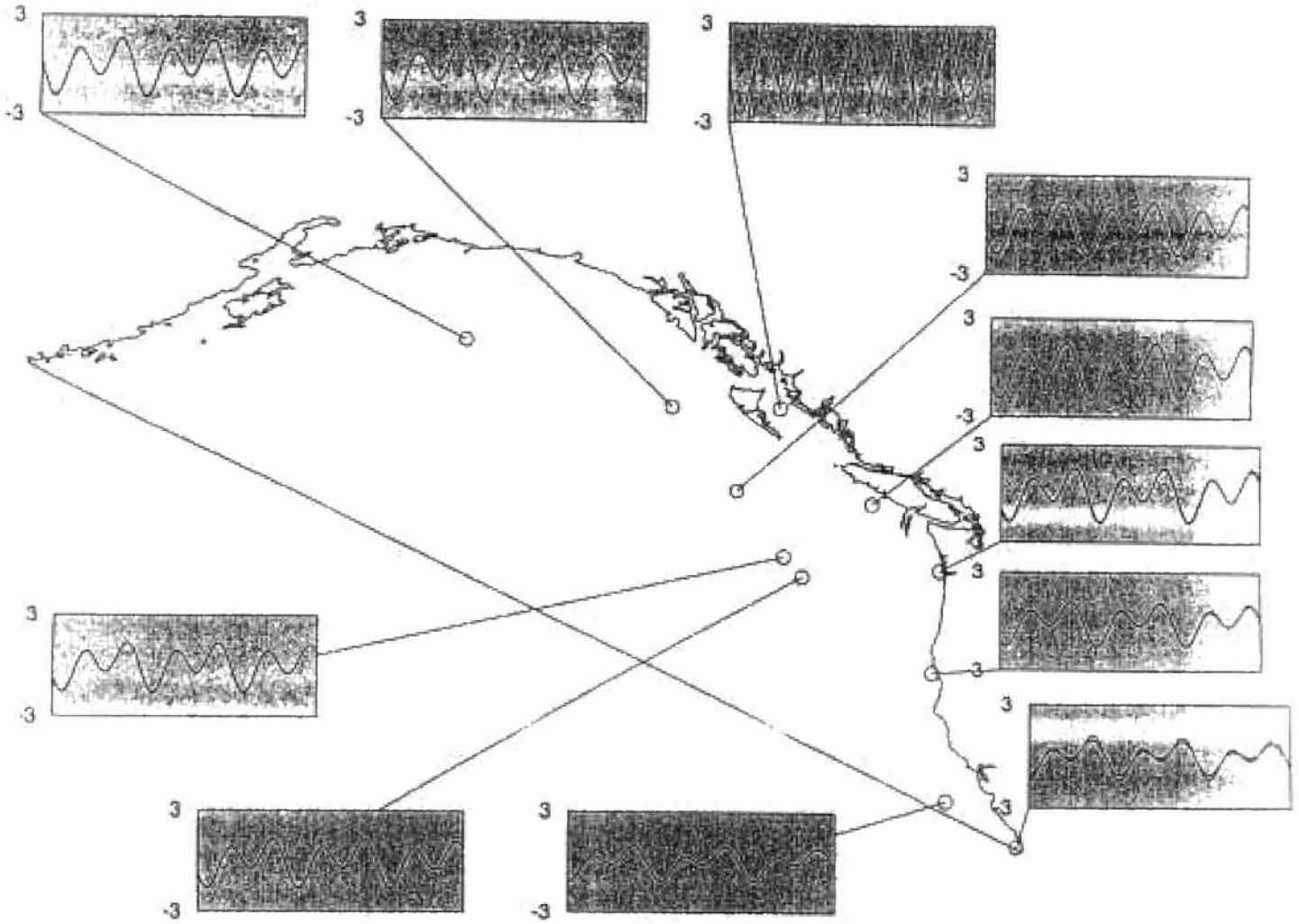


Figure 2.1.

Comparison of calculated and observed tidal elevations at selected pelagic stations of the eastern North Pacific (Myers and Baptista, in preparation)

Hokkaido Nansei-Oki tsunami. The model tends to under-predict observed run-ups, which is partially due to its inability to describe inundation, and to the relatively coarse available bathymetry. However, inherent loss of energy is also identified, a characteristic that may be common to all models based on shallow water equations, and that is currently being investigated in more detail.

While we do not consider the regional PNW tsunami model to be fully validated at this time, there is a large enough base of confidence on the model to use it to define local tsunami forcing for Siletz Bay, within the (large) uncertainties of this study.

**Regional Patterns and Tsunami Wave Heights at 50 m Depth off Siletz Bay**

Regional patterns of maximum wave heights at the "shore" are shown in Figure 2.2, for the three generation scenarios described earlier. Wave patterns obtained (for the reference and second alternative scenarios) at the ocean boundary of the local inundation model, about 50 m of water depth off the Siletz coast, are shown in Figure 2.3. We observe in both figures the much larger wave heights generated by Scenario 3.

## INUNDATION MODELING

The modeling of coastal inundation is a complex exercise, whether the modeling is associated with tsunamis or with other long-waves (e.g., tides and storm surges). Modeling tsunami inundation in Siletz Bay poses an additional challenge: the lack of appropriate data for calibration and validation.

Desirable procedures for calibration and validation would involve as reference both (a) modeling of the wetting and drying of the bay due to tides, with comparison against field observations; and (b) modeling of inundation due to the 1964 Alaska tsunami, with comparison with field evidence. Unfortunately, neither approach was feasible in the context of this study:

- approach (a), which is technically feasible and potentially very valuable, requires a field program that, while relatively modest, was beyond the available funding;
- approach (b) is technically unfeasible, because the signal of the 1964 tsunami was too small in Siletz Bay.

**Table 2.2: Definition of sensitivity runs**

| Run | Initial Sea Level | Subsidence | Forcing wave[a] | Chezy Coefficient (C) |
|---|---|---|---|---|
| 0 | MSL | 1 m | Whitmore (Ax1, Px1) | 50 $m^{1/2}s^{-1}$ |
| 1 | MSL | 1 m | Whitmore (Ax2, Px1) | 50 $m^{1/2}s^{-1}$ |
| 2 | MHHW | 1 m | Whitmore (Ax2, Px1) | 50 $m^{1/2}s^{-1}$ |
| 3 | MHHW | 0 m | Whitmore (Ax4, Px1) | 50 $m^{1/2}s^{-1}$ |
| 4 | MHHW | 1 m | Whitmore (Ax1, Px1) | 50 $m^{1/2}s^{-1}$ |
| 5 | MHHW | 1 m | Whitmore (Ax1, Px1.5) | 50 $m^{1/2}s^{-1}$ |
| 6 | MHHW | 1 m | Whitmore (Ax1, Px2) | 50 $m^{1/2}s^{-1}$ |
| 7 | MHHW | 1 m | Whitmore (Ax1, Px1) | 25 $m^{1/2}s^{-1}$ |
| 8 | MHHW | 1 m | Whitmore (Ax1, Px1) | 75 $m^{1/2}s^{-1}$ |

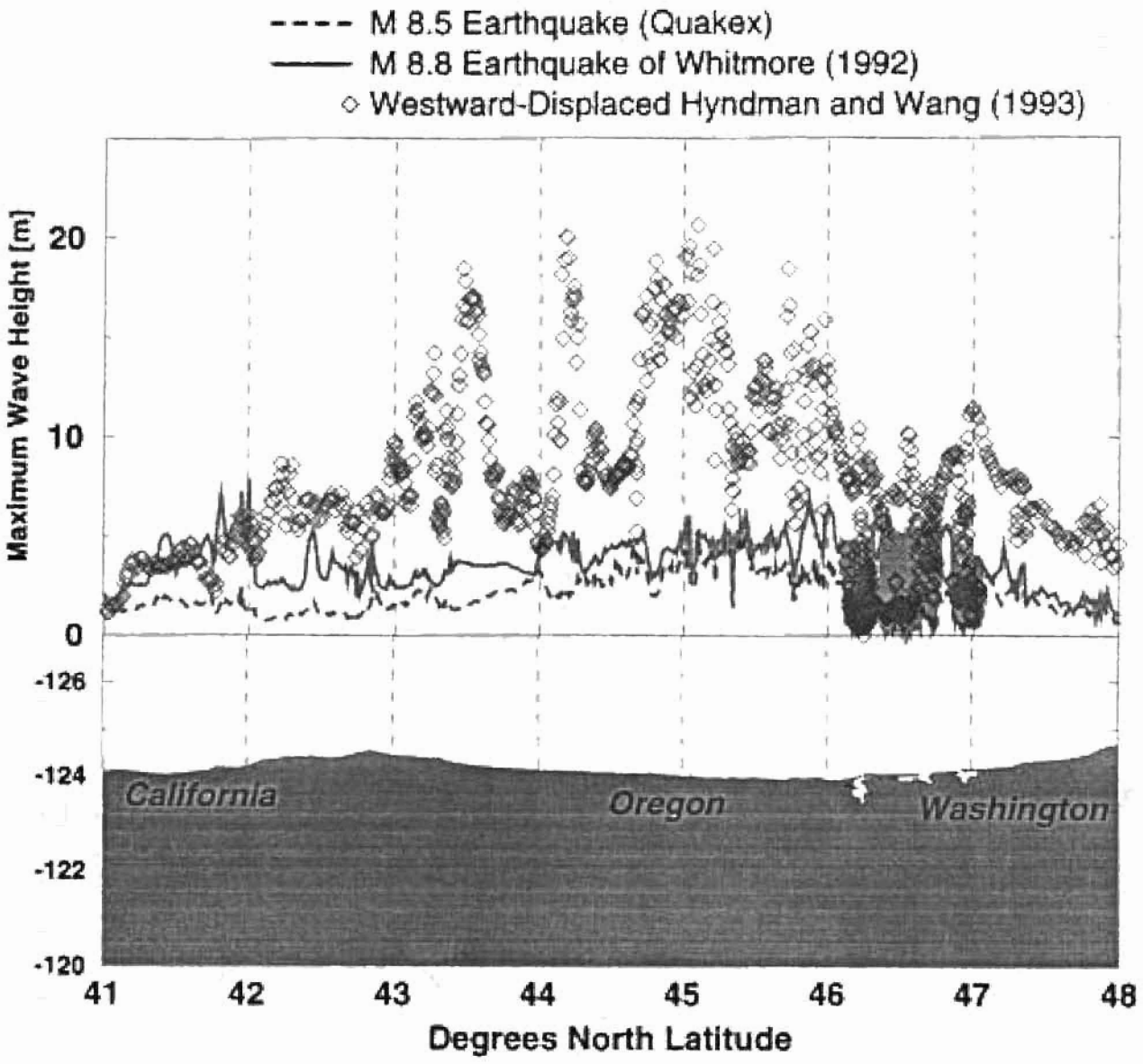


Figure 2.2

Maximum wave heights along the coasts of Washington and Oregon for different source scenarios. Simulations do not include the effect of inundation

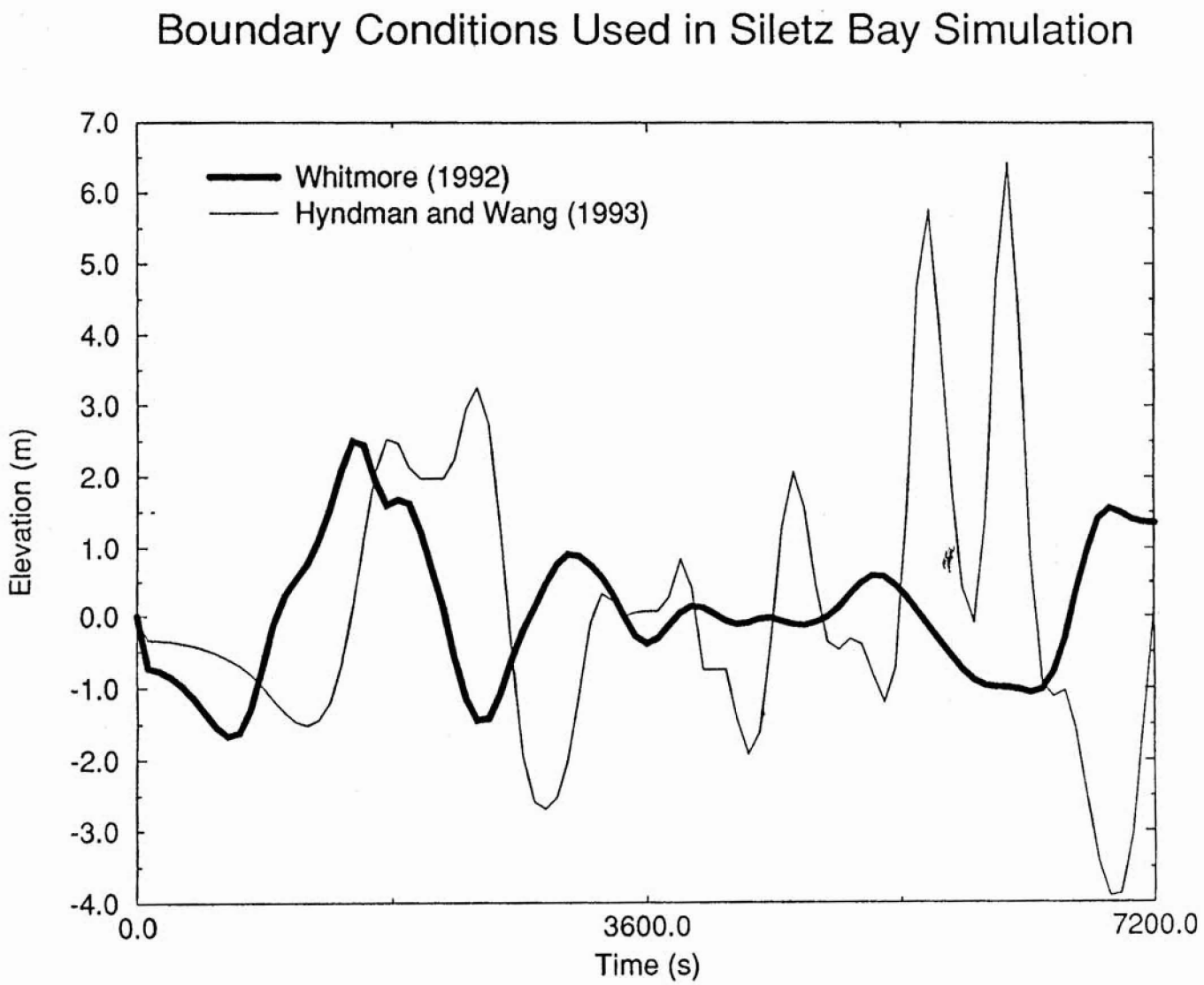


Figure 2.3.
Forcing wave used as ocean boundary condition for the Siletz Bay simulations

| Run | Initial Sea Level | Subsidence | Forcing wave[a] | Chezy Coefficient (C) |
|---|---|---|---|---|
| 9 | MHHW | 1 m | Whitmore (Ax1, Px1) | 10 $m^{1/2}s^{-1}$ |
| 10 | MHHW | 1 m | Hyndman and Wang (Ax1, Px1) | 50 $m^{1/2}s^{-1}$ |

a. Ax and Px denote the multiplying factors for the "amplitude" and "period" of the forcing wave, respectively. All waves were calculated with the regional PNW tsunami model, using source scenarios from either Whitmore (1993) or a laterally displaced Hyndman and Wang (1993).

While we cannot fully circumvent the limitations imposed by the lack of data, we have attempted to minimize such limitations by performing a sensitivity analysis for critical parameters. Table 2.2 summarizes the associated simulations, where the following factors were varied:

- forcing waveform at the ocean boundary of the local inundation model; while the waveform shown in Figure 2.3 for the Whitmore (1993) source scenario was used as reference, its amplitude and period were in a number of cases modified by simple multiplication; also, in one case we used as forcing the waveform shown in the same figure for the laterally displaced Hyndman and Wang scenario.

- sea level at the time of the earthquake;

- extent of land subsidence;

- friction parameterization.

## NUMERICAL MODEL

The model chosen for the inundation simulations is a version of SWAN (Mader, 1988). The algorithm is published in the open literature, and has been used by its author and others in a number of previous tsunami inundation studies.

SWAN solves the shallow water equations using a finite-difference algorithm. In the present application, a grid of 40x40m was used to discretize the domain shown in Figure 2.4. Topo-hydrography was partially obtained from digital elevation maps generated by aerial photography, complemented in deeper water with NOAA/NOS bathymetric data. Time steps of the order of 0.25 seconds were adopted for stability reasons.

## ANALYSIS OF RESULTS

**Sensitivity to Friction**

Friction is a key empirical parameter for modeling flow in general and inundation in particular. In SWAN, friction is parametrized through a domain-wide constant Chezy coefficient. We varied this coefficient from 10 and 25 $m^{1/2}s^{-1}$ (the latter value suggested as typical by Mader (1988)) to 50 and 75 $m^{1/2}s^{-1}$, values more typical of tidal applications in deeper waters). Of these values, the former corresponds to higher friction, i.e., larger resistance to inundation.

Results (Figures. 2.5 and 2.6) show only moderate sensitivity to friction, but the extent of inundation and the maximum wave heights decrease if friction is increased substantially (Chezy coefficient of 25 $m^{1/2}s^{-1}$).

While the recommendation of Mader (1988) bears weight due to his considerable experience, we will argue that both the characteristics of the site (with an estuarine environment that shelters Taft and Cutler City from direct impact of the tsunami wave) and, more importantly in the absence of field data, safety considerations require the use of a parametrization based on low friction. Furthermore, we will show that sensitivity to friction is largely outweighed by sensitivity to the forcing waveform. Hence, we will adopt a Chezy of 50 $m^{1/2}s^{-1}$ for the rest of this study.

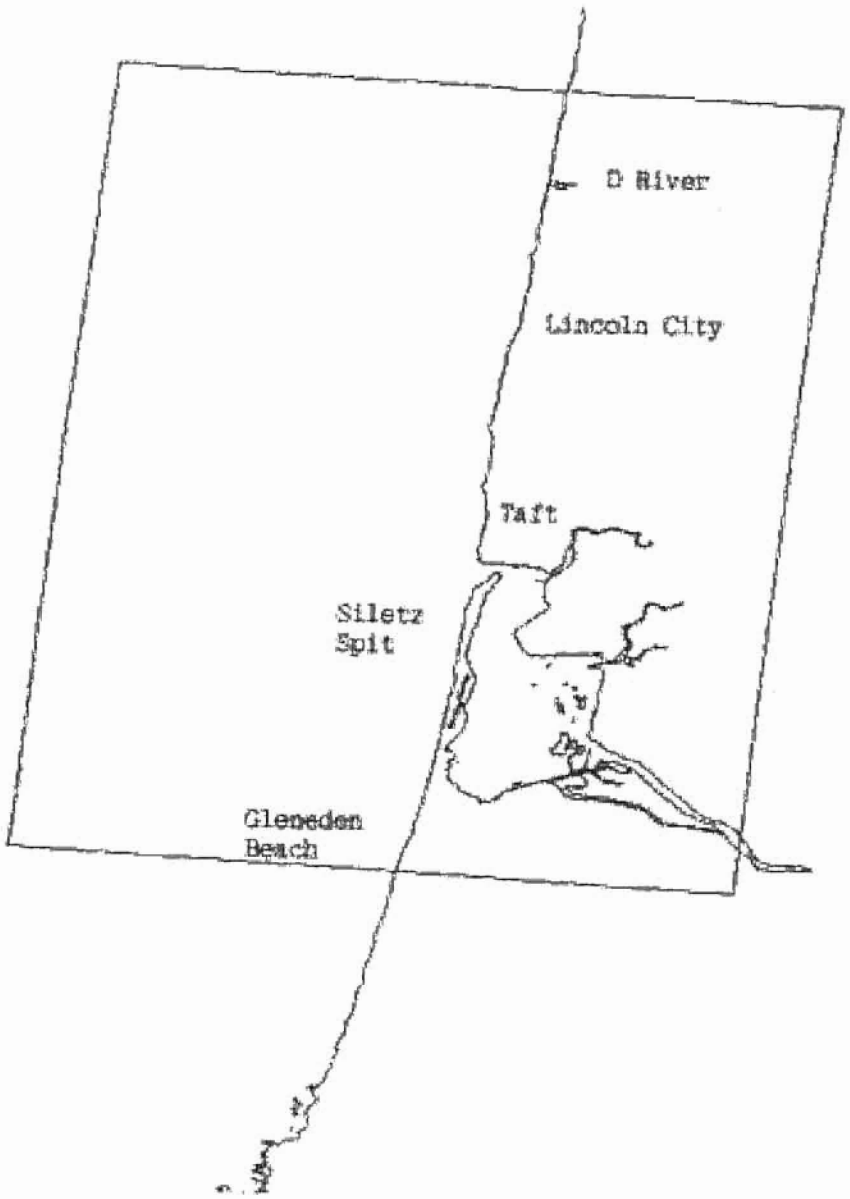


Figure 2.4.
Domain of study

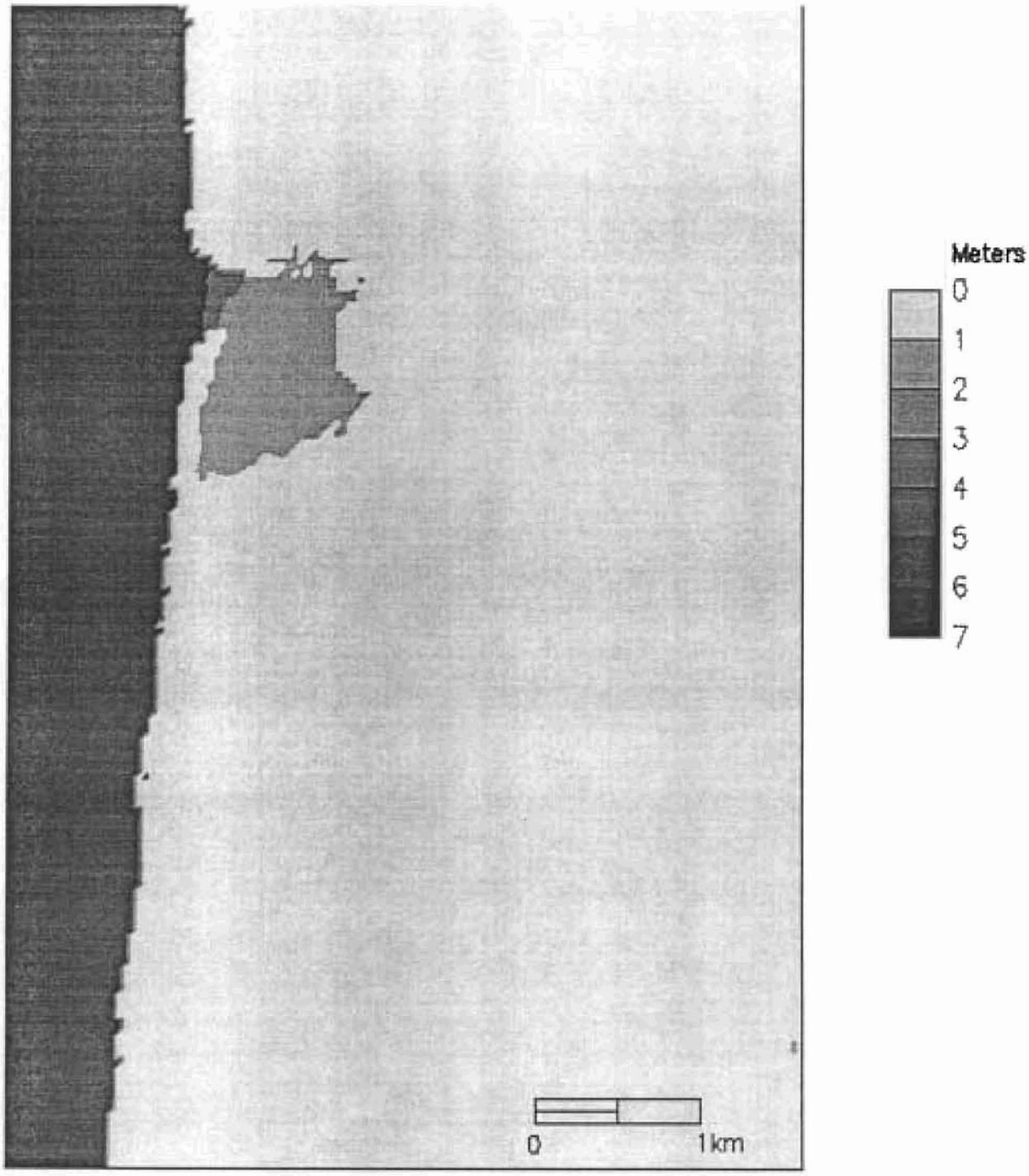


Figure 2.5a. Sensitivity to the friction parametrization. Maps of maximum wave heights in the Siletz Bay area, $C=25 m^{\frac{1}{2}} s^{-1}$.

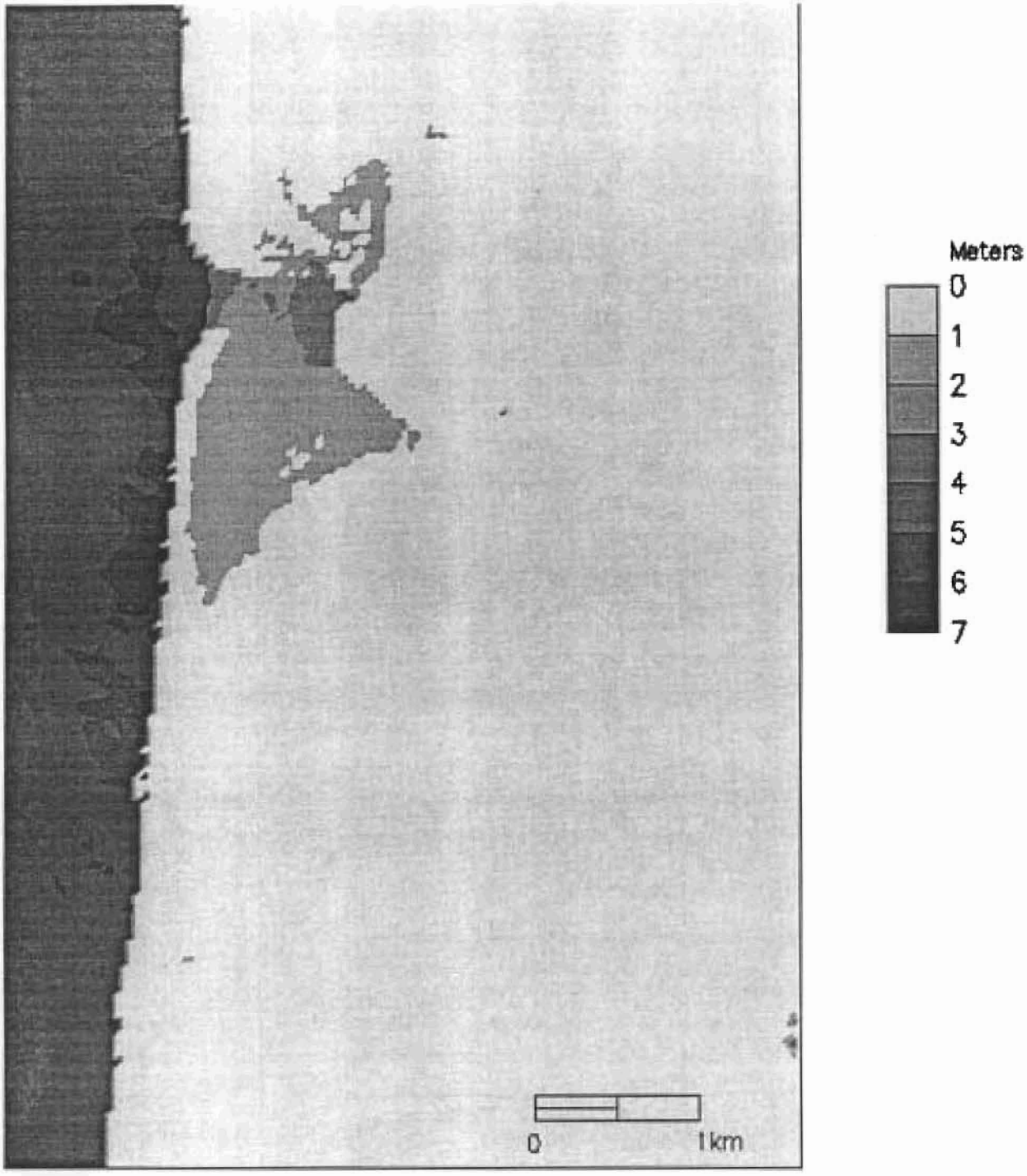


Figure 2.5b. Sensitivity to the friction parametrization. Maps of maximum wave heights in the Siletz Bay area $C=m^2s^{-1}$.

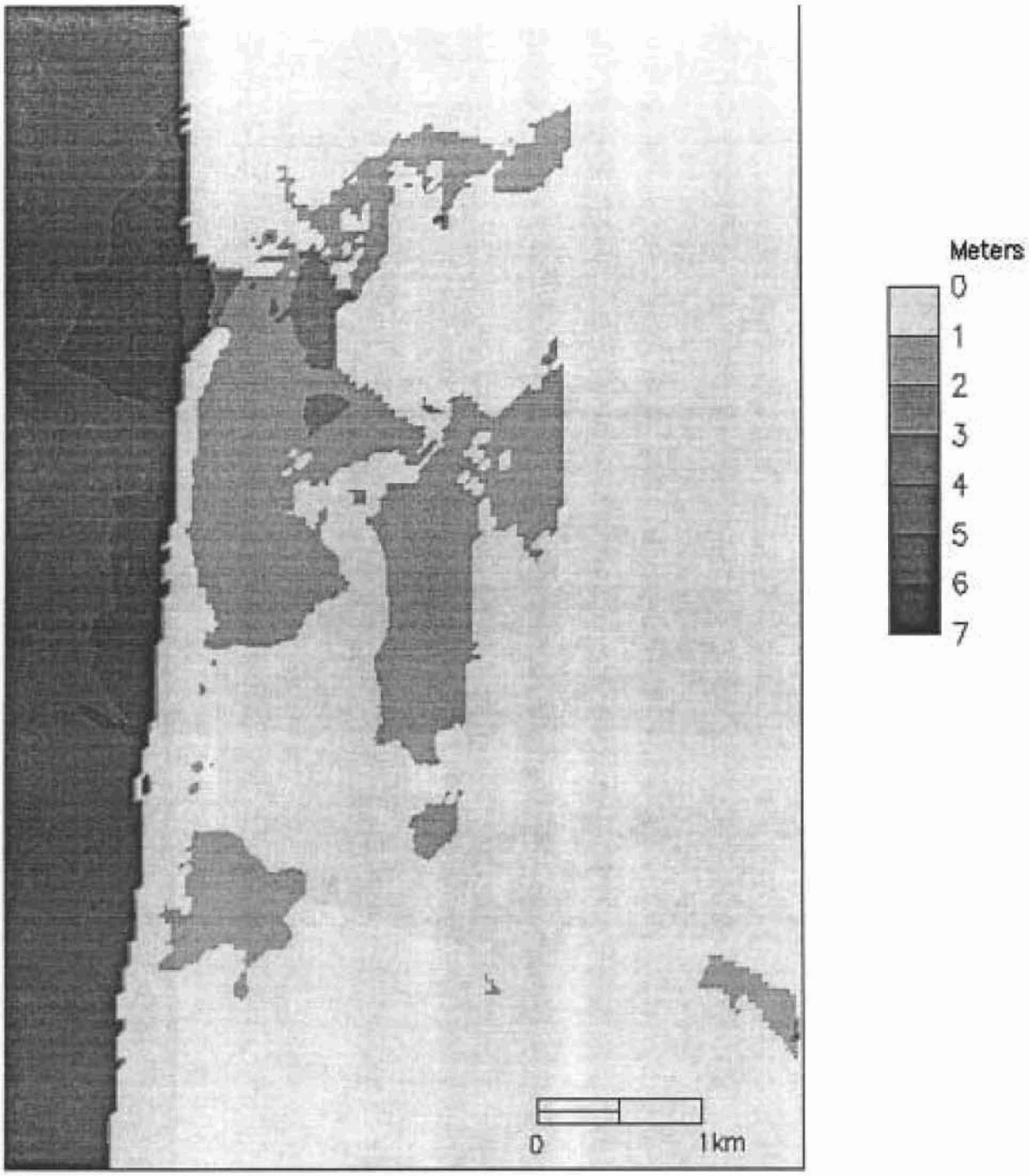


Figure 2.5c. Sensitivity to the friction parametrization. Maximum wave heights in the Siletz Bay area $C=75m^{\frac{1}{2}}n^{-1}$.

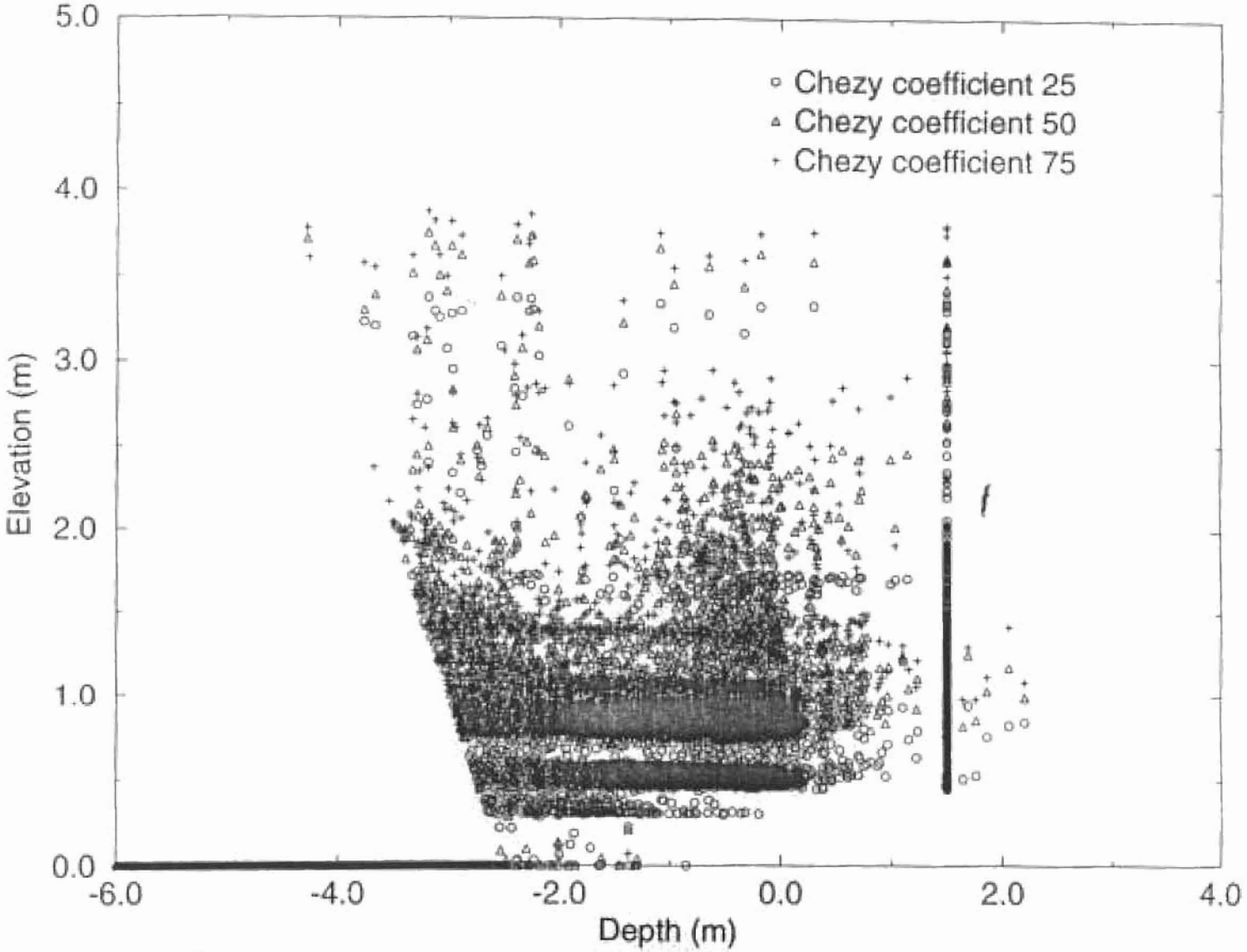


Figure 2.6.

Sensitivity to the friction parapetrization. Maximum wave heights versus water depth, within Siletz Bay, for (a) $C=25m^{\frac{1}{2}}s^{-1}$, (b) $C=50m^{\frac{1}{2}}s^{-1}$, and (c) $C=75m^{\frac{1}{2}}s^{-1}$

**Sensitivity to Forcing**

The sensitivity of the inundation to the amplitude of the forcing wave was tested first by including a multiplicative "safety factor" between 2 and 4. Doubling the wave height is certainly justified because of the demonstrated inability, in recent tsunamis, of numerical models of regional propagation to fully represent observed data. The factor 4 was considered for consistency with the NOAA approach to Crescent City (where a 10 m amplitude wave was used as forcing).

Results show, not surprisingly, that maximum amplitudes in the bay are extremely sensitive to this variation (Figure 2.7). Sensitivity of the limits of inundation (Figure 2.8) to the multiplying factor is significant up to a certain threshold (around 2), but less significant beyond that (mostly because of prevailing sharp topographic slopes). As a warning note, this lessened sensitivity applies only to the limits of inundation, not to the associated maximum amplitudes (Figure 2.7) and current velocities (not shown).

Comparisons of the impact of the reference forcing wave with an amplification of 4 with the forcing wave generated from the laterally displaced Hyndman and Wang scenario are shown in Figure 2.9. Results are strikingly similar with regard to maximum wave heights.

**Sensitivity to Other Factors**

Sensitivity to the prevailing level of the water (due to tides, storm surges, etc.) at the time of the tsunami and due to seismic subsidence, were grouped into the same analysis. The depth of the water in the bay, relative to MSL, was corrected by either 1 m, 1.3 m, or 2.3 meters. A comparison of the first and third cases is shown in Figure 2.10.

Sensitivity to numerical parameters (grid resolution, time step, etc) were also performed, but will not be shown here.

## INUNDATION SCENARIOS

Based on the results of the sensitivity analysis, we defined three inundation scenarios for planning purposes:

*Scenario S1: Reference forcing wave, with initial water level at MSL + 1 m*
Assumes that a large CSZ earthquake occurred ($M_w$=8.8), associated with a local subsidence of the order of 1m, and that the background water level remained during the duration of the tsunami close to MSL (i.e., very low coefficient tide). No safety factors are introduced. Planners should consider that inundated regions are at ***extremely high risk*** for any large CSZ earthquake.

*Scenario S2: Reference forcing wave amplified by a factor of 2, with initial water level at MHHW + 1 m*
Assumes that a large CSZ earthquake occurred (Mw=8.8), associated with a local subsidence of the order of 1m, and that the background water level remained during the duration of the tsunami close to MHHW. Moderate safety factors were included to account for uncertainty. Planners should assume that the inundated regions between S1 and S2 are at ***high risk***.

*Scenario S3: Reference forcing wave amplified by a factor of 4, with initial water level at MHHW*
Assumes that a large CSZ earthquake occurred (Mw=8.8) with no local subsidence and that the background water level remained during the duration of the tsunami close to MHHW. Large safety factors were included to account for uncertainty. Planners should assume that inundated regions between S2 and S3 are at ***moderate risk***.

Inundation lines, defining the transition between the parts of the domain that were ever wet and those that were always dry, were used by Priest et al. (1995) to produce the final inundation maps.

## CONCLUSIONS AND RECOMMENDATIONS

Our investigation provides qualified insight on the potential characteristics of local coastal inundation from a CSZ tsunami. In particular:

- Open coast

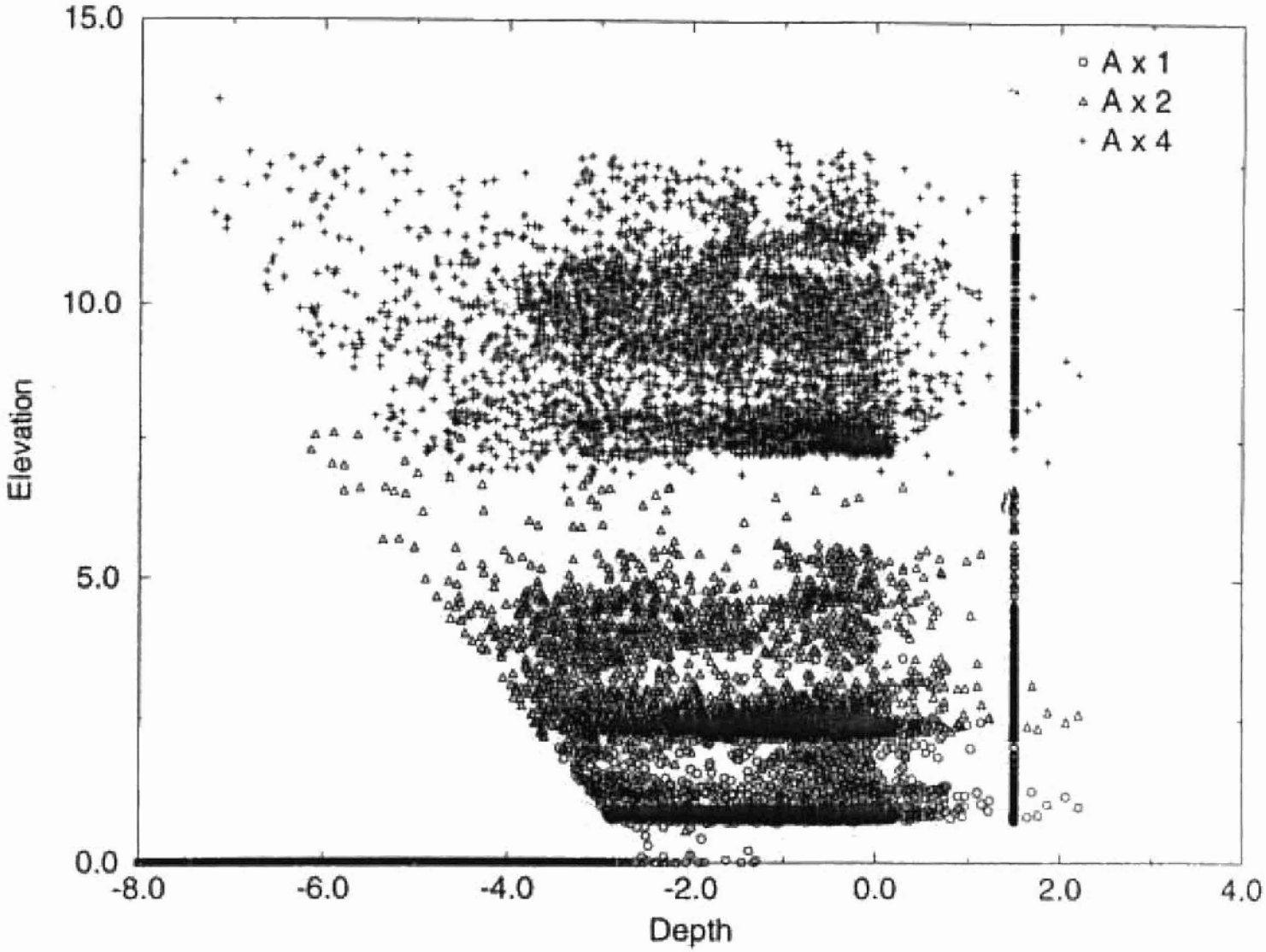


Figure 2.7.

Sensitivity to the forcing wave. Maximum wave heights versus water depth, within Siletz Bay, for different amplification factors for the reference waveform: (a) x1; (b) x2; (c) x4.

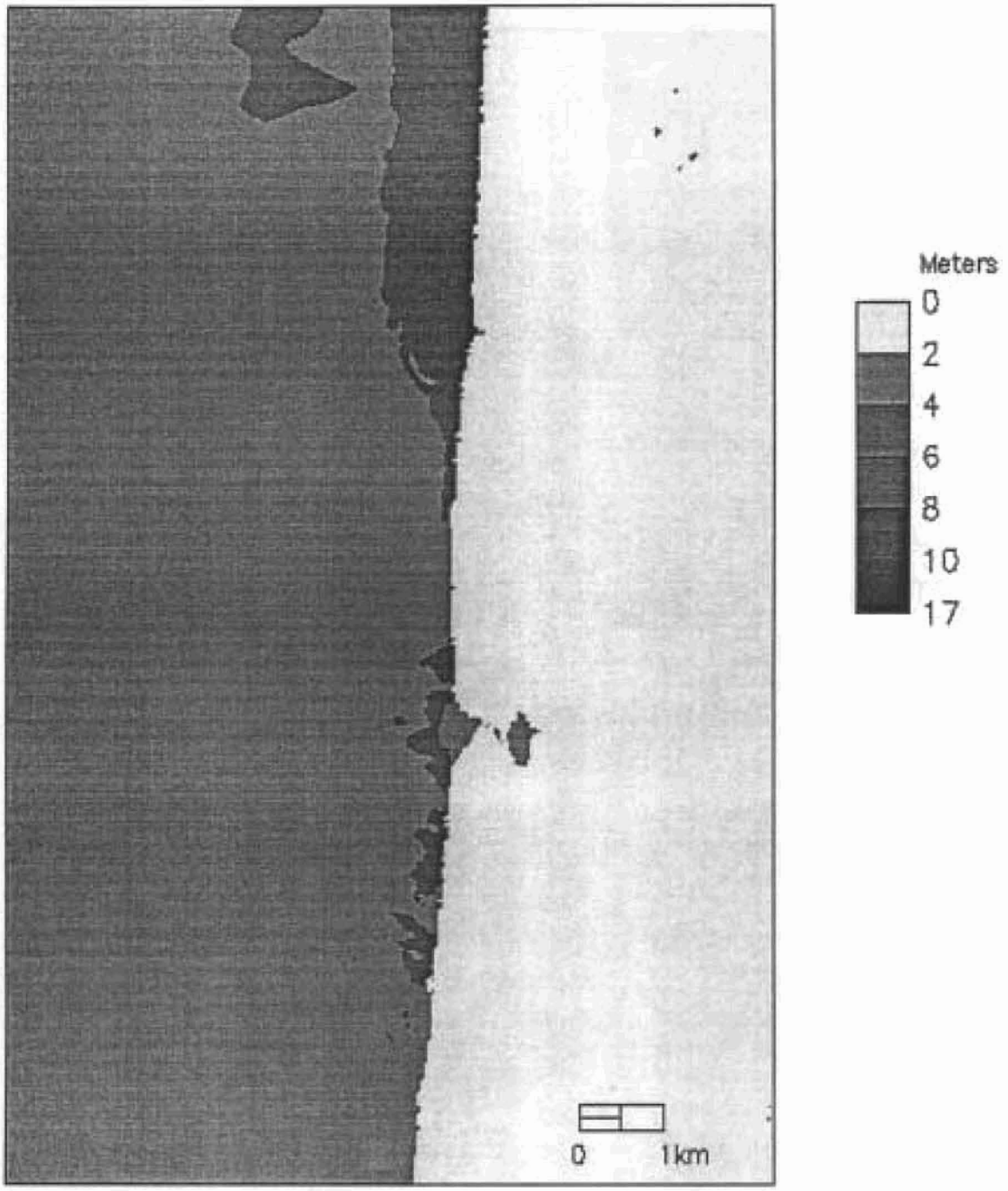


Figure 2.8a. Sensitivity to the forcing wave. Maps of maximum wave heights in the Siletz Bay area, for the following forcing wave scenario x1.

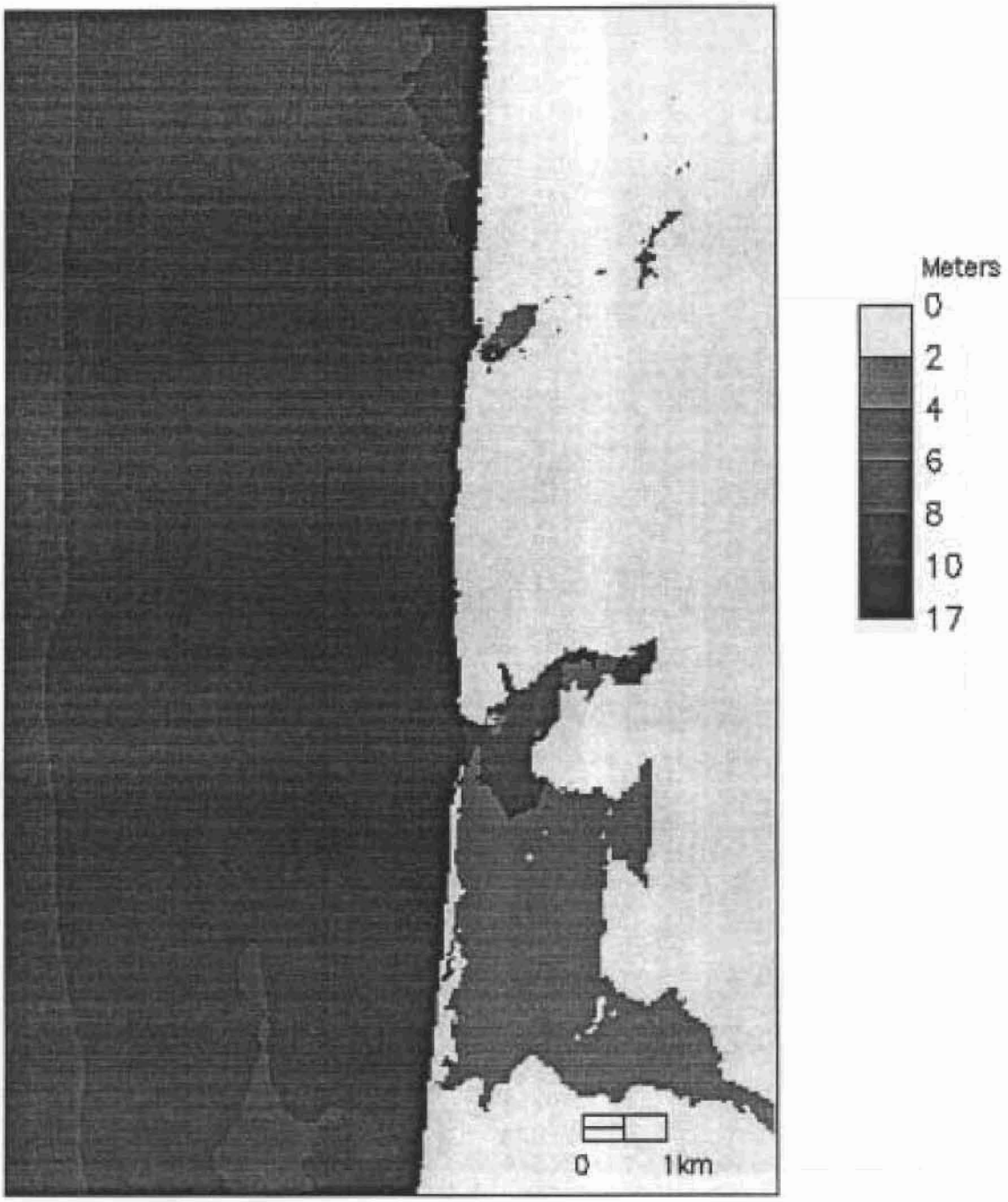


Figure 2.8b. Sensitivity to the forcing wave. Maps of maximum wave heights in the Siletz Bay area, for the following forcing wave scenario x2.

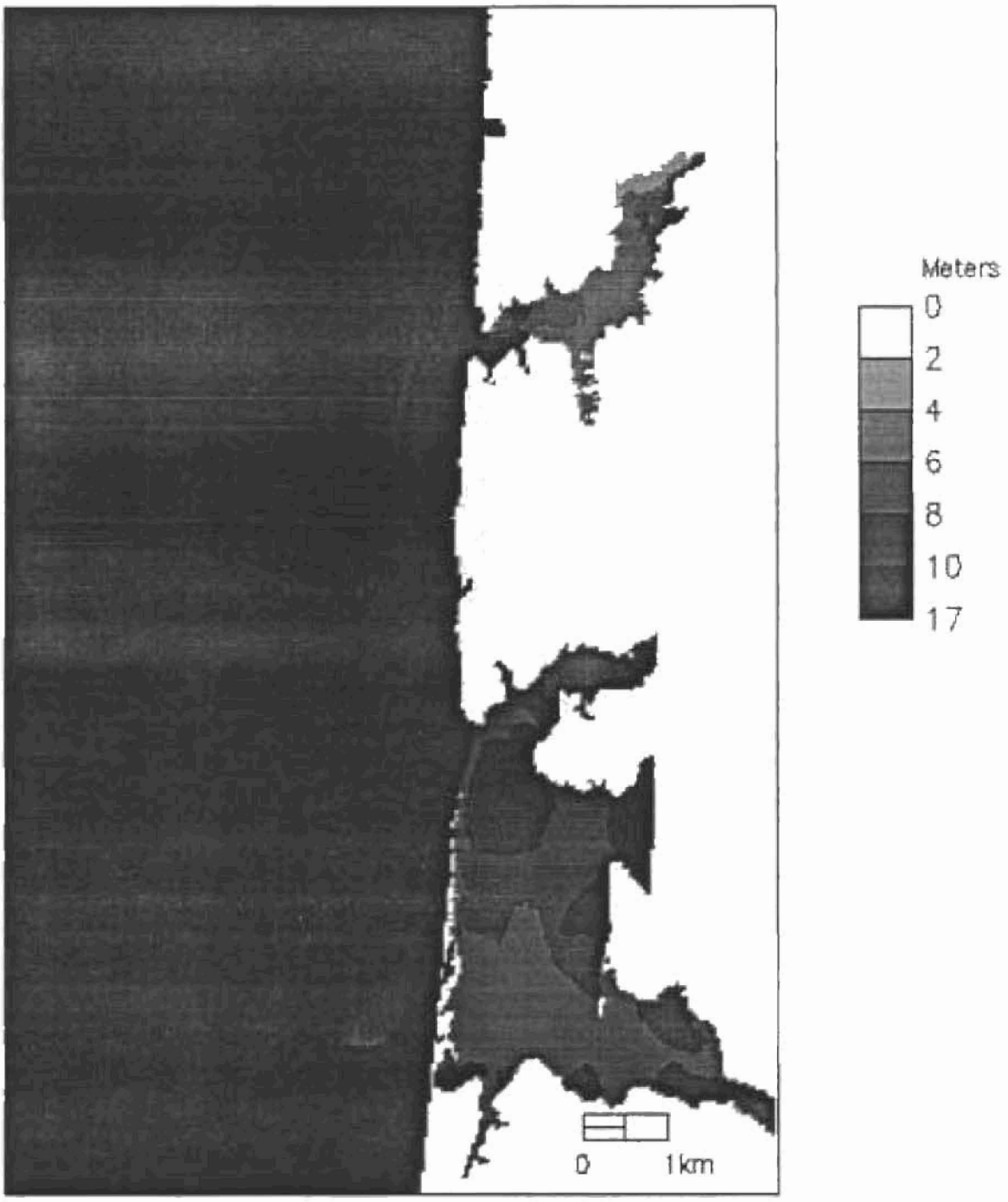


Figure 2.8c. Sensitivity to the forcing wave. Maps of maximum wave heights in the Siletz Bay area, for the following forcing wave scenario x4.

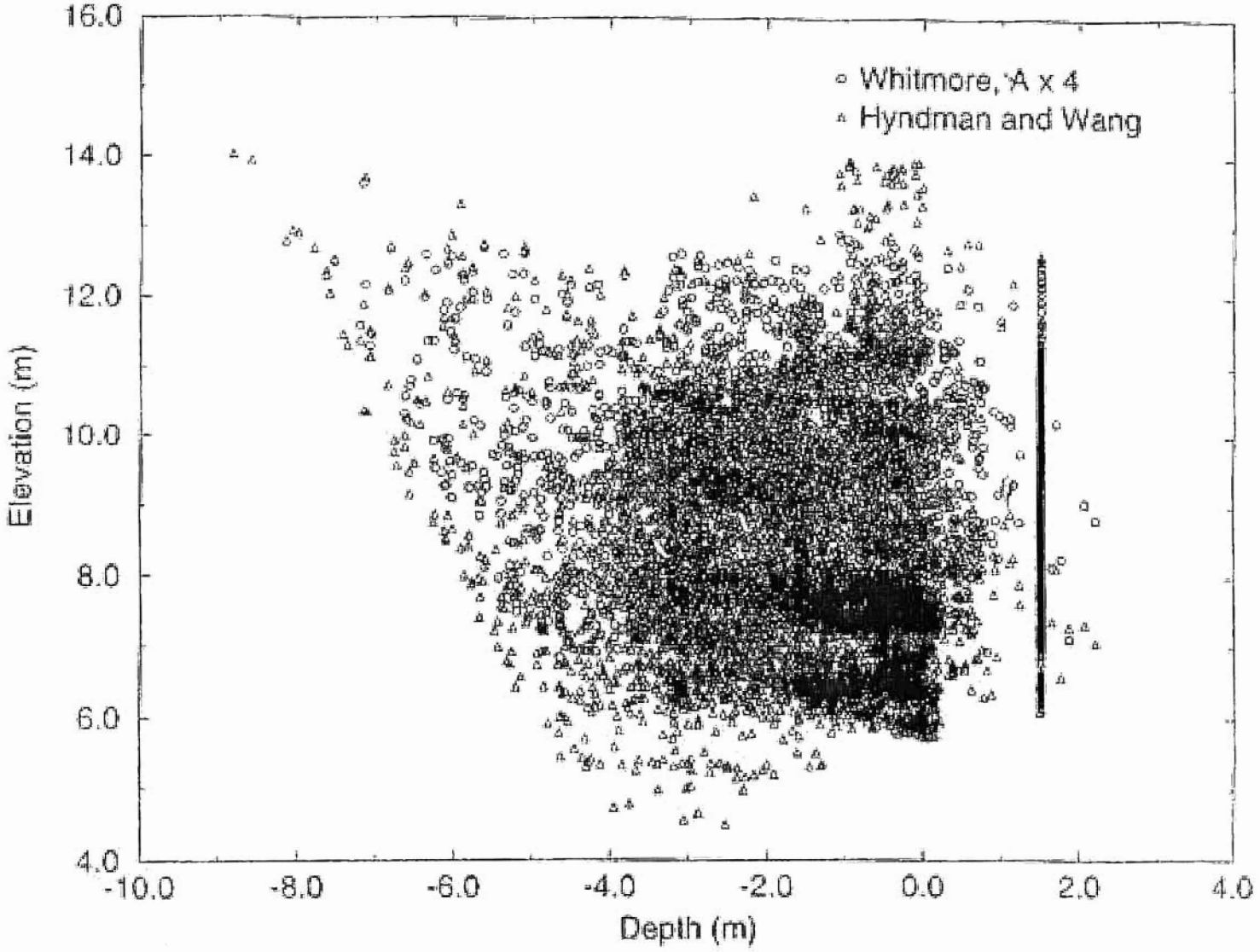


Figure 2.9.

Comparison of maximum wave heights versus water depth, within Siletz Bay, for (a) reference waveform, with quadrupled amplitude; and (b) waveform obtained from the laterally displaced Hyndman and Wang (1995) source scenario.

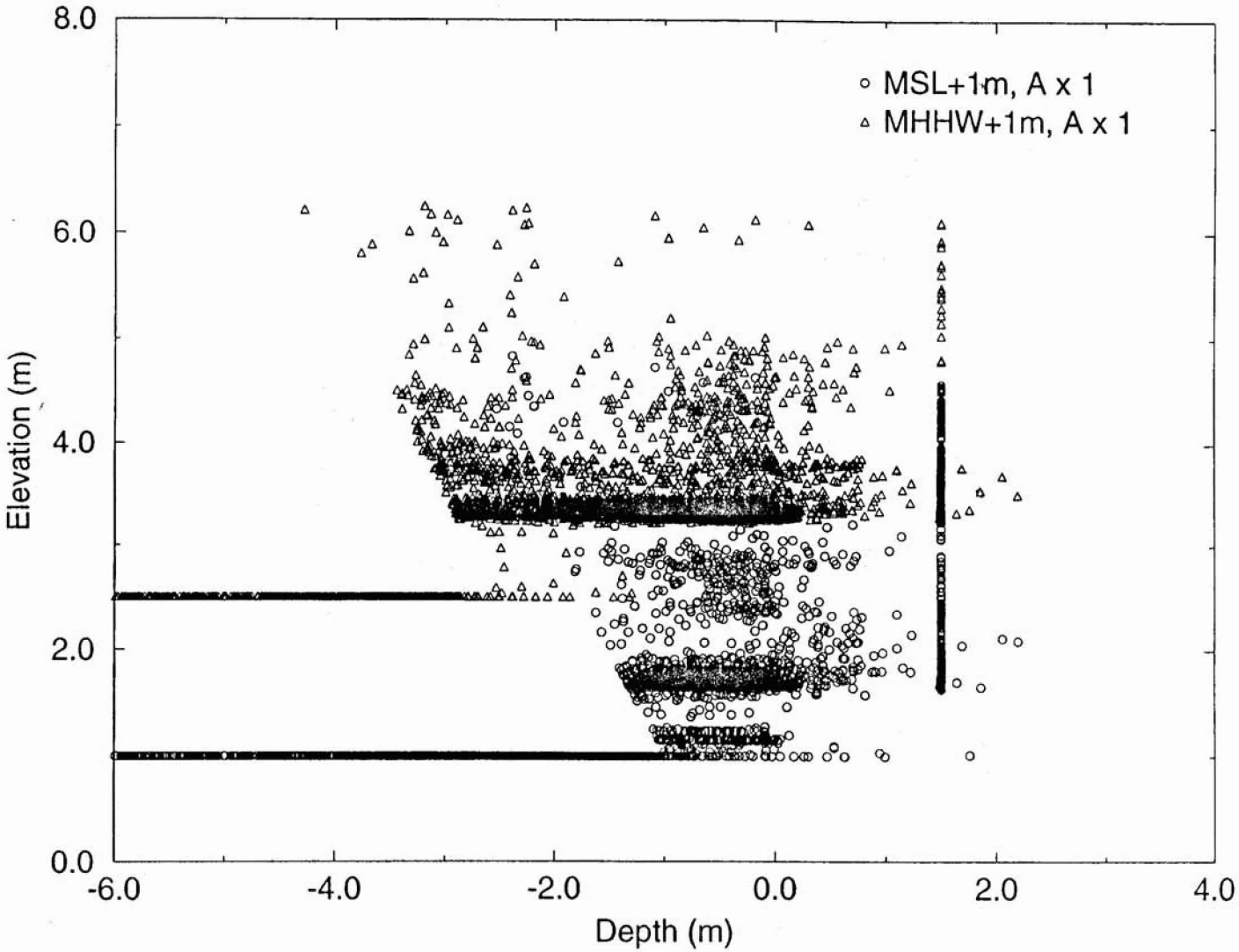


Figure 2.10.

Sensitivity to the initial water level. Maximum wave heights versus water depth, within Siletz Bay, for initial levels at (a) MSL+1 m; and (b) MSL=2.3 m.

CSZ tsunamis are expected to result in significant wave heights at the coast throughout the study area. For a M=8.8 CSZ earthquake, wave heights at the coast should be assumed to be of no less than 4-6 m above the prevailing sea level. This range is consistent with not only our simulations in this investigation, but also with regional tsunami simulations made elsewhere (Myers and Baptista, 1995; Whitmore, 1993).

- Siletz Bay
  Siletz Spit is an important protection mechanism for Siletz Bay. If the spit is not extensively overtopped (Scenario S1), inundation and damage within the bay will be relatively localized. However, if a significant extent of the spit near the mouth of the estuary is overtopped, inundation will likely be generalized and severe. In this case, inundation is essentially limited only when the incoming wave reaches regions of sharp topographic slopes. Because of this, the similarity of the horizontal extents for some of the tsunami scenarios analyzed in this work is misleading: similar horizontal extents do not in any way imply similar wave heights and similar flow velocities.

It has to be recognized that the inundation maps derived in this investigation reflect significant uncertainties and limitations, due to the following key factors:

- uncertainty in the characteristics of the trigger CSZ earthquake[1];
- possibility of associated landslides;
- lack of data to calibrate the tsunami models;

inherent limitations of the numerical models[2].

In addition, the limited budget and scope of this project were constraining with regard to aspects that are technically achievable. In particular, we used a single inundation model (where prudence recommends a cross-check with an independent model, such as Beck and Baptista, 1995), and we had no resources to deploy instrumentation to monitor tidal propagation in the tidal flats (hence, losing the opportunity to obtain field data that are achievable and valuable for partial validation).

Given the uncertainties and limitations discussed above, we recommend that the inundation maps derived in this investigation be used only for:

- emergency planning;
- preparedness through community education; and
- emergency response.

We consider the maps unsuitable for any other purposes, including but not restricted to mandatory land-use planning and establishing insurance policies and/or rates.

## REFERENCES

Adams, J., 1990, Paleoseismeicity of the Cascadia Subduction Zone: evidence from turbidites off the Oregon-Washington margin: Tectonics, v. 9, p. 569-583.

---

1. A more recent investigation into CSZ source parameters (Priest, in preparation) has increased our understanding of this factor. However, uncertainties remain, and the new investigation does not invalidate our conclusions.
2. The regional CSZ tsunami model used to define the incident wave off Siletz Bay has now been refined (Myers and others, in preparation), in particular by accounting for inundation. The new investigation does not invalidate the conclusions of the present study

Atwater, B.F., Nelson, A.R., Clague, J.J., Carver, G.A., Yamaguchi, D.K., Bobrowsky, P.T., Bourgeois, J., Darienzo, M.E., Grant, W.C., Hemphill-Haley, E., Kelsey, H.M., Jacoby, G.C., Nishenko, S.P., Palmer, S.P., Peterson, C.D., and Reinhart, M.A., 1995, Summary of coastal geologic evidence for past great earthquakes at the Cascadia Subduction Zone: Earthquake Spectra, v. 11, no. 1, p. 1-18.

Baptista, A.M., Myers, E., Qi, M., Beck, B., Priest, G.R., and Peterson, C.D., 1985, Tsunami propagation and inundation from Cascadia Subduction Zone earthquakes: tools and approaches: IAPSO, Hawaii, August 1995 (abstract).

Beck, B., and Baptista, A.M., 1995, Accuracy and conservation properties of a 2D inundation model: IAPSO, Hawaii, August 1995 (abstract).

Mader, C.L., 1988, Numerical modeling of water waves: University of California Press.

Myers, E.P., Baptista, A.M., and Priest, G.R., in preparation, Finite element modeling of hypothetical Cascadia Subduction Zone tsunamis.

Myers, E.P., and Baptista, A.M., 1995, Finite element modeling of the July 12, 1993 Hokkaido Nansei-Oki tsunami: Pure and Applied Geophysics, v. 144, no. 3/4, p. 1070-1102.

Hyndman, R.D., and Wang, K., 1993, Thermal constraints on the zone of major thrust earthquake failure: the Cascadia Subduction Zone: Journal of Geophysical Research, v. 98, no. B2, p. 2039-2060.

Okada, Y., 1995, Surface deformation due to shear and tensile faults in a half-space: Bulletin of the Seismological Society of America, v. 75, no. 4, p. 1135-1154.

Priest, G.R., in preparation, Explanation of mapping methods and use of the tsunami hazards maps of the Oregon Coast: Oregon Department of Geology and Mineral Industries, Open-File Report, 0-95-67.

Priest, G.R., Baptista, A.M., Qi, M., and Peterson, C.D., 1995, Tsunami hazard map of the Siletz Bay area, Lincoln County, Oregon: DOGAMI Technical Report.

Savage, J.C., 1983, A dislocation model of strain accumulation and release at a subduction zone: Journal of Geophysical Research, v. 88, p. 4984-4996.

Whitmore, P.M., 1993, Expected tsunami amplitudes and currents along the North American coast for Cascadia Subduction Z

one earthquakes: Natural Hazards, v. 8, p. 59-73.

## APPENDIX 2.1 - FORMULATION OF THE REGIONAL PROPAGATION MODEL

### INTRODUCTION

The model described below was originally developed by Westerink and others (1991) for the study of tides and storm surges (Westerink and others, 1992). Myers (1994) and Myers and Baptista (1995) extended the model to the simulation of tsunamis, through the inclusion of the generation mechanism and of transmissive ocean boundary conditions.

### MODIFIED CONTINUITY EQUATION

To represent the tsunami generation, a time and spatially dependent bottom deformation is introduced in the depth-averaged continuity equation. Rather conventionally, this is accomplished by incorporating the bottom deformation into the kinematic boundary condition, and leads to the following modified equation:

$$\frac{\partial \eta}{\partial t} - \frac{\partial \gamma}{\partial t} + \frac{\partial}{\partial x} uH + \frac{\partial}{\partial y} vH = 0 \tag{1}$$

where $\gamma$ is the bottom deformation (positive for uplift), $\eta$ is the free surface elevation, $u$ and $v$ are the depth-averaged velocities, $H = h + \eta - \gamma$ is the total water depth, and $h$ is the water depth relative to a reference level.

The time interval over which the bottom deformation is imposed should be consistent with the rise time of the earthquake, which, following Geller (1976), can be approximated as:

$$\Upsilon_s = \frac{\overline{D}}{\dot{D}} \approx \frac{\mu \overline{D}}{\beta \Delta\sigma} \tag{2}$$

where $\Upsilon_s$ is the theoretical rise time, $\overline{D}$ the average dislocation, $\dot{D}$ the dislocation velocity, $\mu$ the average rigidity, $\beta$ the shear wave velocity, and $\Delta\sigma$ the mean stress drop.

### GOVERNING EQUATIONS AND NUMERICAL FORMULATION

The adopted finite element model is based on the shallow water equations, with the momentum equations written in non-conservative form, and the continuity equation written in a generalized wave form. The use of wave continuity rather than primitive continuity equations was introduced by Lynch and Gray (1979) and later generalized by Kinnmark and Gray (1984); the approach is effective in eliminating the spurious $2\Delta x$ oscillations often associated with early finite element solutions of coastal flow simulations.

To review the derivation of the generalized wave continuity equation (GWCE), we let $L$ represent the primitive continuity equation written as before:

$$L \equiv \frac{\partial \eta}{\partial t} - \frac{\partial \gamma}{\partial t} + \frac{\partial}{\partial x} uH + \frac{\partial}{\partial y} vH = 0 \tag{3}$$

and let $M$ represent the non-conservative form of the momentum equations subject to the Boussinesq, hydrostatic, and incompressibility assumptions:

$$M \equiv \frac{\partial}{\partial t}\vec{v} + \vec{v} \bullet \nabla\vec{v} + \vec{f} \times \vec{v} + \tau\vec{v} + \nabla\left[\frac{p_s}{\rho_0} + g\,(\eta - \alpha\Psi)\right] + \frac{E_h}{H}\left[\frac{\partial^2}{\partial x^2}\vec{v}H + \frac{\partial^2}{\partial y^2}\vec{v}H\right] + \frac{\tau_{s\vec{x}}}{\rho_0 H} = 0 \tag{4}$$

where $\vec{v}$ is the depth-averaged velocity $(u, v)$, $\vec{f}$ is the Coriolis vector, $\tau = c_f \frac{(u^2 + v^2)^{1/2}}{H}$, $c_f$ is the bottom friction coefficient, $p_s$ is the atmospheric pressure at the free surface, $\rho_0$ is the reference density of water, $g$ is the acceleration due to gravity, $\alpha$ is the effective Earth elasticity factor, $\Psi$ is the Newtonian equilibrium tide potential, $E_h$ is the horizontal eddy diffusion coefficient, and $\tau_{s\vec{x}}$ is the applied free surface stress.

If we represent the conservative form of the momentum equations as:

$$M^c = (H)\,(M) + (\vec{v})\,(L) \tag{5}$$

the continuity wave equation, $W$, is constructed as:

$$W \equiv \frac{\partial L}{\partial t} + \tau L - \nabla \bullet M^c = 0 \tag{6}$$

where $\tau$ is the same as the friction factor used in the momentum equations. The GWCE is an extension of Equation (6) where $\tau$ is replaced by a generic weighting factor $G$:

$$W^G \equiv \frac{\partial L}{\partial t} + GL - \nabla \bullet M^c = 0 \tag{7}$$

or:

$$W^G \equiv \frac{\partial^2 \eta}{\partial t^2} + G\frac{\partial \eta}{\partial t} - \frac{\partial^2 \gamma}{\partial t^2} - G\frac{\partial \gamma}{\partial t} + \frac{\partial}{\partial x}\left\{u\frac{\partial \eta}{\partial t} - uH\frac{\partial u}{\partial x} - vH\frac{\partial u}{\partial y} + fvH - H\frac{\partial}{\partial x}\left[\frac{p_s}{\rho_0} + g\,(\eta - \alpha\Psi)\right]\right\} + \frac{\partial}{\partial x}\left\{-E_h\frac{\partial^2 \eta}{\partial x \partial t} + \frac{\tau_{sx}}{\rho_0} - (\tau - G)\,uH\right\} \tag{8}$$

$$\frac{\partial}{\partial y}\left\{v\frac{\partial \eta}{\partial t} - uH\frac{\partial v}{\partial x} - vH\frac{\partial v}{\partial y} - fuH - H\frac{\partial}{\partial y}\left[\frac{p_s}{\rho_0} + g\,(\eta - \alpha\Psi)\right]\right\} + \left(\frac{\partial}{\partial y}\left\{-E_h\frac{\partial^2 \eta}{\partial y \partial t} + \frac{\tau_{sy}}{\rho_0} - (\tau - G)\,vH\right\} = 0\right)$$

The advective terms in Equation (8) are formulated in non-conservative form in order to be consistent with the non-conservative advective terms in Equation (4) (Kolar and others, 1994). The larger the value of $G$, the more primitive the GWCE will be. Thus, if $G$ is too large, spurious oscillations may arise. However, if $G$ is too small, the solutions will likely be plagued with mass balance errors. A balance must therefore be achieved for an optimal $G$.

Equations (4) and (8) are solved with a Galerkin finite element method. The solution involves three stages (see

Luettich and others, 1991, and Westerink and others, 1992, for details): first, symmetrical weak weighted residual statements are developed for the GWCE and primitive momentum equations; second, the equations are time-discretized, with either two or three time-level schemes applied selectively to different terms within each equation; finally, the finite element method is implemented, by expanding the variables over linear triangular elements, developing discrete equations on an elemental level, assembling global systems of equations, and enforcing boundary conditions.

## BOUNDARY CONDITIONS

The original model allows for the specification at the boundaries of either elevations (enforced in the discrete GWCE equation) or normal velocities (enforced in the discrete momentum equations). We have added the ability to specify transmissive boundary conditions, enforced in the discrete GWCE equation.

Transmissive boundary conditions are imposed by first backtracking from the boundary node in the direction of the incoming wave and then interpolating the elevation from the previous time step at that spatial location. The incident angle of the incoming wave is approximated as,

$$\theta = \text{atan}\left(\frac{v}{u}\right) \tag{9}$$

The wave is backtracked a distance,

$$S = \Delta t\sqrt{gH} \tag{10}$$

in the direction prescribed by $\theta$. Once the backtracked positions $(X_{int}, Y_{int})$ are known, the elevation from the previous time step may be interpolated from the appropriate element. The new elevation at the boundary node may then be set equal to this interpolated old elevation, thus allowing the wave to leave the domain of interest. The transmissive boundary condition should only be imposed if $\hat{v} \bullet \hat{n} \geq 0$ and if the velocities are not relatively small compared to what is expected for a particular simulation.

## REFERENCES


Geller, R.J., 1976, Scaling relations for earthquake source parameters and magnitudes: Bulletin of the Seismological Society of America, v. 66, no. 5, p. 1501-1523.

Kinnmark, I.P.E., and Gray, W.G., 1984, An implicit wave equation model for the shallow water equations: Advances in Water Resources, v. 7, p. 2-14.

Kolar, R.L., Westerink, J.J., Cantekin, M.E., and Blain, C.A., 1994, Aspects of nonlinear simulations using shallow water models based on the wave continuity equation: Computers and Fluids, v. 23, no. 3, p. 523-538.

Luettich, R.A., Westerink, J.J., and Scheffner, N.W., 1991, ADCIRC: an advanced three-dimensional circulation model for shelves, coasts, and estuaries: Dept. of the Army, U.S. Army Corps of Engineers, Washington, D.C.

Lynch, D.R., and Gray, W.G., 1979, A wave equation model for finite element tidal computations: Computers and Fluids, v. 7, no. 3, p. 207-228.

Myers, E.P., 1994, Numerical modeling of tsunamis with applications to the Sea of Japan and the Pacific Northwest: M.Sc. thesis, Department of Environmental Science and Engineering, Oregon Graduate Institute of Science & Technology, Portland, OR.

Westerink, J.J., Luettich, R.Z., Baptista, A.M., Scheffner, N.W., and Farrar, P., 1992,, Tide and storm surge predictions using a finite element model: ASCE Journal of Hydraulic Engineering, v. 118, no. 10, p. 1373-1390.

# CHAPTER 3

# EVIDENCE FOR COSEISMIC SUBSIDENCE AND TSUNAMI INUNDATION DURING THE PAST 3000 YEARS AT SILETZ BAY, OREGON

by
Curt D. Peterson, Mark E. Darienzo, Debra Doyle, and Elson Barnett,
Geology Department, Portland State University

## INTRODUCTION

In this report we summarize the existing geologic evidence of Cascadia earthquakes and some related hazards in the Siletz Bay area of Oregon's central coast (Figure 3.1). The late-Holocene records of episodic coastal subsidence are established from marsh sites in Siletz Bay (Darienzo, 1991; Darienzo and others, 1994). We also describe late Holocene geologic records of anomalous marine-surge deposition in marsh cores from Siletz Bay. The correspondence between episodic subsidence and marine surge deposition is used to test whether apparent paleotsunami inundation resulted from far-field or near-field earthquake sources (Peterson and Darienzo, 1992). Finally, existing beach profile data from the Lincoln City littoral cell (Peterson and others, 1993) are used with estimates of paloesubsidence from Siletz Bay to model potential beach erosion from relative sea-level rise caused by coseismic subsidence. Here the Bruun Rule (Komar and others, 1991) is used to estimate approximate shoreline retreat from predicted, coseismic sea-level rise.

## SCOPE OF WORK


*Figure 3.1. Location of the study area and geographic names used in the text.*

This report consists of a compilation of past paleoseismic-study results and new (extended) mapping of paleotsunami deposits in the Siletz Bay area. Marsh core records of late-Holocene paleosubsidence and paleotsunami deposition in Siletz Bay are reported by Darienzo (1991) and Darienzo and others (1994). In this study we do not assume any particular earthquake source characteristics, such as magnitude or duration. However, an average earthquake recurrence interval is estimated from radiocarbon dated core sequences described in this report. Quantitative analyses of paleotsunami sand mineralogy, grain-size, and organic debris have been performed for selected sites cored during this reconnaissance mapping project. In addition, selected paleosol surfaces in the barrier-spit have been described and radiocarbon dated to establish the prehistoric morphology of the spit. The results from these quantitative analyses are being prepared for publication elsewhere.

Earthquake related hazards of post-subsidence flooding and beach erosion in Siletz Bay are based on estimates of coseismic vertical displacement implied by peat development (paleotidal indicator) in marsh cores (Table 3.1). Verification of the peat development with tidal indicator macrofossils (tree roots and plant rhyzomes) and with tidal indicator microfossils (diatoms) has been performed in Netarts Bay (Darienzo and Peterson, 1990). The application of these paleotidal indicators to infer small amounts of coseismic displacement (less than one meter) on the central Oregon coast has been reported previously (Peterson and Darienzo, 1992). Additional data (unpublished) on regional coastal subsidence associated with the last Cascadia dislocation (about 300 years B.P.) is used to verify local subsidence estimates from the Siletz Bay core sites.

*TABLE 3.1. WETLAND SETTINGS, ELEVATIONS AND PEAT ABUNDANCE IN CENTRAL OREGON BAYS*

| Marsh Settings In Central Oregon Bays | Elevation (m) MTL* | Percent Peaty Visual** | Percent Organics LOI*** | Core Log Key |
|---|---|---|---|---|
| Forest/Shrub | 2.0 ± 0.25 | >80% | >50% | Peat/Tree Roots |
| High Marsh | 1.5 ± 0.25 | 50-80% | 20-50% | Muddy Peat |
| Transitional Marsh | 1.25 ± 0.25 | 20-50% | 10-20% | Peaty Mud |
| Low Marsh | 0.75 ± 0.25 | 5-20% | -10% | Slightly Peaty Mud |
| Colonizing Marsh/ Mud Flat | 0.5 ± 0.25 | 1-5% | <5% | Rooted Mud or Mud |

* Meters above Mean Tidal Level (MTL). Note: that there is significant overlap of marsh setting elevations shown in this regional compilation. Marsh settings at individual marsh sites typically show less variability in tidal elevation. The marsh settings, tidal elevations, percent peaty and percent organics used in this table are compiled from data from several central Oregon bays including Yaquina Bay (Darienzo and Peterson, 1990; Darienzo, 1991; Peterson and Darienzo, 1992).
** Visual estimate of peaty material as percentage of core surface area.
*** Organic weight fraction from Loss On Ignition (LOI).

## FIELD STUDY METHODS

A total of 51 core sites have been logged in late-Holocene marsh deposits of Siletz Bay (Figure 3.2; Table 3.2). The strategy of core site selection was based on tracing the landward limit of apparent deposition of anomalous sand-sheets capping abruptly buried marsh surfaces. Hand coring by gouge cores (2.5 cm diameter) was used for reconnaissance surveying of marsh and sand capping layer (SCL) stratigraphy. Representative sites were vibra-cored (7.5 cm diameter) for radiocarbon dating of peaty layers (Darienzo, 1991). Core depths of one to several meters were limited by either refusal, or termination of peaty deposits in basal sands or barren mud. Recovered cores were logged to the nearest centimeter for lithology, contact relations, paleotidal-level indicators, and SCL thickness (Darienzo, 1991). Marsh cores were taken in high marsh -to spruce wetland settings, 1.5 ±0.5 m above mean tidal level (MTL). Some of the sites have been surveyed into MTL (Darienzo, 1991) but for this report all site elevations are estimated from point elevation data and 1.5 m (5 ft) topogrphic contours on the 1:4800 scale orthophotographic base map (Table 3.2). Errors in the contours are about ±0.8 m (2.5 ft); errors in the point elevation data are ±0.4 m (1.25 ft). The extremely low relief of the marsh sites and density of point elevation data allowed vertical control for nearly all sites to approach ±0.4 m (1.25 ft). Differences between geodetic mean sea level assumed for the base maps and local mean sea level does not exceed 0.45 m (1.5 ft), so total root mean square error on most elevation measurements is about ±0.6 m (2.0 ft).

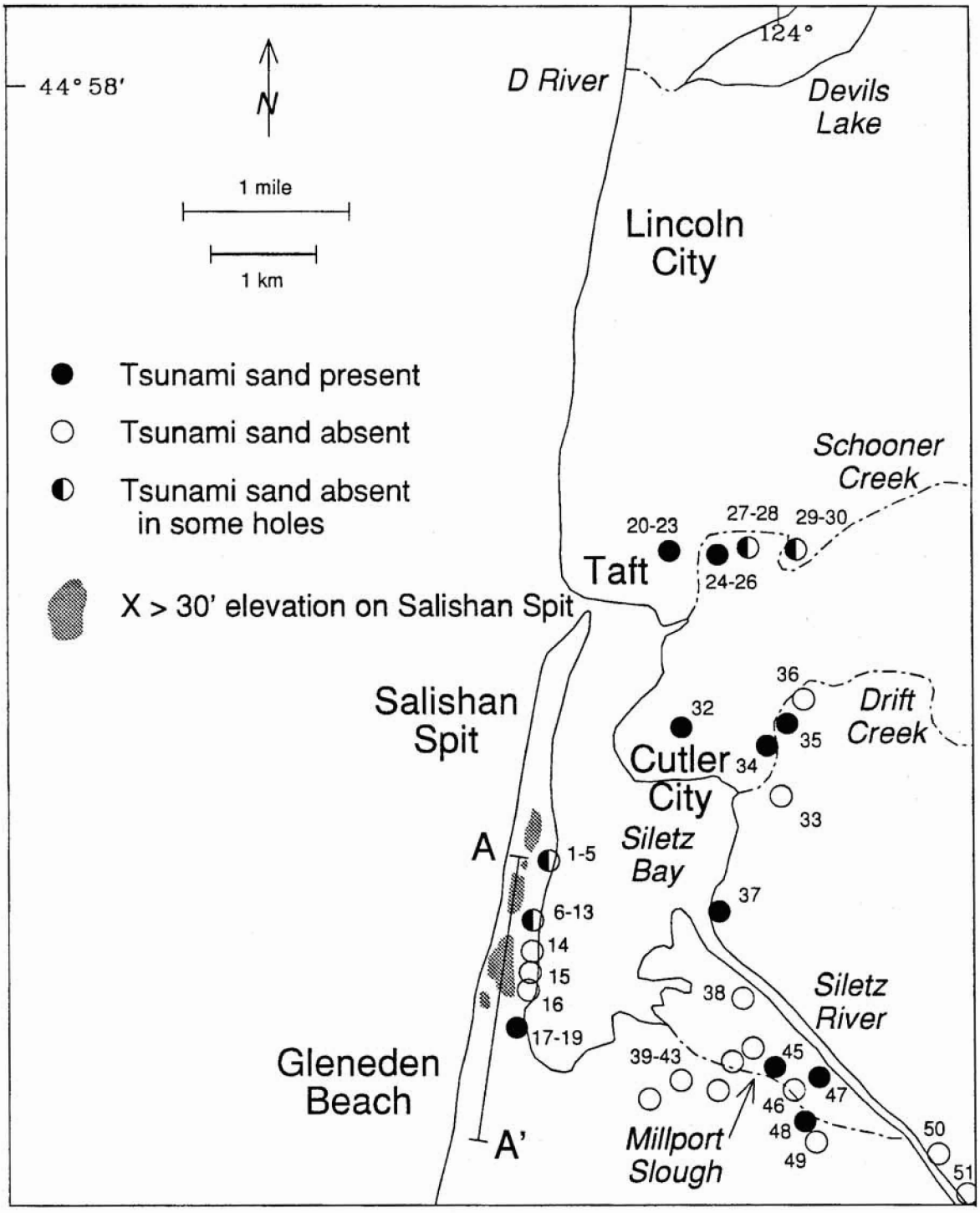


*Figure 3.2. Location of core sites. See the tsunami hazard map for detailed locations and topography.*

*TABLE 3.2 SILETZ BAY CORE SITE DATA (all elevation data is in increments of 0.25 m, but this does not imply accuracy to two decimal places).*

| Core Site | State Plane N | State Plane E | Modern Site Elev. MSL m ±0.25 | Event #1 SCL Isopach (cm) | Event #1* Subsidence m ±0.5 | Event #1 Elev. PMTL m ±0.25 | Event #2 SCL Isopach (cm) | Event #2 Elev. PMTL m ±0.25 | Event #4 SCL Isopach (cm) | Event #4 Elev. PMTL m ±0.25 |
|---|---|---|---|---|---|---|---|---|---|---|
| 1 | 470310 | 7288250 | 1.75 | 0 | 0.75 | 1.5 | 0 | no data | no data | no data |
| 2 | 470730 | 7288470 | 1.5 | 14 | 0.75 | 1.5 | 7 | 0.5 | no data | no data |
| 3 | 470410 | 7288150 | 1.75 | 0 | no data | 1.5 | no data | no data | no data | no data |
| 4 | 470310 | 7288340 | 1.5 | 4 | no data | 1.5 | no data | no data | no data | no data |
| 5 | 470120 | 7288200 | 1.75 | 3 | 0.75 | 1.5 | 5 | 1 | no data | no data |
| 6 | 469810 | 7287840 | 1.75 | 0 | 0.75 | 1.5 | no data | no data | no data | no data |
| 7 | 469600 | 7287710 | 1.75 | 0 | 0.75 | 1.5 | no data | no data | no data | no data |
| 8 | 469390 | 7287580 | 1.75 | 2 | 0.75 | 1.5 | 0 | no data | 7 | 1.5 |
| 9 | 469350 | 7287770 | 1.5 | 1 | 0.75 | 1.5 | no data | no data | no data | no data |
| 10 | 469340 | 7287970 | 1.5 | 0 | no data | 1 | no data | no data | no data | no data |
| 11 | 469310 | 7287660 | 1.75 | 0 | 1 | 1.5 | 0 | 1.5 | 26 | 1 |
| 12 | 469310 | 7287570 | 1.75 | 2 | no data | 1.5 | 0 | no data | 5 | 1 |
| 13 | 469230 | 7287560 | 1.75 | 5 | no data | 1.5 | 2 | 1 | 8 | 1.5 |
| 14 | 468830 | 7287780 | 1.75 | 0 | 1 | 1.5 | 0 | no data | no data | no data |
| 15 | 468180 | 7287610 | 2 | 0 | 0.75 | 1.5 | 0 | no data | no data | no data |
| 16 | 467580 | 7287600 | 1.5 | 0 | no data | 1.5 | no data | no data | no data | no data |
| 17 | 467230 | 7287500 | 2 | 24 | no data | 1.5 | 5 | 1 | 25 | 1 |
| 18 | 466880 | 7287760 | 1.75 | 4 | no data | 1.5 | 3 | 1.5 | 12 | 0.5 |
| 19 | 467220 | 7287740 | 1.5 | 0 | no data | 1.5 | 0 | no data | no data | no data |
| 20 | 480060 | 7292270 | 2.5 | 7 | no data | 2.5 | no data | no data | no data | no data |
| 21 | 480550 | 7292410 | 2 | 4 | no data | 2 | no data | no data | no data | no data |
| 22 | 480570 | 7292320 | 2.5 | 8 | no data | 2.5 | no data | no data | no data | no data |
| 23 | 480690 | 7292510 | 2.5 | 15 | no data | 2.5 | no data | no data | no data | no data |
| 24 | 480998 | 7293495 | 1.75 | 1 | no data | 1.5 | no data | no data | no data | no data |
| 25 | 481160 | 7293550 | 1.75 | 20 | no data | 1.5 | no data | no data | no data | no data |
| 26 | 481280 | 7293620 | 1.75 | 10 | no data | 1.5 | no data | no data | no data | no data |
| 27 | 481090 | 7294650 | 1.75 | 0 | 0.75 | 1.5 | no data | no data | no data | no data |
| 28 | 481390 | 7294940 | 2 | 5 | no data | 1 | no data | no data | no data | no data |
| 29 | 480500 | 7295840 | 1.75 | 5 | no data | 1 | no data | no data | no data | no data |
| 30 | 480540 | 7295860 | 2 | 0 | no data | 1 | no data | no data | no data | no data |
| 31 | **4976140 | **422100 | 2.25 | 0 | no data | 1 | no data | no data | no data | no data |

| Core Site | State Plane N | State Plane E | Modern Site* Elev. MSL m ±0.25 | Event #1 SCL Isopach (cm) | Event #1** Subsidence m ±0.5 | Event #1 Elev. PMTL m ±0.25 | Event #2 SCL Isopach (cm) | Event #2 Elev. PMTL m ±0.25 | Event #4 SCL Isopach (cm) | Event #4 Elev. PMTL m ±0.25 |
|---|---|---|---|---|---|---|---|---|---|---|
| 31 | ***4976140 | ***422100 | 2.25 | 0 | no data | 1 | no data | no data | no data | no data |
| 32 | 476410 | 7292510 | 2 | 0 | 0.5 | 1.5 | no data | no data | no data | no data |
| 33 | 473590 | 7295500 | 1.5 | 0 | 0.75 | 1.5 | 0 | no data | no data | no data |
| 34 | 475450 | 7295400 | 1.75 | 5 | no data | 0.5 | no data | no data | no data | no data |
| 35 | 476090 | 7295850 | 2 | 2 | no data | 1 | no data | no data | no data | no data |
| 36 | 476390 | 7296070 | 2 | 0 | no data | 1.5 | no data | no data | no data | no data |
| 37 | 470900 | 7293400 | 1.5 | no data | 0.75 | 1.5 | 5 | 1 | no data | no data |
| 38 | 468150 | 7294060 | 1.75 | 0 | no data | 1 | no data | no data | no data | no data |
| 39 | 465310 | 7292850 | 1.25 | 0 | no data | 1 | no data | no data | no data | no data |
| 40 | 465240 | 7292970 | 1.5 | 0 | no data | 1 | no data | no data | no data | no data |
| 41 | 465157 | 7292990 | 1.75 | 0 | no data | 1 | no data | no data | no data | no data |
| 42 | 465440 | 7293600 | 1.25 | 0 | no data | 1 | no data | no data | no data | no data |
| 43 | 466220 | 7294510 | 1.5 | 0 | 0.75 | 1.5 | no data | no data | no data | no data |
| 44 | 466050 | 7294180 | 1.25 | 0 | no data | 1 | no data | no data | no data | no data |
| 45 | 465660 | 7295580 | 1.5 | 0 | no data | 1 | 0 | no data | 20 | 1 |
| 46 | 465270 | 7295690 | 1.5 | 0 | no data | 1 | no data | no data | no data | no data |
| 47 | 465460 | 7296590 | 1.75 | 5 | no data | 1.5 | 5 | 1.5 | no data | no data |
| 48 | 464850 | 7296250 | 1.5 | 0 | 0.5 | 1.5 | 0 | no data | 7 | 1 |
| 49 | 464450 | 7296240 | 1.25 | 0 | 0.25 | 1 | no data | no data | no data | no data |
| 50 | 463590 | 7299120 | 2 | 0 | no data | 1.5 | no data | no data | no data | no data |
| 51 | ***4970150 | ***423920 | 2 | 0 | no data | 1 | no data | no data | no data | no data |

* Modern Site Elevation is taken from averaged pasture surface, or 0.5 m below vegetation surface in high marsh as shown the orthophotographic base base map

** Data from selected cores that do not include paleotidal indicators such as barren tidal flat muds or forest soils with no well defined upper or lower elevation limit..

*** UTM coordinates (used for sites immediately east of the study area for easy reference to USGS quadrangles)

*Abbreviations*

MSL=Mean Sea Level

PMTL=Paleo-mean tidal level

## MARSH CORING RESULTS

### SALISHAN SPIT CORE SITES

Core logs from 51 sites in Siletz Bay are shown in Appendix 3.1, and corresponding radiocarbon dates are in Appendix 3.2. The cores were examined for the presence of abruptly buried marsh surfaces and anomalous sand capping layers (SCLs). Beginning with the Siletz Bay back-barrier (Salishan Spit) sites SB1-SB19 there are 16 marsh core sites showing evidence of at least one subsidence event at roughly 0.5 m depth subsurface. Radiocarbon dates (SB17) suggest that this latest Holocene subsidence event at the western end of Siletz Bay corresponds to the last Cascadia dislocation event (300 calendric years ago; Darienzo and others, 1994). Anomalous sand layers (1-15 cm thick) cap this buried peaty horizon in ten of the 19 core sites. Sites SB8, SB11, SB12, SB13, and SB18 also have sand or muddy sand layers above the last subsidence event, possibly representing marine surge overwash or dune slipface advance, not associated with local coseismic subsidence. Additional coring is needed to establish the origin of these young (possibly historic) sandy layers.

Nine of the back-barrier marsh sites have two or more recorded subsidence events denoted by buried peaty horizons (Appendix 3.1). Sites SB11 and SB17 have four to five buried peats each. Upcore transitions include peaty mud to slightly peaty mud, slightly peaty mud to rooted/barren mud, and peaty mud to barren mud. These transitions indicate a range of 0.5 to 1.0 m submergence (Table C.1). The fourth buried peaty horizon in site SB17 (subsurface depth of 220 cm) has a radiocarbon age of about 1,700 Radiocarbon Years Before Present (RCY B.P. or $^{14}$C yr B.P.).

An anomalous sandy layer (2-5 cm thick) occurs within peaty horizons at about 75 cm subsurface depth in core sites SB2, SB5, and SB17. Additional core sites at the eastern margin of the bay also record this anomalous sandy layer, which is not associated with a local paleosubsidence event. The thickest SCL (up to 25 cm thick) found in deep marsh sites SB11, SB17, and SB18 occurs at about 1.5 m depth subsurface. The peat underlying this unusually thick SCL has a radiocarbon date of 1,500 RCY B.P. at site SB17.

The distributions of cores with SCLs appear to correspond to locations either (1) just landward of low passes in the southern end of the barrier spit or (2) along the bay margins of the northernmost back-barrier marsh (Figure 3.2; see tsunami hazard map). These distributions argue for two origins of marine surge deposition, including localized barrier-spit overtopping from the west (sites SB17, and sites SB8, SB12 and SB13) and bay shoreline deposition from the east (sites SB2, SB4 and SB5). SCL deposition is absent along the bay side of the back-barrier marsh south of site SB5. This SCL pinchout to the south implies surge attenuation with increasing distance from either the tidal inlet and/or from the river-tidal channels to the northeast. Additional work is needed to test for possible SCL deposition along the southern bay shorelines, which are presently diked and filled.

### SCHOONER CREEK CORE SITES

A total of eleven marsh cores (SB20-SB31) have been taken from wetlands in back of the Taft Elementary and Intermediate Schools, and along Schooner Creek (Figure 3.2; Appendix 3.1). One anomalous sand horizon (2-10 cm thick) is correlated by relative depth (about 0.5 m subsurface) among the Taft core sites (SB20-SB23). This anomalous sand layer occurs in wetland (forest) soils that are younger than 1,100 RCY B.P. These Taft wetland sites are separated from the bay mouth shoreline to the west by an eolian bay-barrier shoreline (present elevation +3.5 m MSL). The anomalous sandy layer pinches-out to the northeast of site SB23, indicating a marine surge origin from the west, over the bay-shore barrier.

By comparison, SCLs are associated with a buried peaty horizon correlated by depth (about 0.7 cm subsurface) in Schooner Creek marsh sites SB24-SB26, and SB28-SB29 (Appendix 3.1). This SCL reaches a maximum thickness of about 20 cm at a point bar site SB25, where it overlies a peaty horizon dated at about 600 RCY B.P. This SCL is derived from a marine surge which propagated up Schooner Creek from its confluence with the main channel at the bay mouth. The SCLs along Schooner Creek upstream of the sewage treatment plant (see ponds on Plate 3.1) decrease in thickness with distance away from the present channel (sites SB27-SB28, and SB29-SB30).

No evidence of SCL deposition was found upstream of site SB29 where the river valley widens into a broad flood plain (Figure 3.2).

## CUTLER CITY AND DRIFT CREEK CORE SITES

A total of 10 cores were taken in a small wetland locality (represented by core site SB32) due east of Cutler City (Fgure 3.2). This site is presently separated from the flood-tide delta bar to the north by an eolian bay-shore barrier (present elevation +3.3 m MSL). This wetland/pond represents the northernmost limit of a diked tidal marsh which previously connected to the Drift Creek channel to the south. There is no evidence of SCL deposition over the buried wetland horizon (about 0.3 m depth subsurface) in any of the cores at a radius of 20-30 m from site SB32. The buried peaty horizon at SB32 is dated at about 500 RCY B.P. (Appendix 3.1). The lack of any sand or organic debris cap on top of the subsidence event contact argues against substantial marine-surge overtopping of the bay-shore barrier at Cutler City during the last coseismic subsidence event.

About a dozen core sites were occupied in pasture fields on either side of Drift Creek (Figure 3.2). Four representative core sites (SB33-SB36) were logged from the lower Drift Creek marshes (Appendix 3.1). At least three paleosubsidence intervals are recorded at SB33. Upcore transitions of peaty mud -to- rooted/barren mud indicate subsidence displacements of 0.5-1.0 m (Table 3.1). Thin SCLs (1-5 cm thickness) are associated with a shallow subsidence event contact (0.8 m depth) in core sites adjacent to the Drift Creek channel (sites SB34 and SB35). This subsidence interval is assumed to correlate with that dated at the north end of the Cutler City marsh (site SB33). The SCLs at sites SB34 and SB35 pinchout within 50 m distance away from the present channel levee. No SCLs were found upstream of SB35, however recent lateral migrations of the Drift Creek channel have reduced the SCL record preservation upstream of SB36. Overall, the SCL development in the Drift Creek marshes are comparatively weak, suggesting substantial attenuation of the marine surge or a lack of available sand supply in the Drift Creek tidal channel-marsh system.

## SILETZ RIVER AND MILLPORT SLOUGH CORE SITES

A total of 15 core sites (SB37-SB51) are logged from the Siletz River and Millport Slough areas at the southeastern end of Siletz Bay (Figure 3.2). The stratigraphy in this area is complex, with low preservation potential of paleoseismic records at sites adjacent to the Siletz River and Millport Slough channels. The longest intact sections (greater than 3 m depth subsurface) are found between the Siletz and Millport channels at the upstream terminus of the Millport Slough marsh (sites SB45 and SB48). Site SB48 records at least six subsidence events in the last 2,900 RCY B.P. (Appendix 3.1). Upcore transitions of peaty muds or slighty peaty muds -to- rooted/barren muds indicate paleosubsidence displacements of 0.5-1.2 m. Three thick SCLs (5-20 cm in thickness) at sites SB45 and SB48 are associated with subsidence intervals older than a dated peaty horizon (1,600 RCY B.P.) at 150 cm subsurface depth.

By comparison, two SCLs are well developed in the upper one meter section at site SB47 adjacent to the Siletz River channel (Appendix 3.1). The lower SCL at SB47 and the only SCL at SB37 are both developed within a peaty section, i.e., they are not associated with local subsidence. SCL deposition was not observed in marsh cores (SB50 and SB51) upstream of the confluence of the Millport Slough and Siletz River channels (Figure 3.2). Apparent SCL deposition is also absent from core sites along the southeastern margin of Siletz Bay (sites SB39-SB42). Like the Schooner and Drift Creek localities, the SCLs in the Millport Slough marsh are best developed adjacent to the paleotidal channel. Overbank surge attenuation and/or diminished sand supply in back-levee environments are potential causes of SCL pinchouts with distance away from the tidal channels.

The lack of SCL development in the upper one meter sections of the Millport Slough marsh sites SB43-SB46 and SB48 is unexpected. It is not known whether this reflects (1) a different bay morphology prior to 1,000 years ago, or (2) more energetic SCL depositional events prior to 1,000 years ago. Available field evidence might support both hypotheses. For example, particularly thick SCLs are found at 150 cm depth at the spit sites (SB11 and SB17). Alternatively, a lack of marsh development below one meter depth at sites SB42, SB44, and SB45 attests to deeper tidal-flat environments under what is now the Millport Slough marsh. This area might have been more exposed to marine surge propagation during the earlier SCL deposition events.

Three core sites SB39-SB41 (Figure 3.2) were taken at the foot of a debris flow chute along the southeastern margin of Millport Slough marsh. At least two debris flow events are shown in the cores (Appendix 3.1). The debris flows are separated by two subsidence intervals in SB41 and by one subsidence interval in SB39. The bottom contacts of these debris flow deposits are not associated with peaty horizons. Therefore, it is not possible to show any correlation between paleosubsidence and debris flow deposition at these core sites. Additional work is needed to test potential correspondence between debris flow deposition (upland land sliding) and coseismic subsidence of marsh surfaces in Siletz Bay.

## DISCUSSION

### EARTHQUAKE RECURRENCE INTERVAL

The subsidence events and associated marine surge (SCL) deposition recorded in the Siletz Bay marsh cores are interpreted to represent near-field tsunamigenic dislocations of the Cascadia megathrust (Darienzo, 1991; Darienzo and others, 1994). The paleosubsidence and tsunami deposition stratigraphy at sites SB17 and SB48 are interpreted as follows: event #1 subsidence and tsunami inundation at core depths of about 0.5 m subsurface (at 300 years B.P.); event #2 tsunami inundation with no subsidence at 0.75-1 m core depths; event #3 subsidence with no observed tsunami deposition at 1-1.25 m core depths (younger than 1,300 RCY B.P.); event #4 subsidence and tsunami inundation at 1.5 m core depths (younger than 1,600 RCY B.P.); event #5 subsidence and tsunami inundation (younger than 1,800 RCY B.P.); event #6 subsidence at about 2.5 m core depth, and event #7 subsidence with tsunami inundation at about 3.0 m core depth (younger than 2,800 RCY B.P.).

Although event #2 was not associated with local subsidence in Siletz Bay, it appears to have caused subsidence in Yaquina and Alsea Bays to the south (Darienzo and Peterson, 1994). From the standpoint of tsunami runup and potential shaking in Siletz Bay, this event should probably be included in estimates of average recurrence intervals between events in the Lincoln City area. Therefore, in Siletz Bay a total of seven events are recorded roughly between 2,800 and 300 years. This is equivalent to six recurrence intervals in 2,500 years or an average recurrence interval of about 400 years between earthquake events. The actual recurrence intervals between specific events cannot be resolved by carbon-14 dating, but might vary by several hundred years from the average. The last Cascadia earthquake event recorded along the northern Oregon coast occurred about 300 years ago (Darienzo and others, 1994).

### ESTIMATES OF COSEISMIC SUBSIDENCE IN SILETZ BAY

The subsidence aspects of the Cascadia earthquakes are probably the least life-threatening of the earthquake hazards. However, post-subsidence bay flooding and ocean beach erosion might last for decades after a Cascadia earthquake. The persistent flooding and beach erosion could impact bay circulation and marsh habitat, drainage systems and roads, and the stability of sea cliffs and beach foredunes (Peterson and Priest, 1991).

Measures of past coseismic subsidence displacements in Siletz Bay can be used to estimate future coseismic subsidence hazards for the bay and adjacent coastlines. Estimates of vertical displacement (sea-level rise) corresponding to the last several subsidence events are based on upcore transitions of paleotidal indicators (Table 3.1) as discussed in the Results sections. Paleosubsidence estimates range from 0.5 to 1.0 meters for core sites along the Salishan Spit, Schooner Creek, Drift Creek, and the Millport Slough. These estimates do not include event #2 which did not produce apparent subsidence in Siletz Bay. Based on the Siletz Bay core data, a potential coseismic subsidence of 0.75±0.25 m should be expected for the next Cascadia dislocation event.

Recently, there has been some speculation that the subsidence events recorded in Siletz Bay are possibly produced by local faults or folds that might exist only within the bay (Robert Yeats, pers. comm., 1994). To test this hypothesis we compare the estimated subsidence associated with the last (youngest) subsidence event from several northern Oregon sites (Table 3.3). A plot of estimated subsidence versus site distance from the trench shows a clear trend of increasing subsidence with increasing distance from the trench in northern Oregon (Figure 3.3).

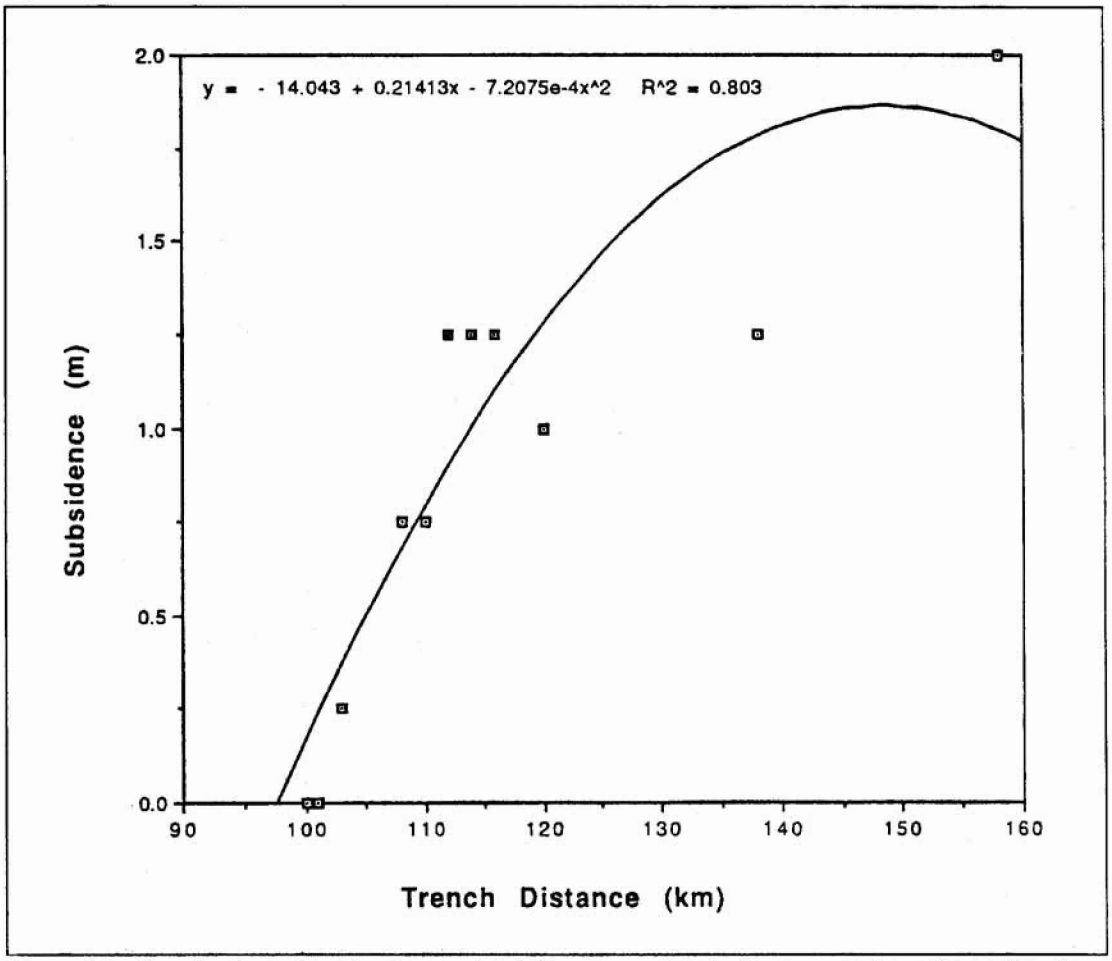


*Figure 3.3. Plot of estimated coseismic coastal-subsidence associated with youngest Cascadia earthquake (300 years B.P.) as a function of site distance (due east) from the base of the continental slope (buried trench). Second order polynomial "best fit curve" yields about 0.8 $r^2$ correlation coefficient.*

These results demonstrate that the most recent coseismic subsidence observed in Siletz Bay is due to a regional elastic response rather than from local fault/fold deformation within the bay.

*TABLE 3.3. COASTAL COSEISMIC SUBSIDENCE FOR THE LAST CASCADIA-DISLOCATION EVENT IN NORTHERN OREGON*

| **Location** | **UTM coordinates.** |
|---|---|
| **Subsidence (m)** | **downcore/transition** |
| A. Young's Bay | 433500, 5111700 |
| 1. (1-1.5) | mud/peat |
| B. Columbia River | |
| 1. Blind Slough | 455800, 5116400 |
| (2) | mud/peat with spruce roots |
| C. Necanicum | |
| 1. Core site 2 | 428900, 5092300 |
| (0.5-1) | peaty mud/muddy peat with tree roots |
| D. Netarts | |
| 1. Site 5 | 424400, 5024200 |
| (1-1.5) | mud with brackish-marine diatoms/peat with freshwater diatoms |
| 2. Oyster Farm | 426800, 5029900 |
| (1-1.5) | mud with *Triglochin*/muddy peat with Juncus |
| 3. Wee Willies | 427200, 5027700 |
| (1-1.5) | mud/peaty mud |
| E. Nestucca | |
| 1. Nestucca Duck | 425500, 5004200 |
| (1-1.5) | mud/muddy peat |
| F. Siletz | |
| 1. Salishan House | 418700, 4971500 |
| (0.5-1) | slightly peaty mud/25cm sand layer/peaty mud |
| 2. Drift Creek | 421100, 4973300 |
| (0.5-1) | mud/peaty mud |
| G. Yaquina | |
| 1. Conser 1 | 427200, 4938300 |
| (0.5-1) | mud/slightly peaty mud |
| H. Alsea | |
| 1. AB10 | 419000, 4918700 |
| (>0) | mud (5-10 cm thick)/slightly peaty mud |
| 2. AB2 | 417500, 4919300 |
| <0.5 | mud (5-10 cm thick)/peaty mud |

Using a best fit relation for the regional subsidence data (Figure 3.3) the Siletz Bay locality (about 110 km from the trench) corresponds to 0.5-1.0 m subsidence. This result confirms the predicted coseismic subsidence estimated locally from the Siletz Bay cores. This magnitude of potential coseismic subsidence needs to be factored into long-term flood zones in the Siletz Bay area. For example, annual and 100 year flood levels in tidally influenced areas would reach about one meter higher than those currently predicted following a coseismic subsidence event.

## PALEOTSUNAMI RUN-UP IN SILETZ BAY

The core record of SCL deposition in the salt marshes represents the minimum inundation distances reached by paleotsunamis in Siletz Bay. For example, older stratigraphic sequences (subsidence events) are not preserved along some tidal channel margins in Siletz Bay. Core sites in these areas only record the last one or two paleotsunami events. There is some tentative field evidence that earlier paleotsunami surges, such as that associated with Cascadia earthquake event #4 (between 1600 and 1300 RCY B.P.), were more energetic than the better recorded paleotsunami surge(s) associated with Cascadia earthquake event #1 (300 RCY B.P.). Furthermore, the sand deposited by a tsunami surge is dependent on available sand supply, distance of surge transport, and very-local conditions of surge turbulence and sand deposition. Paleotsunami surge flooding is likely to have extended further inland than those sites that record SCL deposition.

The distribution of SCL deposition in Siletz Bay indicates widespread paleotsunami flooding of low-lying bay marsh and shorelines west of Highway 101. Channel levee overtopping is also demonstrated along Schooner Creek, Drift Creek, and the Siletz River at distances of at least one kilometer upriver of the Highway 101 crossings. At least one paleotsunami surge (probably event #1) locally overtopped the downtown Taft area (at an elevation of +3.5 m MSL) directly inshore of the present bay mouth. However, this paleotsunami did not substantially overtop the Cutler City barrier-ridge at about 3.3 m MSL elevation. Further attenuation of the most recent paleotsunami surge is indicated by very-restricted SCL deposition in Drift Creek and along the bay marshes at the south end of the Salishan Spit. However, well-developed SCLs along the Siletz River marshes upstream of the Highway 101 bridge suggest effective surge propagation up the Siletz River channel.

Finally, apparent paleotsunami overtopping of the Salishan Spit is recorded at several core sites located just landward of present low-passes in the barrier dunes. These low passes are presently between six and eight meters in elevation. By comparison, there is no evidence of the most recent paleotsunamis (Cascadia earthquake events #1 and #2) leaving beach sand deposits in marshes just landward of the highest dune ridges (greater than 10 m elevation) at the south end of the spit. Additional work is needed to constrain paleotsunami runup estimates from apparent localized overtopping of the Salishan Spit. See Priest and others, this volume, for further discussion of the overtopping evidence.

## POST-SUBSIDENCE BEACH EROSION IN THE LINCOLN CITY LITTORAL CELL

The active beach-sand deposits in the Lincoln City littoral cell (Figure 3.2) act as a buffer to winter wave erosion of the shoreline. Specifically, the beach sand dissipates wave energy which attacks the base of the unconsolidated marine terrace deposits (sea cliffs) and/or foredunes. Over a period of years the loss of beach sand translates into increased shoreline erosion and retreat. Beach sand deposits in the Lincoln City littoral cell (Figure 3.1) have been profiled in eight across-shore traverses from Roads End to Fogerty Creek (Peterson and others, 1993). The profiles extend from the base of the sea cliff, or sand dunes along Salishan Spit, to the beach toe or inner surf zone. The accumulation and elevation of the beach deposits correspond to local conditions of sand supply, wave energy and mean sea level.

Following a coseismic subsidence event in the central Cascadia margin the Lincoln City littoral cell should experience beach sand loss due to the abrupt rise in sea level. Several models of beach erosion resulting from sea-level rise have recently been reviewed with regards to potential global sea-level rise (Komar and others, 1991). One of the earliest models (Bruun, 1962) appears to be most applicable to the case of coseismic sea-level rise along the Lincoln City area beaches. Bruun's model of beach retreat (R) resulting from sea level rise (S) is based on the displacement of onshore beach sands (berm height B) to the offshore as the beach establishes a new equilibrium

profile. The beach sand is displaced over the profile length (L) to the offshore to a maximum water depth of sand displacement (h). The relation is thus R={L/(B+h)}S.

For this analysis we use a sea-level rise of 0.75 m and a maximum water depth 15 m below sea level (Peterson and Burris, 1993). Beach backshore heights are taken at the half-way point between the mid-beach face and the back edge of the beach. This point generally corresponds to the backshore just landward of the summer berm. The profile length (about one kilometer) is measured from the beach backshore out to the 15 m water depth on NOAA bathymetric charts. Estimated beach retreat from a 0.75 m coseismic subsidence event in the Lincoln City cell is on the order of 40-45 meters (Table 3.4). Summer backshore widths in the littoral cell presently range from 20 to 70 meters. Additional work is needed to establish the sensitivity of the Bruun model to variable input parameters for the Lincoln City littoral cell. Potential net sand loss from the Lincoln City cell, around Cascade Head or into Siletz Bay, is not considered in this analysis, but could increase the estimates of local beach retreat (Komar and others, 1991).

*TABLE 3.4. ESTIMATED BEACH RETREAT (all numbers are in meters; R={L/(B+h)}S, where R = retreat, L= profile length, B = beach berm height, h = maximum water depth of sand displacement = 15 m, and S = sea level rise from coseismic subsidence = 0.75 m. Note that a subsidence of 1 m, assumed for tsunami run-up scenarios 1 and 2 would yield retreats 25 percent larger than those listed here).*

| UTM | Retreat | Backshore |
|---|---|---|
| 4985000 | 45.83 | 51.10 |
| 4981000 | 46.70 | 58.50 |
| 4977310 | 45.45 | 36.20 |
| 4974480 | 44.03 | 62.50 |
| 4969550 | 39.94 | 38.50 |
| 4966500 | 44.57 | 69.76 |
| 4965700 | 43.33 | 22.57 |
| 4965460 | 39.77 | 60.55 |

| UTM | R | L | B | S | Backshore to berm (m) | BEACH WIDTH (m) | MTL to 15 m depth |
|---|---|---|---|---|---|---|---|
| 4985000 | 45.83 | 1051.1 | 2.20 | 0.75 | 51.10 | 127 | 1000 |
| 4981000 | 46.70 | 1058.5 | 2.00 | 0.75 | 58.50 | 130 | 1000 |
| 4977310 | 45.45 | 1036.2 | 2.10 | 0.75 | 36.20 | 174 | 1000 |
| 4974480 | 44.03 | 1062.5 | 3.10 | 0.75 | 62.50 | 167 | 1000 |
| 4969550 | 39.94 | 1038.5 | 4.50 | 0.75 | 38.50 | 66 | 1000 |
| 4966500 | 44.57 | 1069.77 | 3.00 | 0.75 | 69.76 | 147 | 1000 |
| 4965700 | 43.33 | 1022.58 | 2.70 | 0.75 | 22.57 | 55 | 1000 |
| 4965460 | 39.77 | 1060.55 | 5.00 | 0.75 | 60.55 | 128 | 1000 |

The potential beach retreats (estimated above) and the corresponding backshore widths of the present beaches are plotted as a function of location (UTM) in Figure 3.4. Following a coseismic subsidence event of 0.75 m the

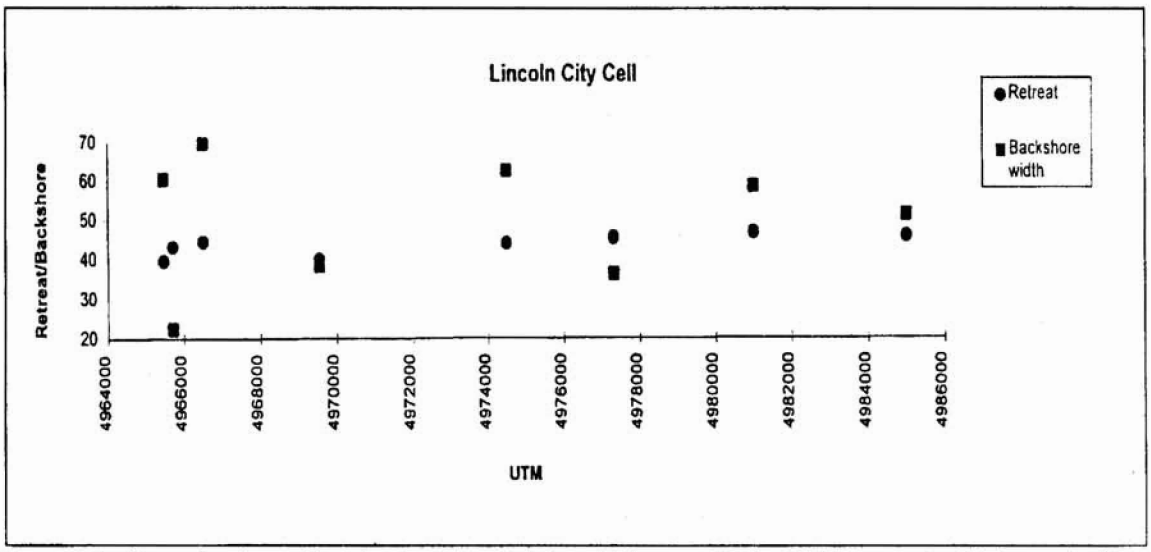


*Figure 3.4. Plots of estimated beach retreat (meters) from 0.75 m coseismic subsidence and width (meters) of modern beach backshore (to seasonal berm) at eight beach profile sites in the Lincoln City littoral cell, from Fogerty Creek (UTM-N 4964000) to Roads End (UTM-N 4986000); (see Figure 3.2 for littoral cell location).*

ensuing beach erosion is estimated to remove most of the summer beach backshore buffer. No beach backshore

buffer is expected to survive during winter months of high wave energy and seasonal sand transport to the offshore. Due to assumed global sea-level rise of about 2 mm per year during the last 300-year interseismic period the Lincoln City sea cliffs would experience a net 0.5 m rise in sea level from the previous (coseismic) high-sea-level stand. Wave-attack undermining of present terrace sea cliffs, foredunes and shoreline protection structures would be expected to greatly accelerate shoreline retreat and slope failures in the Lincoln City littoral cell.

## ACKNOWLEDGMENTS

This study was funded in part through contract from the Oregon Department of Geology and Mineral Industries (see acknowledgments section of Priest and others, this volume, for funding sources). Additional support was provided by Oregon Sea Grant #NA36RG0451.

## REFERENCES

Bruun, P., 1962, Sea level as a cause of shore erosion: Journal of Waterways and Harbors Division, Amer. Society of Civil Engineers, v. 88:, p. 117-130.

Darienzo, M.E., 1991, Late Holocene paleoseismicity along the northern Oregon coast: unpublished Ph.D. Thesis, Portland State University, 168 p.

Darienzo, M.E., and Peterson, C.D., 1990. Episodic tectonic subsidence of late-Holocene salt marsh sequences in Netarts Bay, Oregon, Central Cascadia Margin, USA.: Tectonics, v. 9, p. 1-22.

Darienzo, M.E., Peterson, C.D., and Clough, C., 1994. Stratigraphic evidence for great subduction zone earthquakes at four estuaries in northern Oregon: Journal of Coastal Research, v. 10, p. 850-876.

Komar, P.D., Lanfredi, N., Baba, M., Dean, R.G., Dyer, K., Healy, T., Ibe, A.C., Jterwindt, H.J., and. Thom, B.G, 1991, The response of beaches to sea-level changes: a review of predictive models: Journal of Coastal Research, v. 7, p. 895-921.

Peterson, C.D., and Burris, W.K., 1993, Evaluation of littoral sediment composition and volume, Coos Bay-Umpqua littoral subcell, Oregon: Report to U.S. Army Corps of Engineers, Portland District, Portland, Oregon. 20 p.

Peterson, C.D. and Darienzo, M.E., 1992, Discrimination of flood, storm and tectonic subsidence events in coastal marsh records of Alsea Bay, Central Cascadia Margin, USA: U.S. Geological Survey Open-File Report, OF91-441-C, 53 p.

Peterson, C.D., Darienzo M.E., Burns, S.F., and Burris, K., 1993. Field trip guide to Cascadia paleoseismic evidence along the northern Oregon coast: Evidence of subduction zone seismicity in the central Cascadia margin. Oregon Geology, v. 55, p. 99-114.

Peterson, C.D., Darienzo, M.E., Hamilton, D., Pettit, D.J., Yeager, R.K., Jackson, P.L., Rosenfeld, C.L., and Terich, T.A., 1994, Cascadia beach-shoreline data base, Pacific Northwest Region, USA: Oregon Department of Geology and Mineral Industries, Open-File Report O-94-2, 29 p., and 3 digital database files.

Peterson, C.D., and Priest G.R., 1991. Initiative for the focus of a coastal geology program on catastrophic coastal hazards in the Cascadia margin of the U.S. Pacific Northwest *in* Good, J.W., and Ridlington, S.S., eds., Coastal natural hazards, science, engineering and public policy: Oregon Sea Grant ORESU-B-92-001, Corvallis, Oregon, p. 33-38.

## APPENDIX 3.1: CORE LOGS FOR MARSH SITES IN THE SILETZ BAY AREA

KEY


Peat


Muddy to sandy peat


Peaty mud to sand


Slightly peaty mud to sand


Rooted mud to sand


Slightly rooted to barren mud


Slightly rooted to barren sand


Tsunami deposit


Debris flow

a abrupt contact
g gradual contact
sl sand laminae
tri triglochin rhizomes

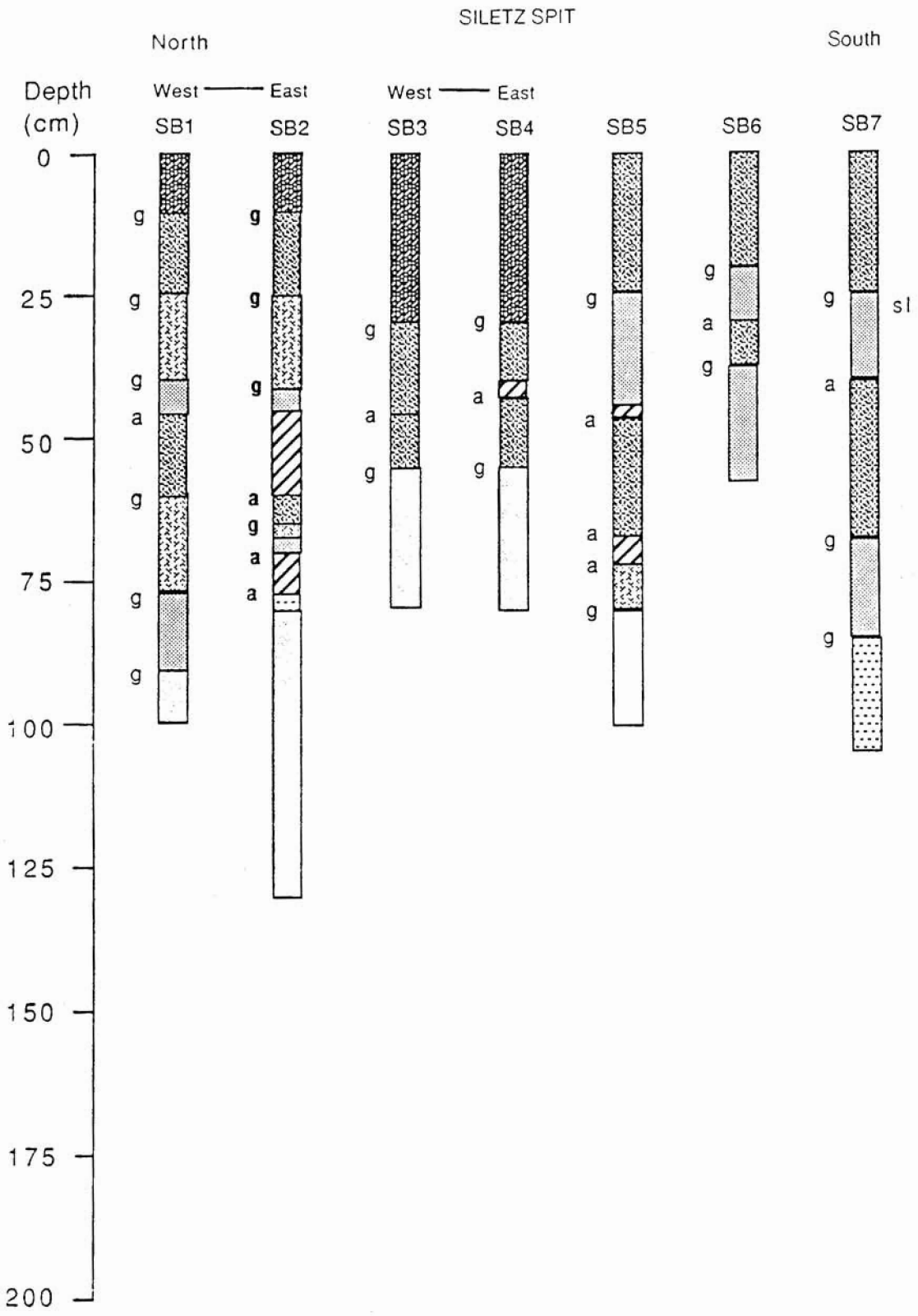
SILETZ SPIT
North
South
Depth
(cm)
West
East
West
East
SB1
SB2
SB3
SB4
SB5
SB6
SB7
0
25
50
75
100
125
150
175
200
g
a
sl

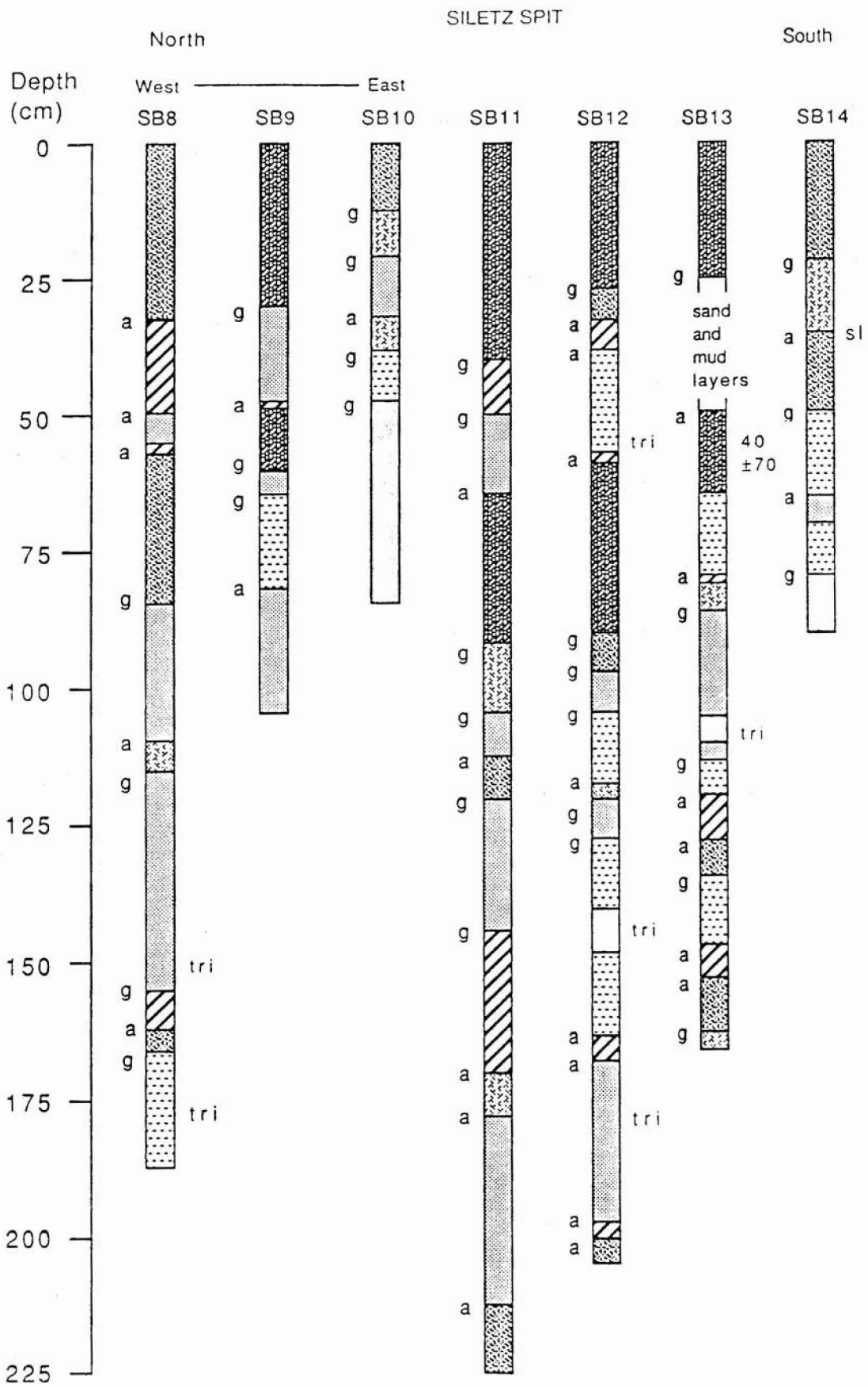
SILETZ SPIT
North
South
Depth (cm)
West
East
SB8
SB9
SB10
SB11
SB12
SB13
SB14
0
25
50
75
100
125
150
175
200
225
tri
sand and mud layers
40 ±70
sl


250
275
a
a
g

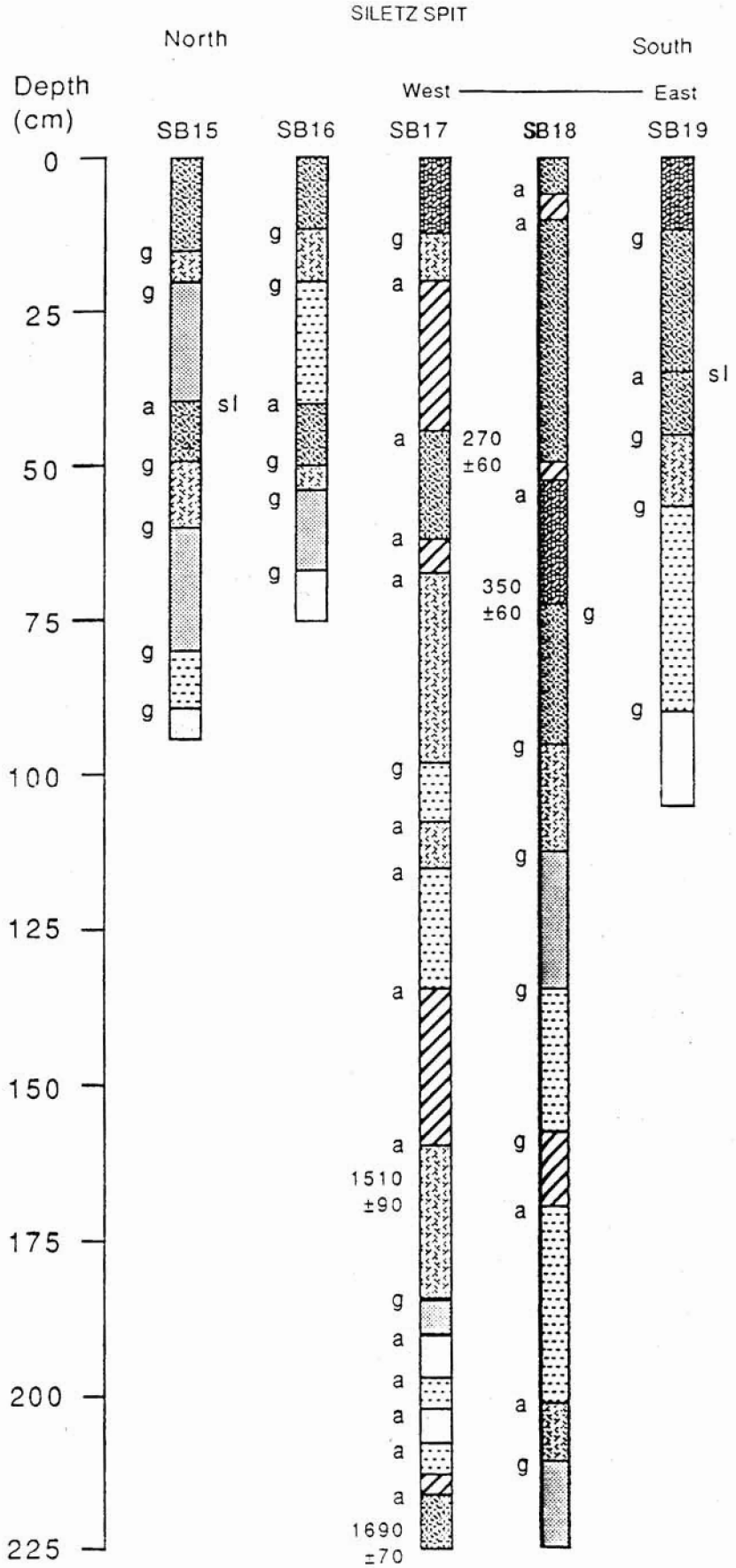
SILETZ SPIT
North
South
Depth (cm)
West
East
SB15
SB16
SB17
SB18
SB19
0
25
50
75
100
125
150
175
200
225
sl
270 ±60
350 ±60
1510 ±90
1690 ±70

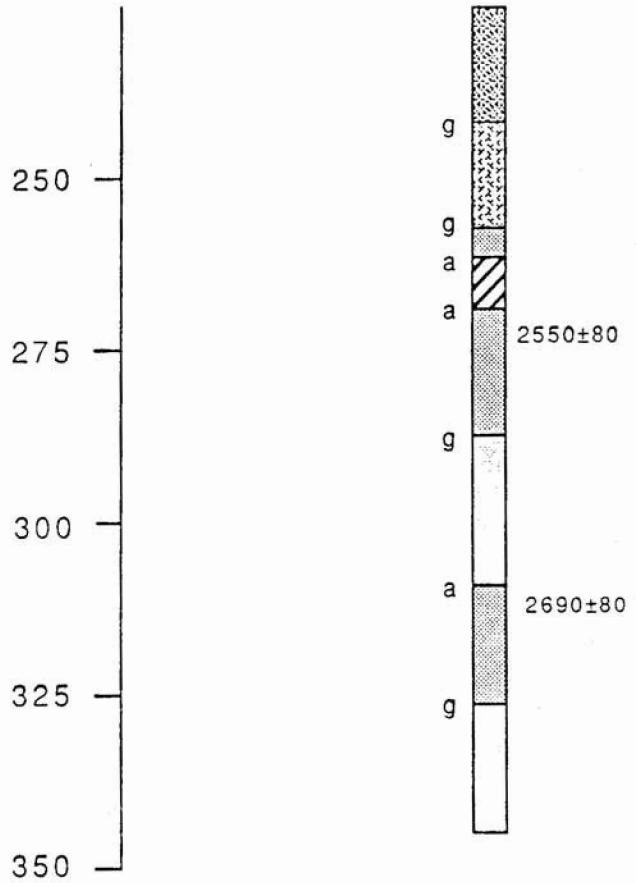
250
275
300
325
350
g
g
a
a
2550±80
g
a
2690±80
g

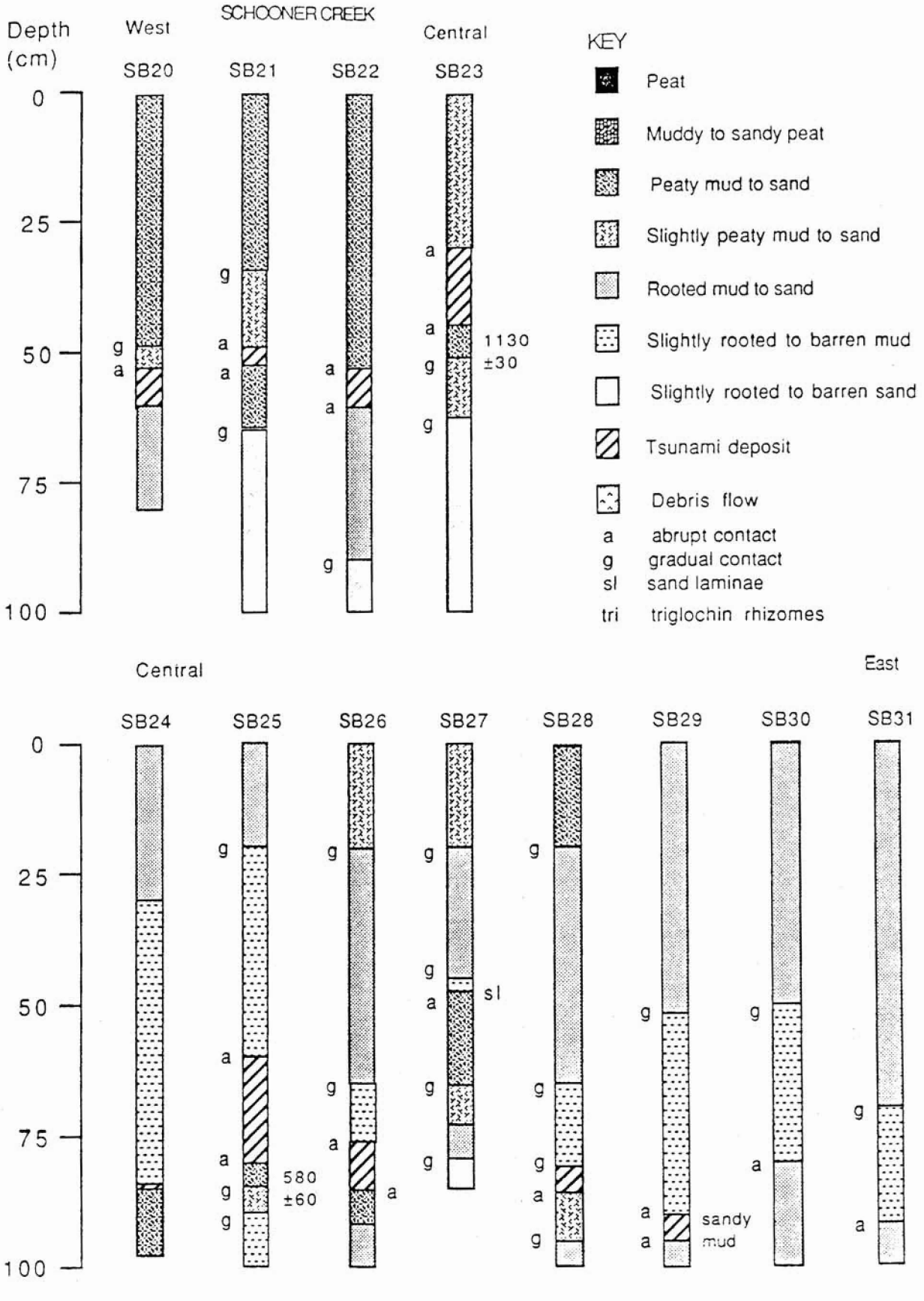
SCHOONER CREEK
Depth (cm)
West
Central
SB20
SB21
SB22
SB23
0
25
50
75
100
1130 ±30
KEY
Peat
Muddy to sandy peat
Peaty mud to sand
Slightly peaty mud to sand
Rooted mud to sand
Slightly rooted to barren mud
Slightly rooted to barren sand
Tsunami deposit
Debris flow
a abrupt contact
g gradual contact
sl sand laminae
tri triglochin rhizomes
Central
East
SB24
SB25
SB26
SB27
SB28
SB29
SB30
SB31
580 ±60
sl
sandy mud

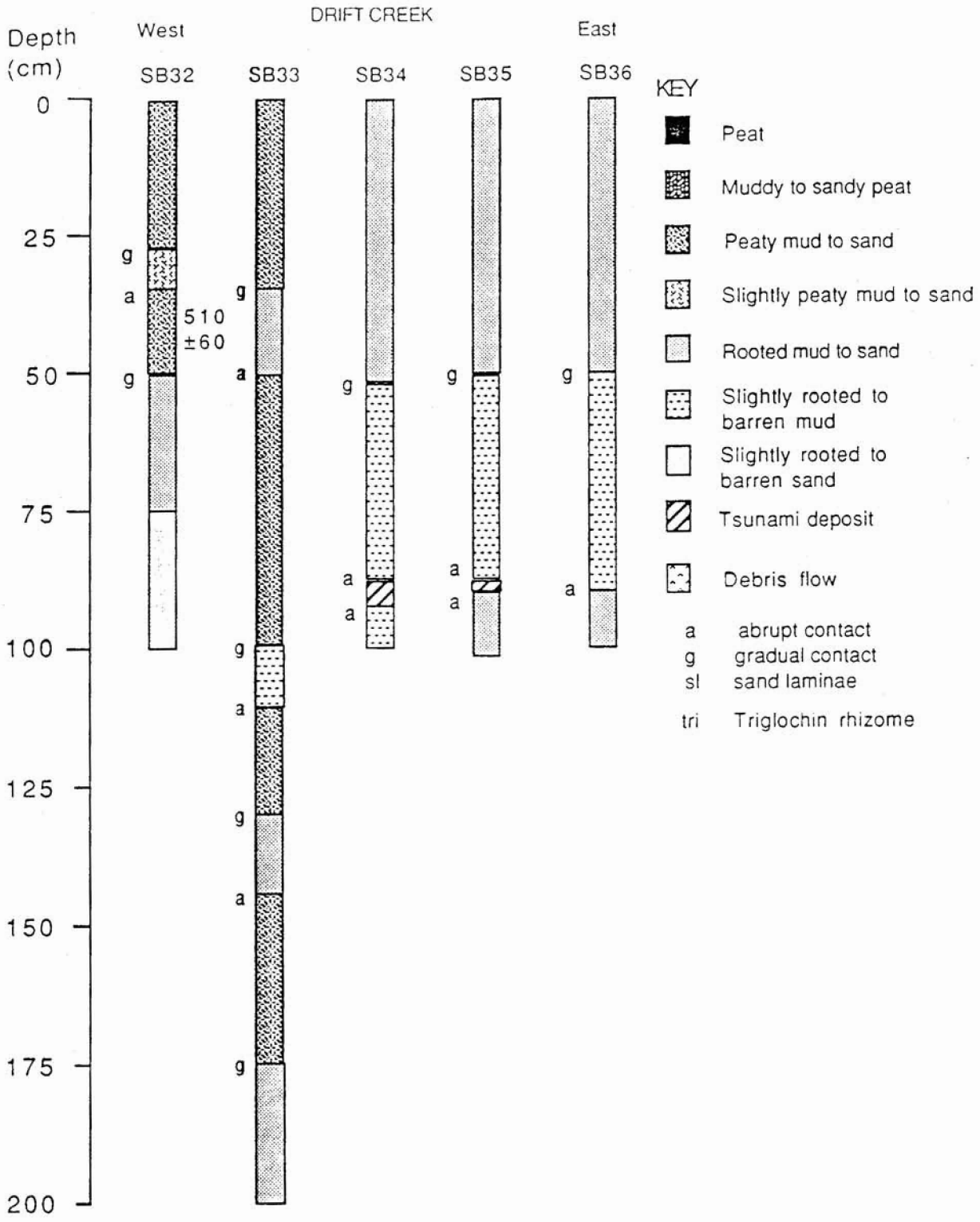
DRIFT CREEK
Depth (cm)
West
East
SB32
SB33
SB34
SB35
SB36
0
25
50
75
100
125
150
175
200
g
a
510 ±60
KEY
Peat
Muddy to sandy peat
Peaty mud to sand
Slightly peaty mud to sand
Rooted mud to sand
Slightly rooted to barren mud
Slightly rooted to barren sand
Tsunami deposit
Debris flow
a abrupt contact
g gradual contact
sl sand laminae
tri Triglochin rhizome

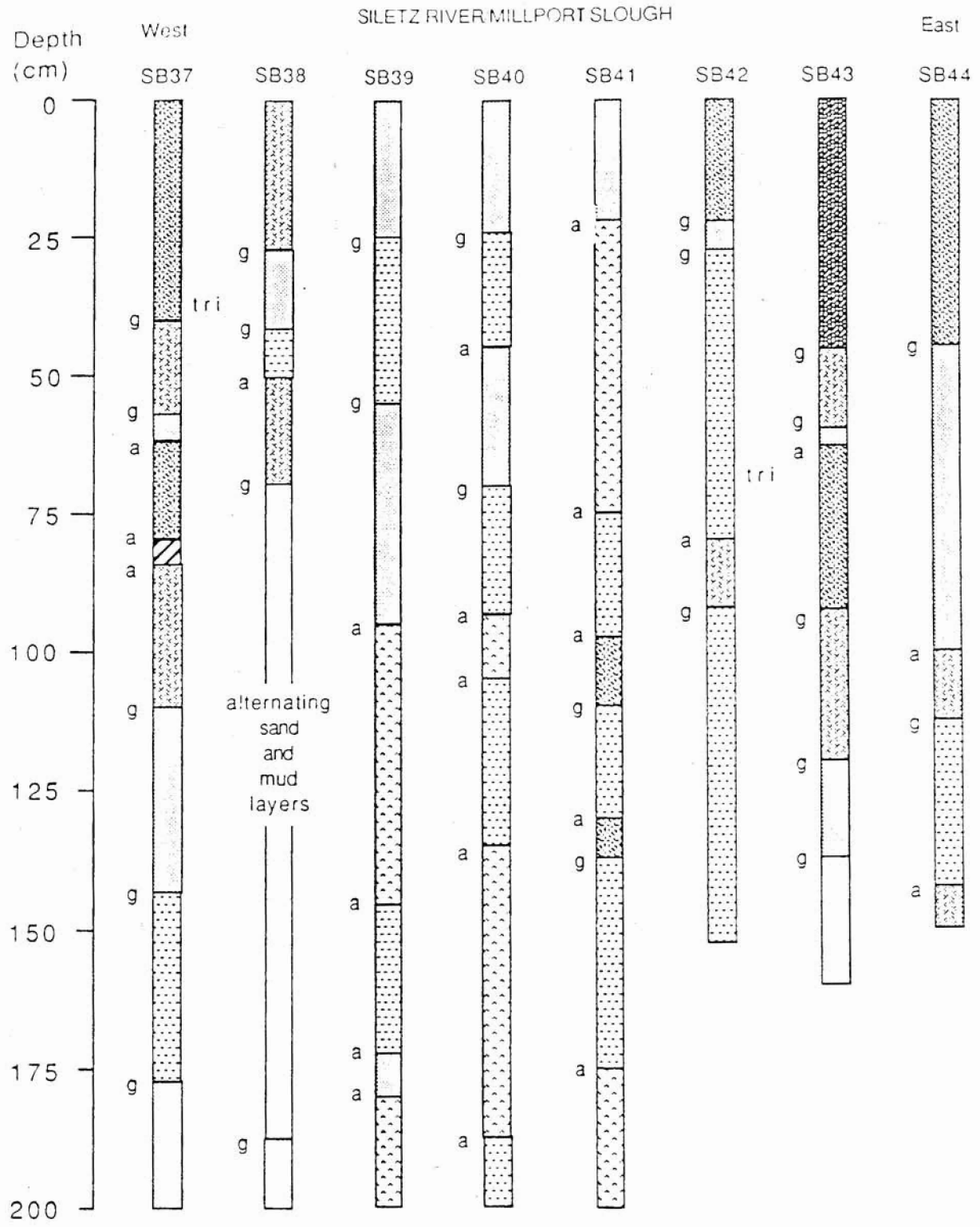
SILETZ RIVER MILLPORT SLOUGH
Depth (cm)
West
East
SB37
SB38
SB39
SB40
SB41
SB42
SB43
SB44
0
25
50
75
100
125
150
175
200
tri
alternating sand and mud layers

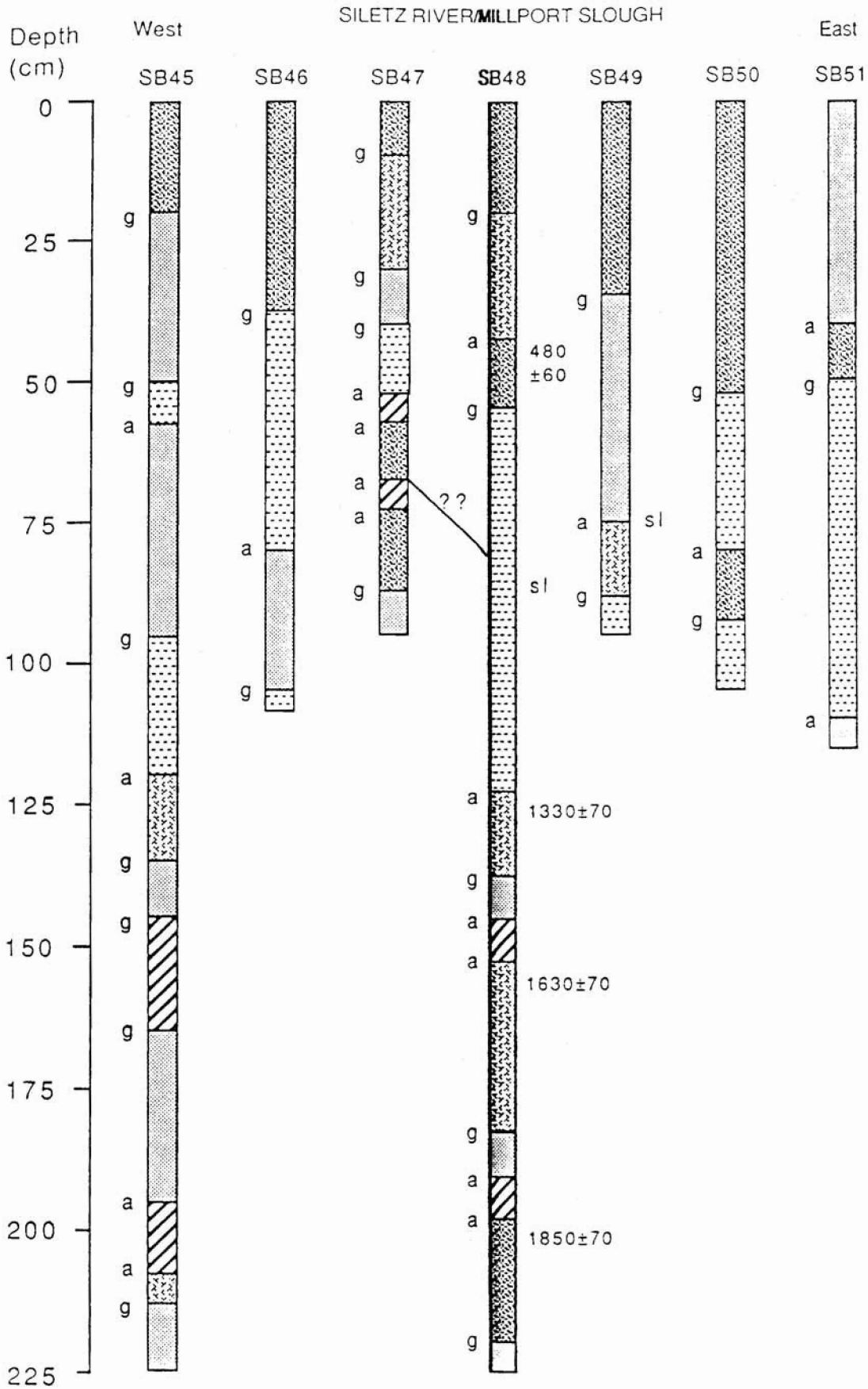
SILETZ RIVER/MILLPORT SLOUGH
Depth (cm)
West
East
SB45
SB46
SB47
SB48
SB49
SB50
SB51
0
25
50
75
100
125
150
175
200
225
??
480 ±60
1330±70
1630±70
1850±70
sl
sl

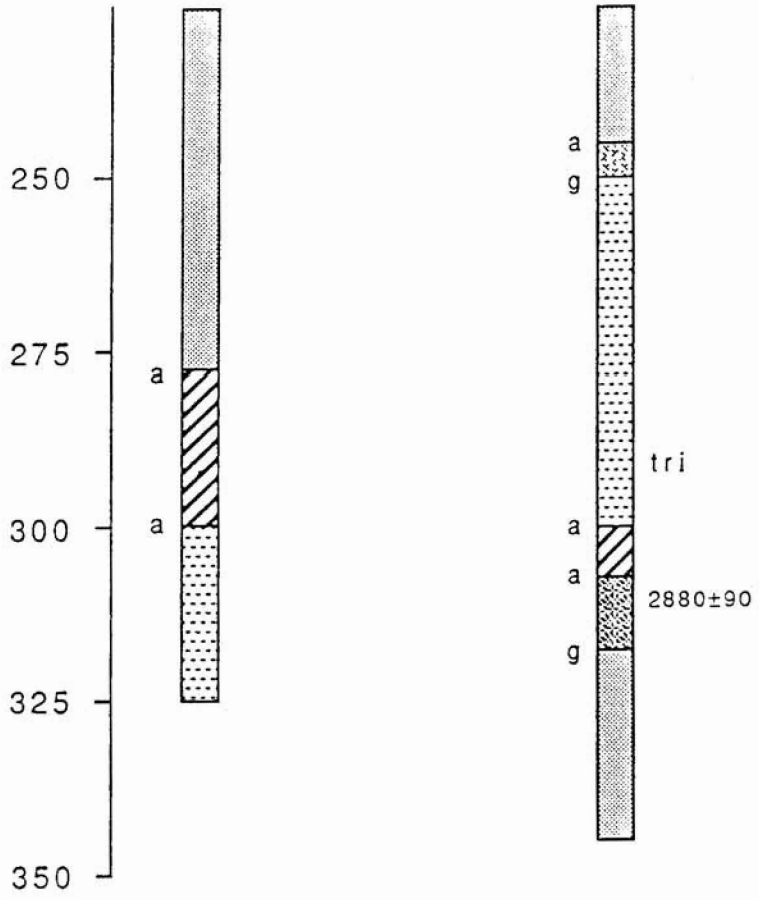
250
275
300
325
350
a
a
a
g
tri
a
a
2880±90
g

## APPENDIX 3.2: RADIOCARBON DATES FROM SILETZ BAY CORES

| Core Site | Depth (cm) | Age (RCY B.P.)[1] | Laboratory No. (Beta Analytic) |
|---|---|---|---|
| SB13 | 50 | 40±70 | 73252 |
| SB17 | 45 | 270±60 | 42089 |
| " | 70 | 350±60 | 42090 |
| " | 150 | 1,510±90 | 42001 |
| " | 215 | 1,690±70 | 42091 |
| " | 270 | 2,550±80 | 42002 |
| " | 310 | 2,690±80 | 42003 |
| SB23 | 45 | 1,130±50 | 73253 |
| SB25 | 80 | 580±60 | 73254 |
| SB32 | 35 | 510±60 | 73247 |
| SB48 | 45 | 480±60 | 42085 |
| " | 110 | 1,330±70 | 43126 |
| " | 155 | 1,630±70 | 43125 |
| " | 200 | 1,850±70 | 42086 |
| " | 305 | 2,880±90 | 42087 |

[1] RCY B.P. = Radiocarbon years before present.